Finite-Difference Time-Domain (FDTD) modeling of metamaterial structures

Professor Costas D. Sarris

The Eugene V. Polistuk Chair in Electromagnetic Design

The Edward S. Rogers Sr. Department of Electrical & Computer Engineering
UNIVERSITY OF TORONTO

Professor Costas Sarris

cEMPACT

Computational Electromagnetics for Wireless Communication, Sensing And Biomedical Applications

The Edward S. Rogers Sr. Department of Electrical & Computer Engineering
UNIVERSITY OF TORONTO

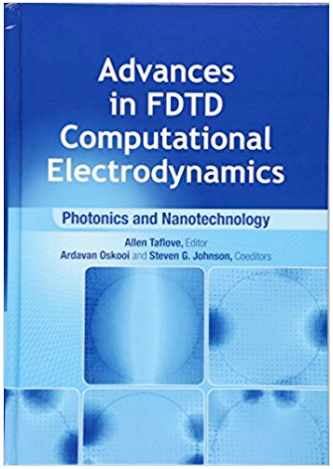

Acknowledgments

- Prof. Dongying Li, Dr. Roberto Armenta, Dr. Yaxun Liu, Dr. Alon Ludwig, Titos Kokkinos

- Prof. George Eleftheriades

Overview

- Finite-Difference Time-Domain (FDTD) modeling of metamaterials:
    - Dispersive models of negative index media.
    - Periodic structures.
    - Plasmonic metamaterials.
    - Driven periodic structures.
- Transformation optics inspired numerical methods:
    - Low and high-order methods on implicitly defined conformal meshes.
    - Moving meshes.

Negative Refractive Index (NRI) Media

$\varepsilon > 0, \mu > 0$

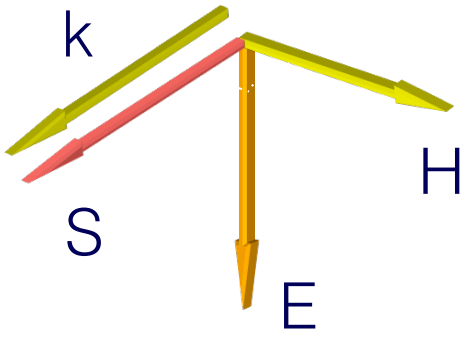

Right -Handed Media

$$n = \sqrt{\varepsilon\mu}$$

$\varepsilon < 0, \mu < 0$ [*]

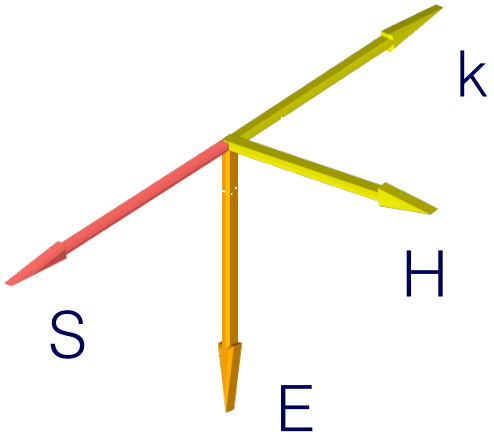

Left-Handed Media

$$n = -\sqrt{\varepsilon\mu}$$

* V. G. Veselago, "The electrodynamics of substances with simultaneously negative values of ε and μ", Soviet Phys. USPEKHI, vol 10, 1968

Veselago-Pendry Super-Lens

- Conventional lens:

$$k_x^2 + k_y^2 = k_0^2 \Rightarrow$$
$$k_y = \sqrt{k_0^2 - k_x^2}$$
$$= -j\alpha_y,\ k_x > k_0$$

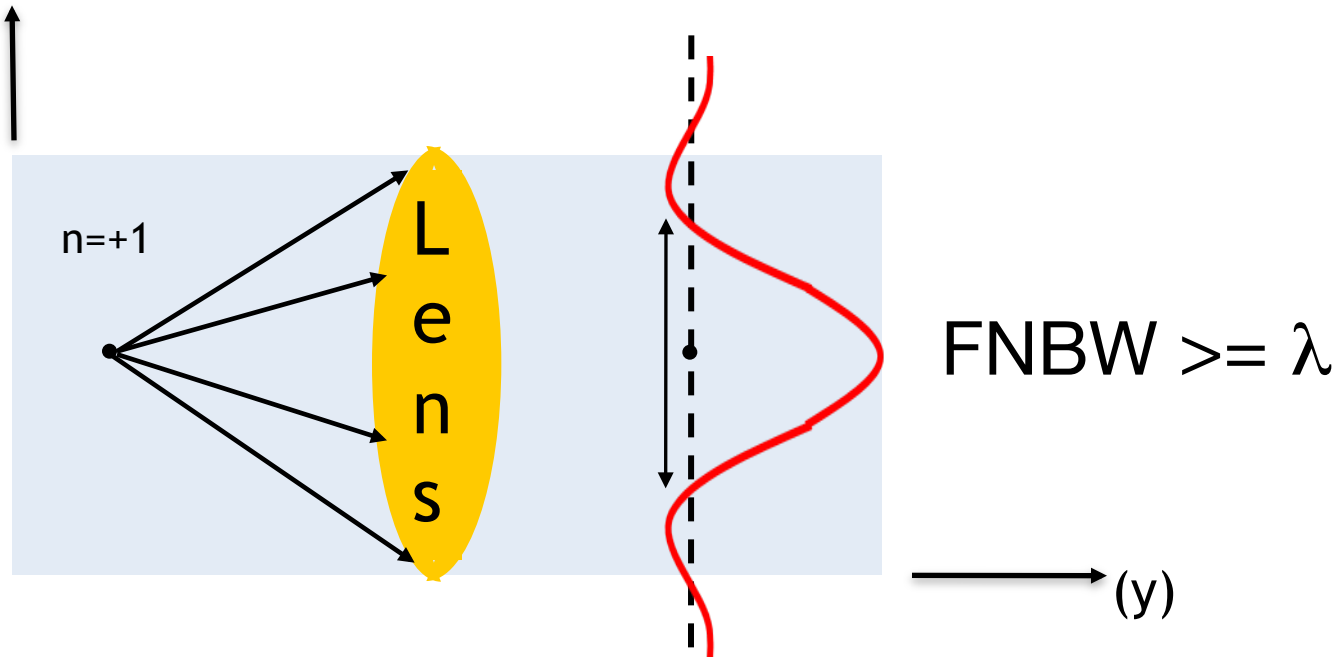

- First null beamwidth (FNBW) cannot be smaller than one wavelength of the source.
- Evanescent field components ($k_x > k_0$), are absent from the image spectrum, even if the lens aperture is infinite.

• J.Pendry, "Negative index makes a perfect lens", PRL 85, 3966 (2000).

Veselago-Pendry Super-Lens

- Veselago's planar lens:

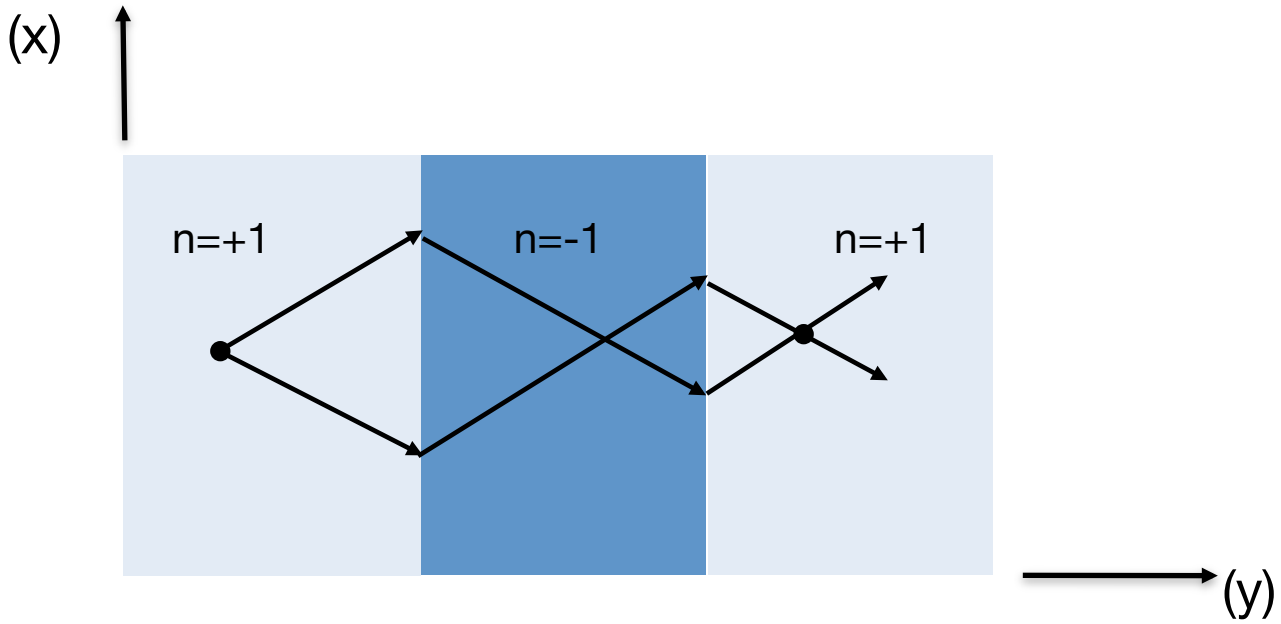

* V. G. Veselago, "The electrodynamics of substances with simultaneously negative values of ε and μ", Soviet Phys. USPEKHI, vol 10, 1968

Veselago-Pendry Super-Lens

- A planar lens beyond the diffraction limit*:

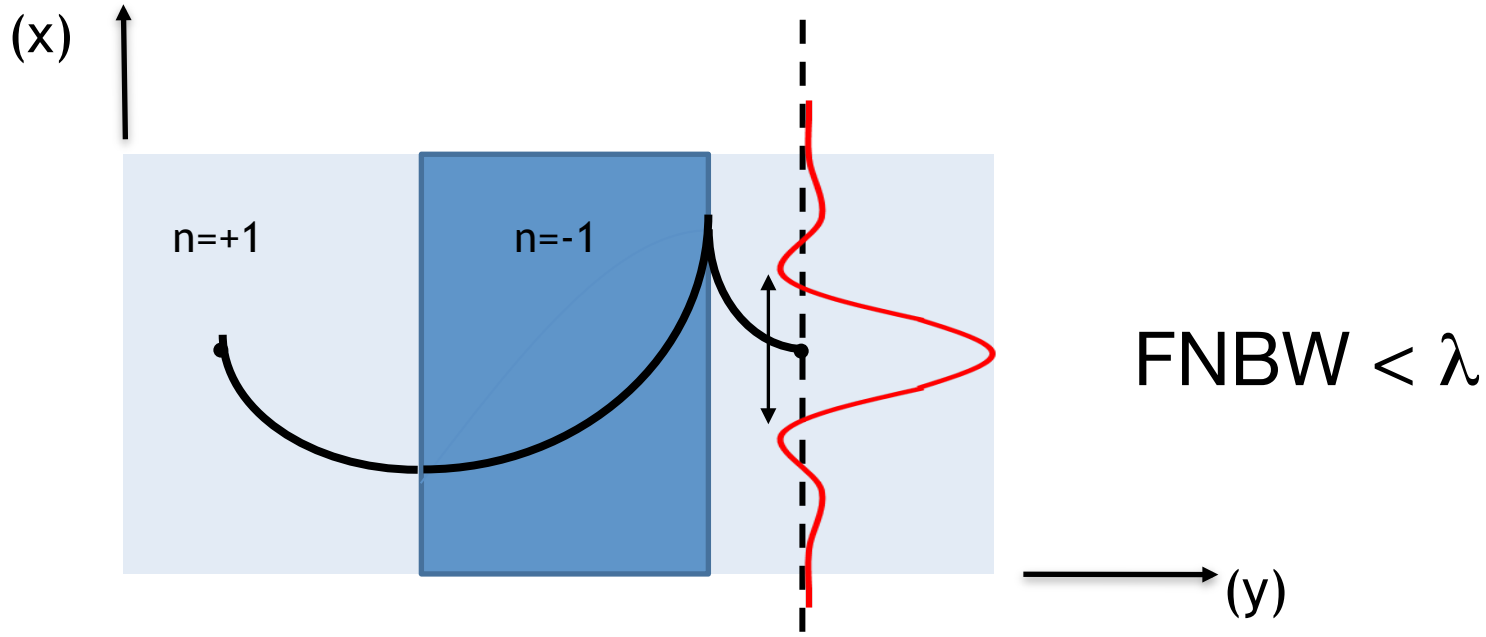

The negative index slab “amplifies” evanescent field components ($k_x > k_0$), restoring the spectrum of the source at the image plane, to obtain sub-wavelength resolution.

• J.Pendry, “Negative index makes a perfect lens”, PRL 85, 3966 (2000).

Super-Lens: FDTD Implementation

- Lorentz dispersion models for negative index media:

$$\varepsilon_r = 1 - \frac{\omega_{pe}^2}{\omega^2 - j\omega\nu_e}, \mu_r = 1 - \frac{\omega_{pm}^2}{\omega^2 - j\omega\nu_m}$$

Example: Perfect lens design at 1 GHz (ε_r, μ_r = -1).

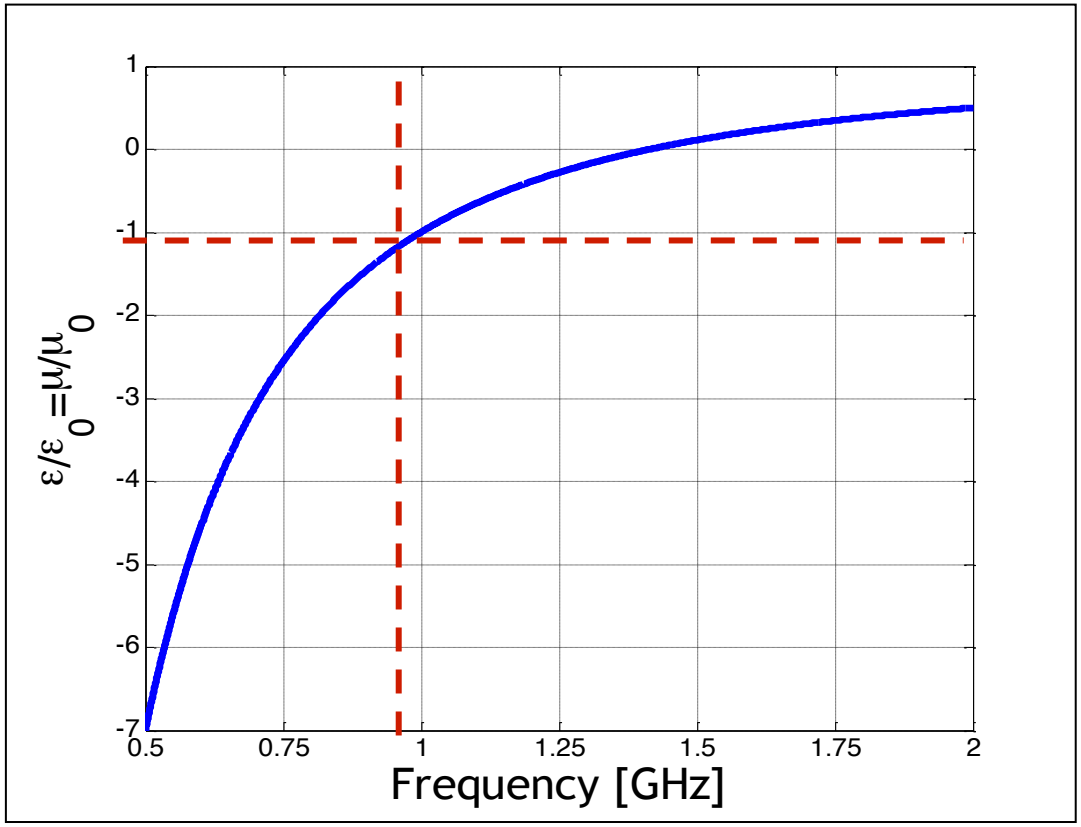

Super-Lens: FDTD Implementation

- Electric and magnetic dispersion incorporated in electric/magnetic currents:

$$\nabla \times \bar{E} = -\bar{M} - j\omega\mu_0 \bar{H}, \quad \bar{M} = -j\omega\mu_0 \frac{\omega_{pm}^2}{\omega^2 - j\omega\nu_m} \bar{H}$$

$$\nabla \times \bar{H} = \bar{J} + j\omega\varepsilon_0 \bar{E}, \quad \bar{J} = -j\omega\varepsilon_0 \frac{\omega_{pe}^2}{\omega^2 - j\omega\nu_e} \bar{E}$$

- Auxiliary differential equation for electric current:

$$\bar{J}^{n+1} = \frac{4\bar{J}^n + (\nu_e \Delta t - 2)\bar{J}^{n-1} + \varepsilon_0 \omega_{pe}^2 \Delta t \left(\bar{E}^{n+1} - \bar{E}^n\right)}{\nu_e \Delta t + 2}$$

Veselago-Pendry Super-Lens: Results

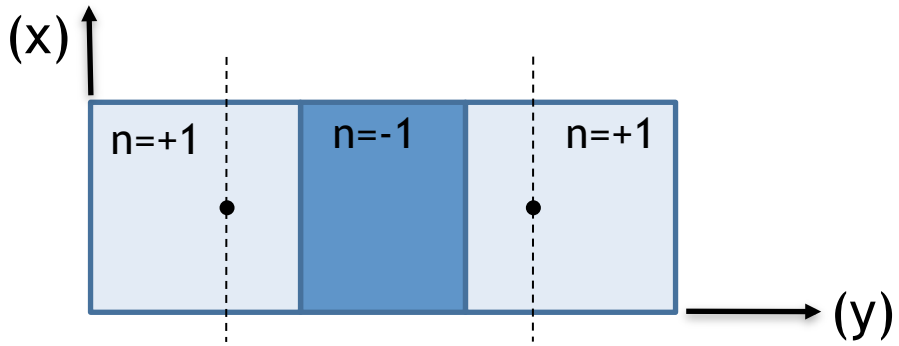

Negative index slab:
Drude medium with
index -1 at 1 GHz

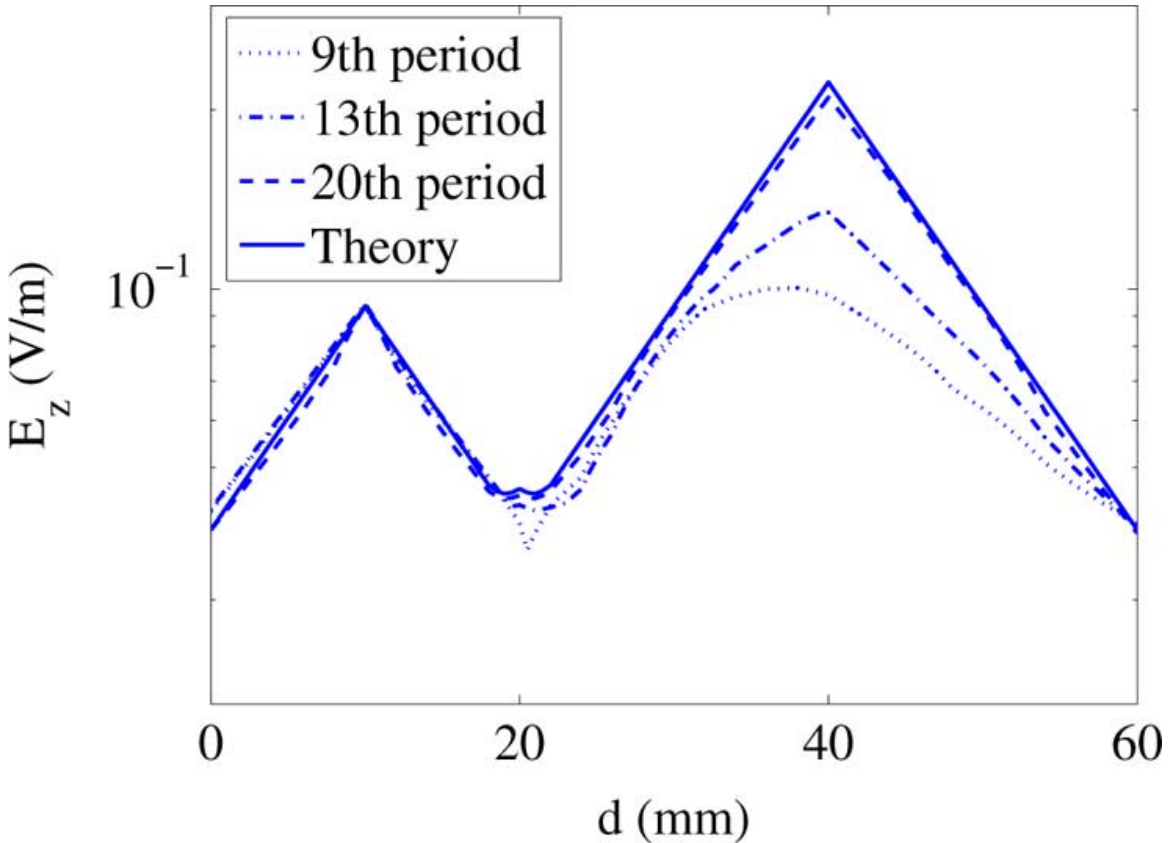

Veselago-Pendry Super-Lens: Results

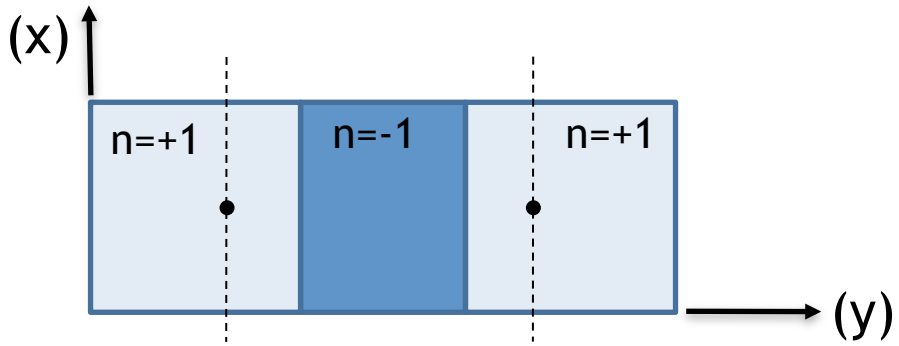

Negative index slab: Drude medium with index -1 at 1 GHz

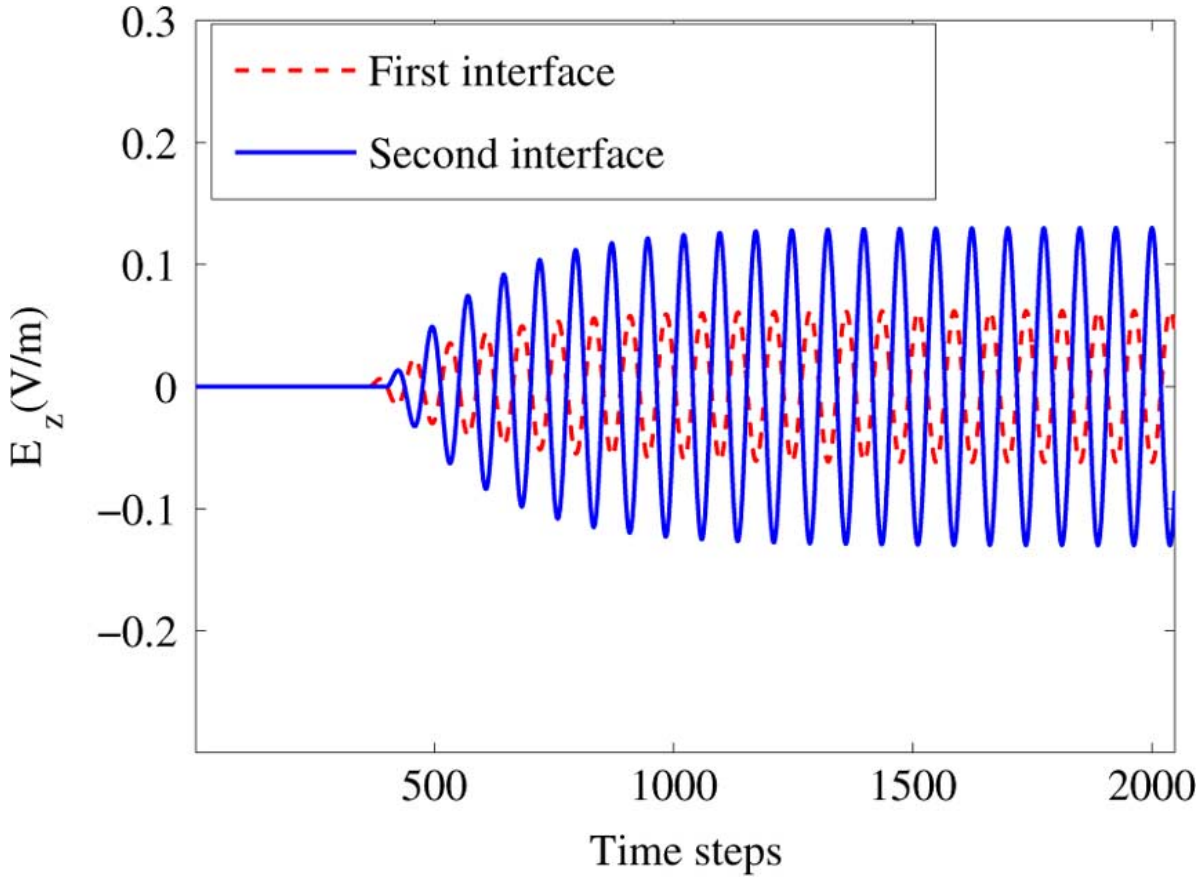

Veselago-Pendry Super-Lens: Results

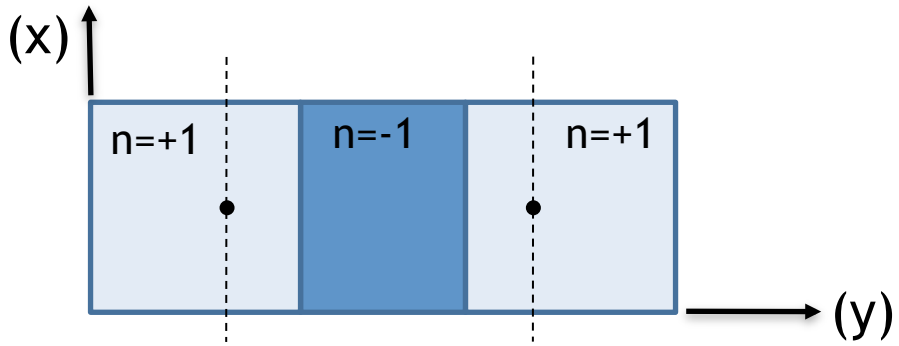

Negative index slab:
Drude medium with
index -1 at 1 GHz

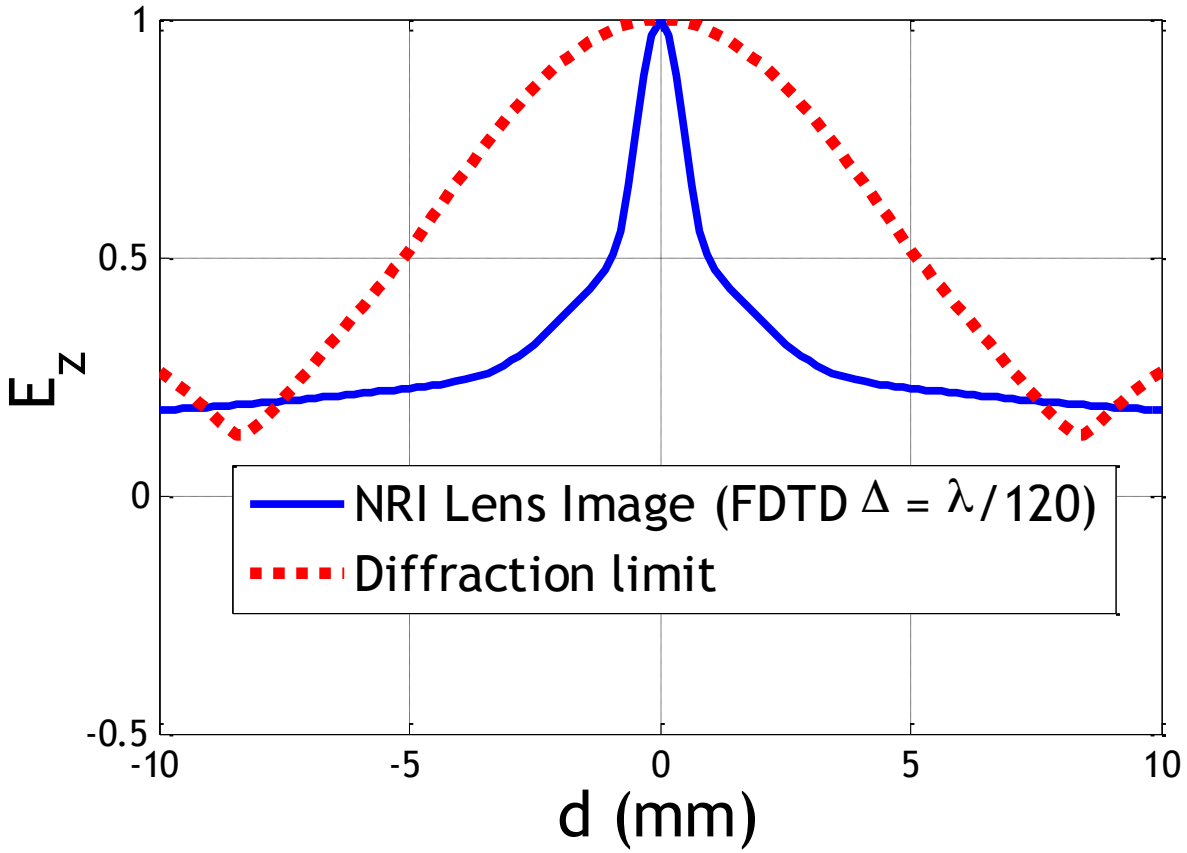

Veselago-Pendry Super-Lens: Results

- Temporal field evolution

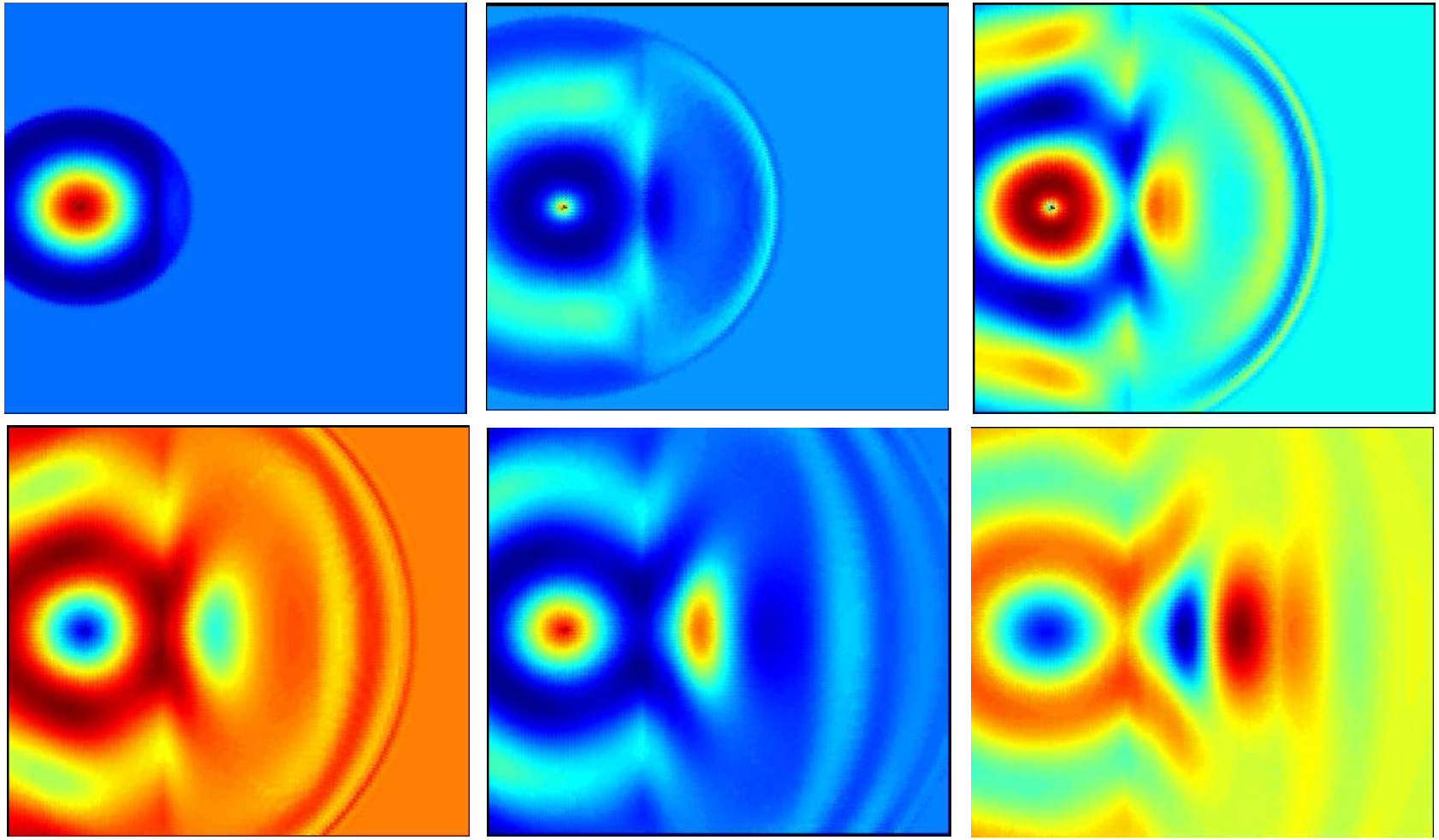

Numerical Dispersion Effects (1)

- Consider an inhomogeneous plane wave (k_x, k_y), with:

$$k_x^2 + k_y^2 = k^2 \Rightarrow k_y = \sqrt{k^2 - k_x^2} = -j\alpha_y$$

for $k_x > k$; back-substituting:

$$\sin^2\frac{\omega\Delta t}{2}\tilde{\varepsilon}_r\tilde{\mu}_r = \left\{\frac{c\Delta t}{\Delta x}\sum_{p=0}^{L_s-1}\alpha(p)\sin\left(\tilde{k}_x\left(p+\frac{1}{2}\right)\Delta x\right)\right\}^2 - \left\{\frac{c\Delta t}{\Delta y}\sum_{p=0}^{L_s-1}\alpha(p)\sinh\left(\tilde{\alpha}_y\left(p+\frac{1}{2}\right)\Delta y\right)\right\}^2$$

Allows for the evaluation of the numerical dispersion of evanescent waves, for general FDTD and high-order FDTD schemes (α's are the stencil coefficients).

Numerical Dispersion Effects (2)

- To focus on the evanescent wave spectrum ($k_x > k_0$), parameterize: $k_x = k_0 \cosh\zeta$, $\alpha_y = k_0 \sinh\zeta$.

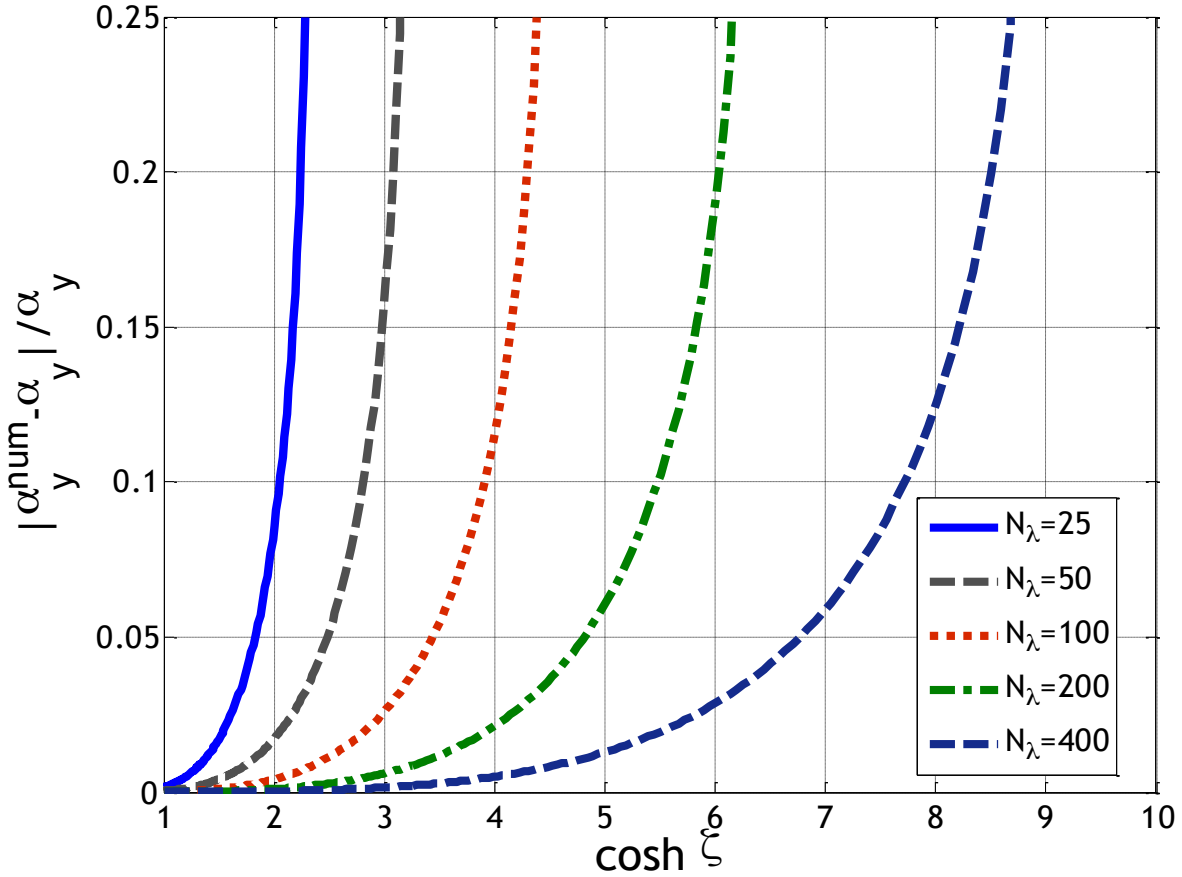

FDTD:
For evanescent wavenumber beyond 5 free space wavelengths, more than N_λ=100 ppw are needed.

Numerical Dispersion Effects (3)

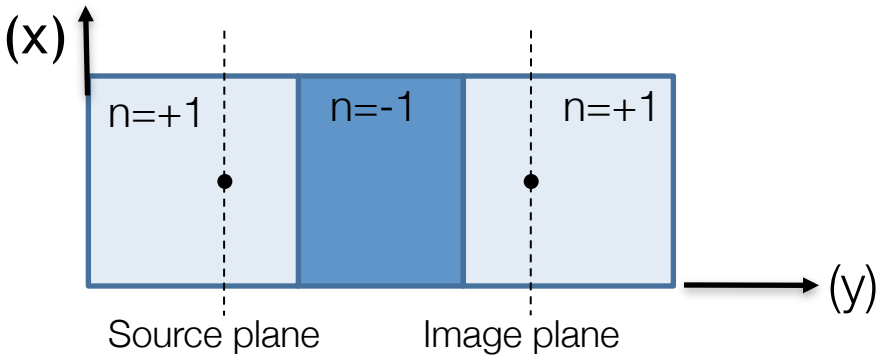

- Negative index slab: Drude medium with index -1 at 16 GHz
- 3-dB beamwidth found

- For the same medium, the resolution enhancement changes from 1.1 to 5.3, by changing the cell size.

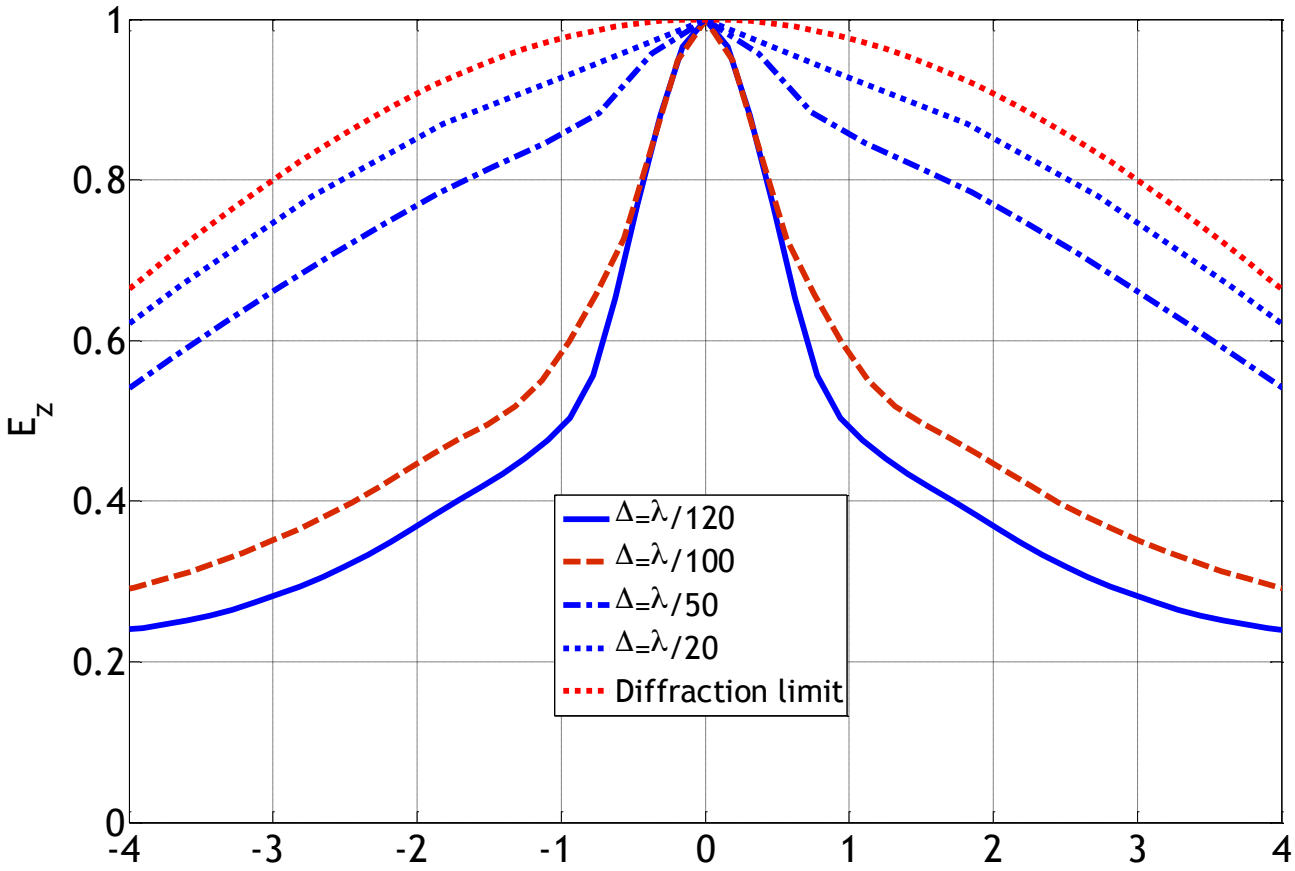

Super-Lens: Limitations

Physical Limitations

- Negative index slab index different from -1 (design / fabrication issues).
- Losses (source spectral components attenuated).
- If periodic media are used to implement the lens, resolution is limited by periodicity.

Numerical Limitations

- Negative index slab index different from -1 (numerical dispersion/ anisotropy).
- Dispersion of STRONGLY evanescent waves.
- Resolution limited by cell size.

*D. R. Smith, D. Schurig, M. Rosenbluth, S. Schultz, S. A. Ramakrishna, J. B. Pendry, "Limitations on subdiffraction imaging with a negative refractive index slab", Appl. Phys. Lett. , 82, 1506 (2003).

Microwave NRI Media

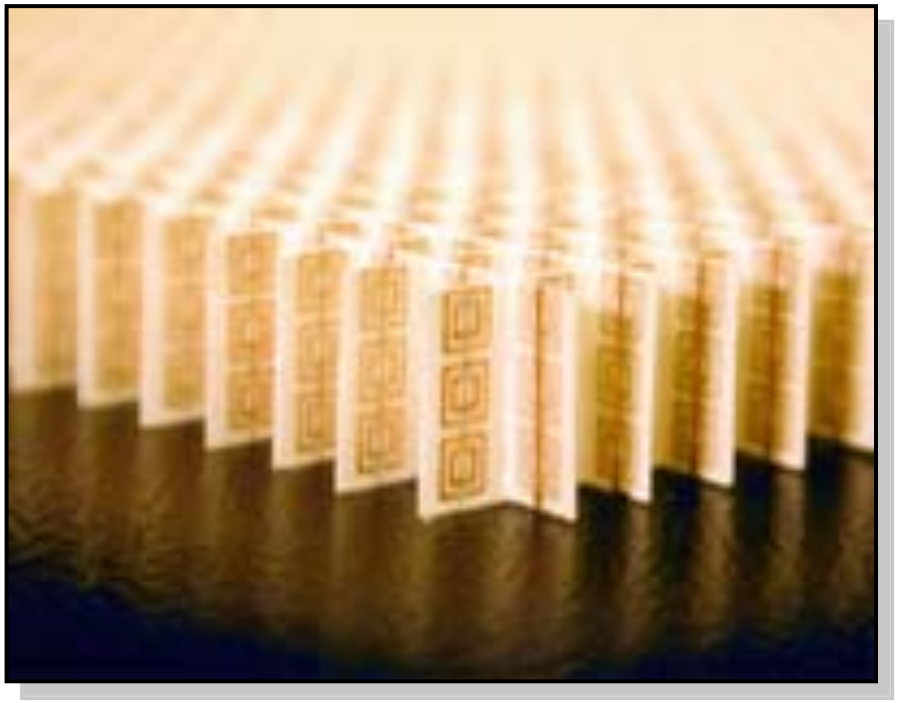

Split-Ring Resonators (SRR) and Straight Wires [D. R. Smith et al., Phys.Rev. Let. ,vol. 78, 2933, May 2000.]

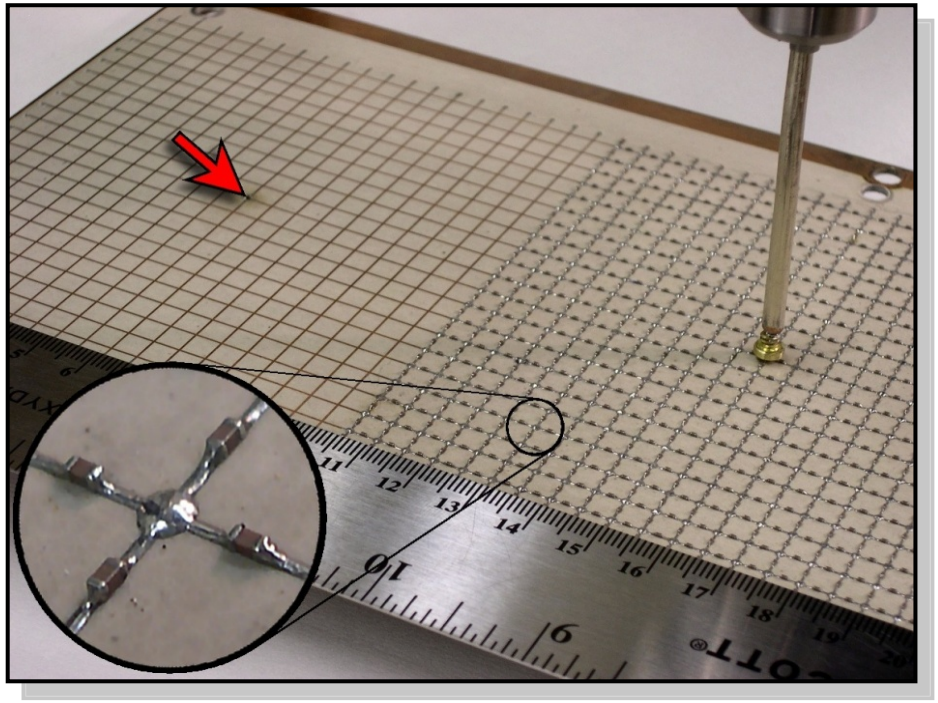

2D Negative Refractive Index Transmission-Line (NRI-TL) Media [G.V.Eleftheriades et al., IEEE Trans. MTT, vol. 50, 2702, Dec. 2002]

Periodic Boundary Conditions

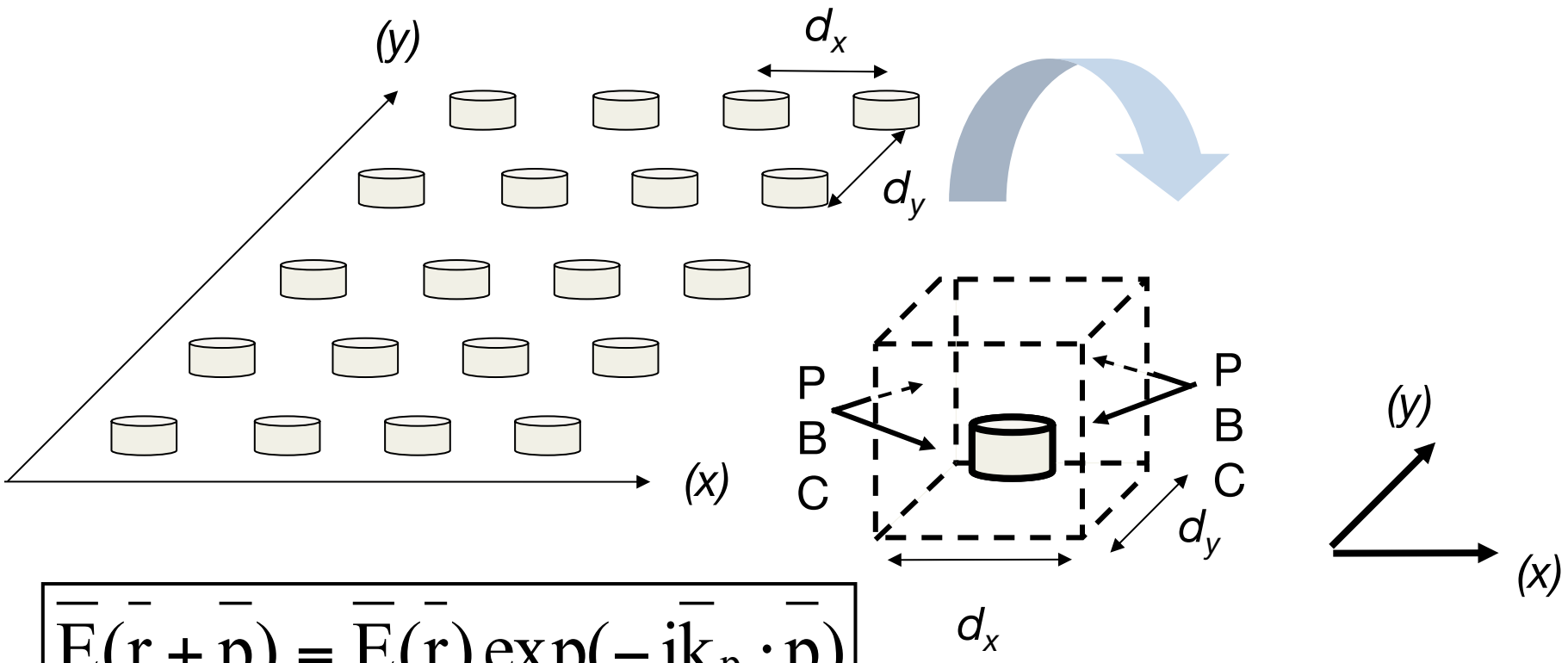

$$\bar{E}(\bar{r}+\bar{p}) = \bar{E}(\bar{r})\exp(-j\bar{k}_p \cdot \bar{p})$$

$$\bar{p} = d_x\hat{x} + d_y\hat{y}$$ Lattice vector

$$\bar{k}_p = k_x\hat{x} + k_y\hat{y}$$ Bloch wavevector

Periodic Boundary Conditions in FDTD

- Sine-cosine method [Harms, Mittra, Ko, IEEE T-AP, Sept. 1994], split-field [Roden et al, IEEE T-MTT, Apr. 1998].

- Basic process:
  - Enforce a Floquet wave vector k within the irreducible Brillouin zone.
  - Sample the field in the time-domain, find $\omega(k)$ from spectral analysis.

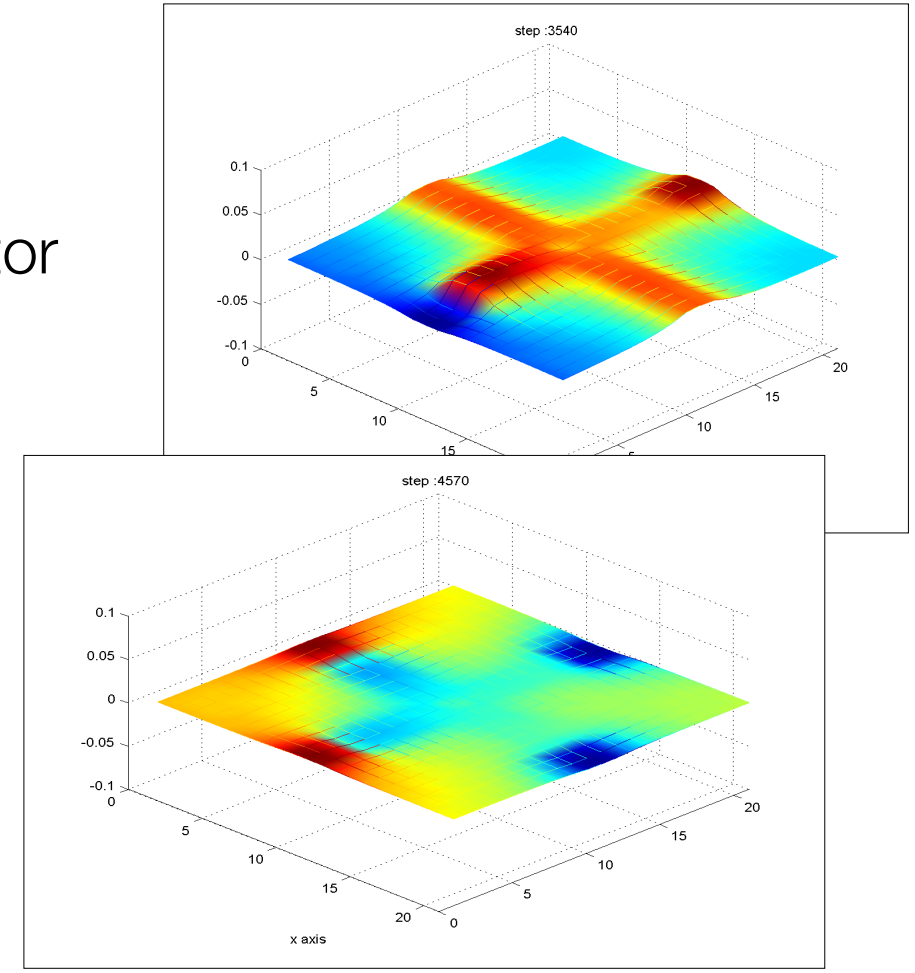

Broadband Periodic FDTD Analysis (1)

Example: The NRI Transmission-Line Unit Cell

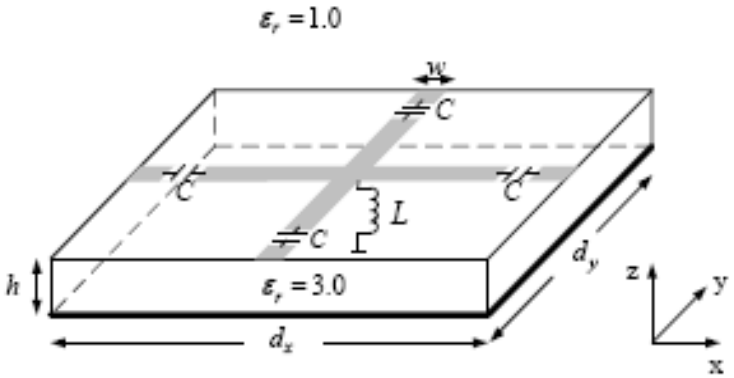

C=3.34 pF
L=16.02 nH

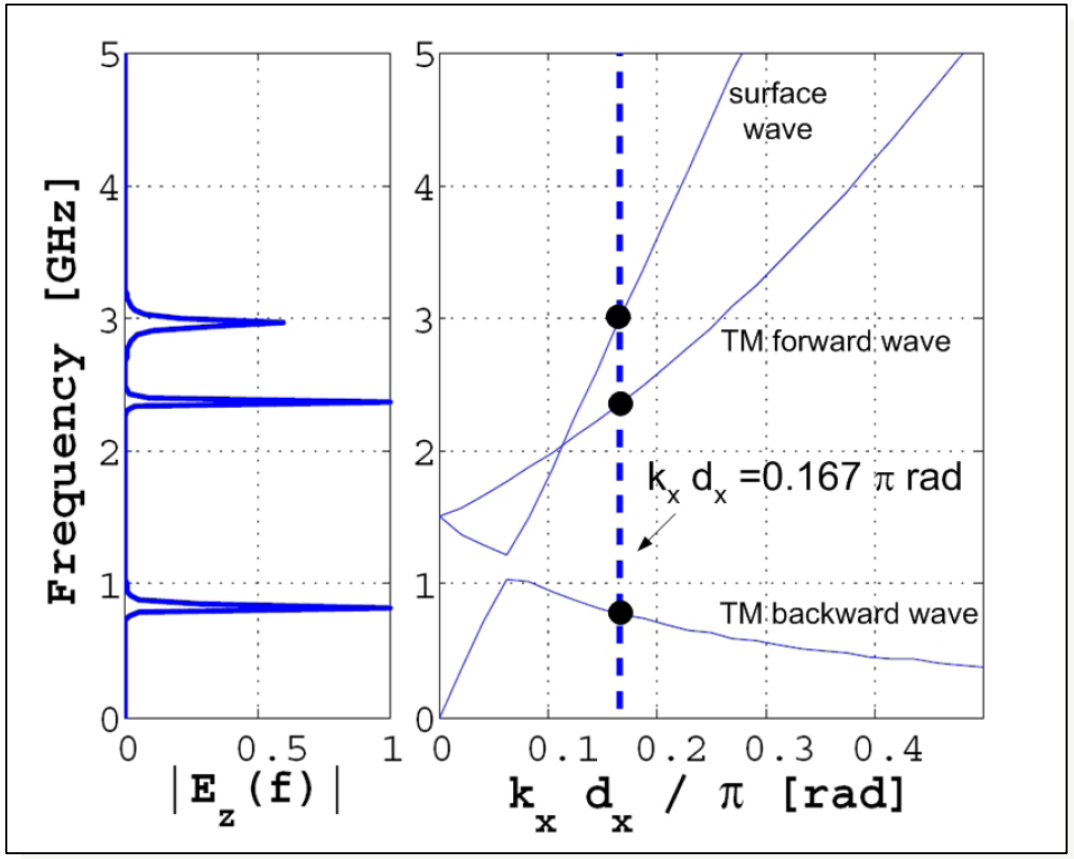

FDTD analysis based on a wideband pulse excitation (0.5-3 GHz)

Broadband Periodic FDTD Analysis (2)

Example: The NRI Transmission-Line Unit Cell

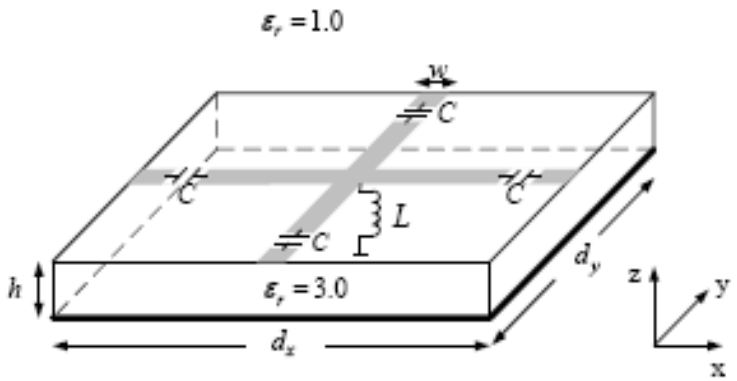

C=3.34 pF
L=16.02 nH

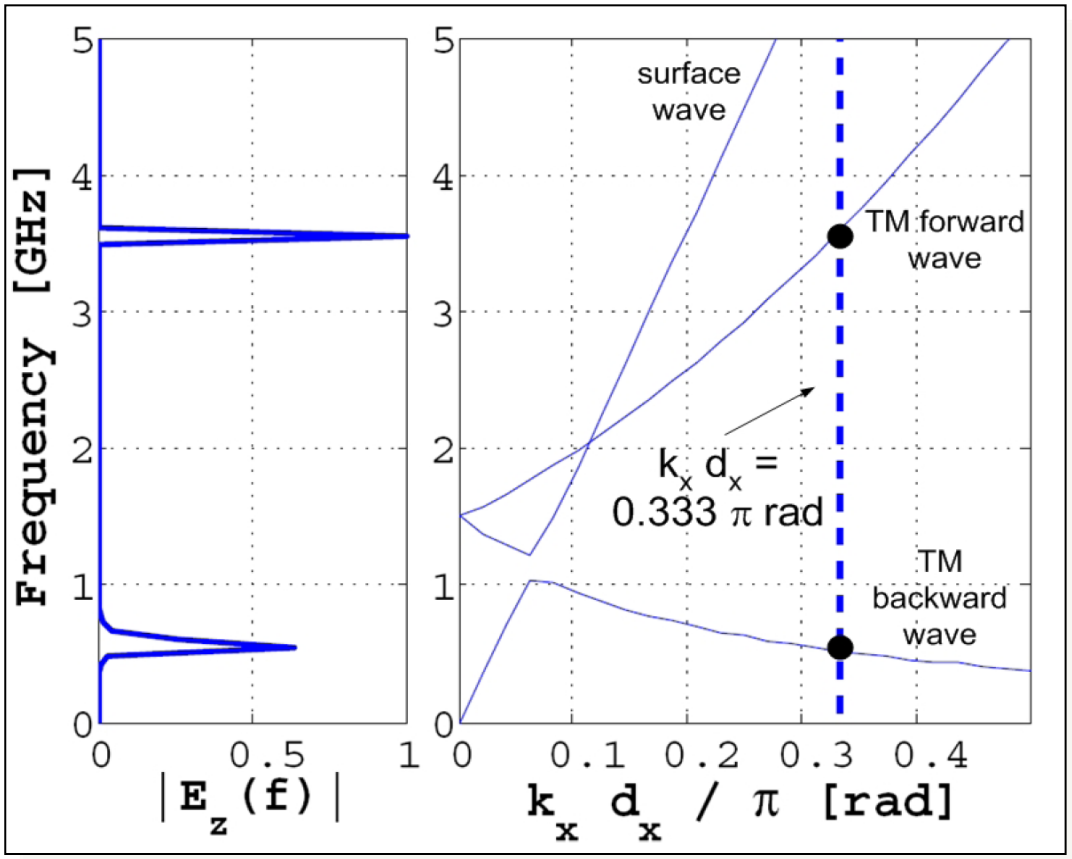

FDTD analysis based on a wideband pulse excitation (0.5-3 GHz)

Leaky-Wave Radiation from the NRI -TL

- Leaky-Wave Antennas:
  - Periodic structures supporting leaky-wave radiation.
  - Renewed interest stemming from recent advances in metamaterials.

$|\beta_x|/k_0 < 1$:

Fast (leaky) waves emerging at angle θ,

$$\sin\theta = \beta_x / k_0$$

Forward Endfire: $\beta_x = k_0$

Broadside: $\beta_x = 0$

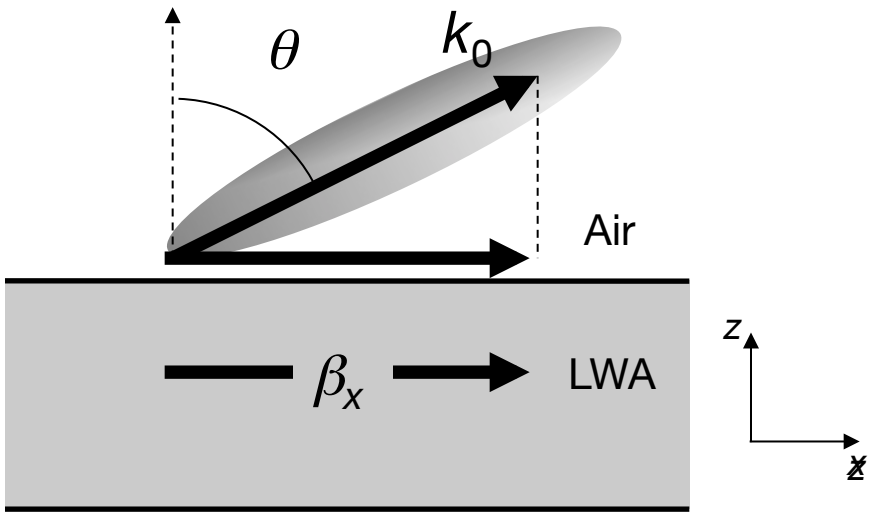

Leaky-Wave Radiation from the NRI -TL

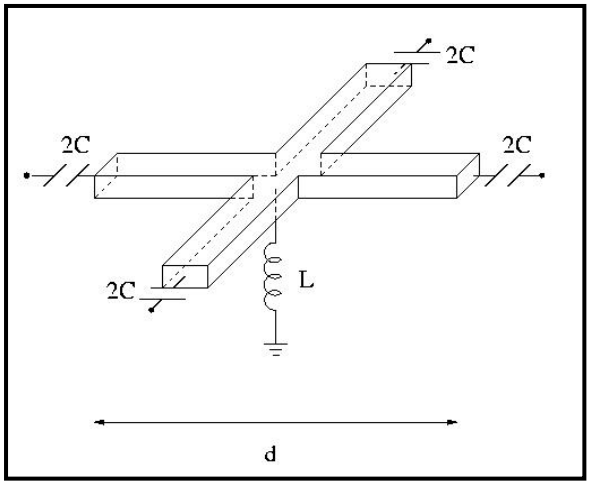

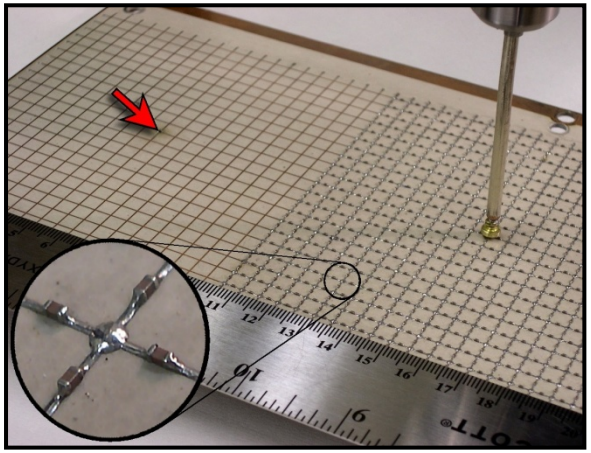

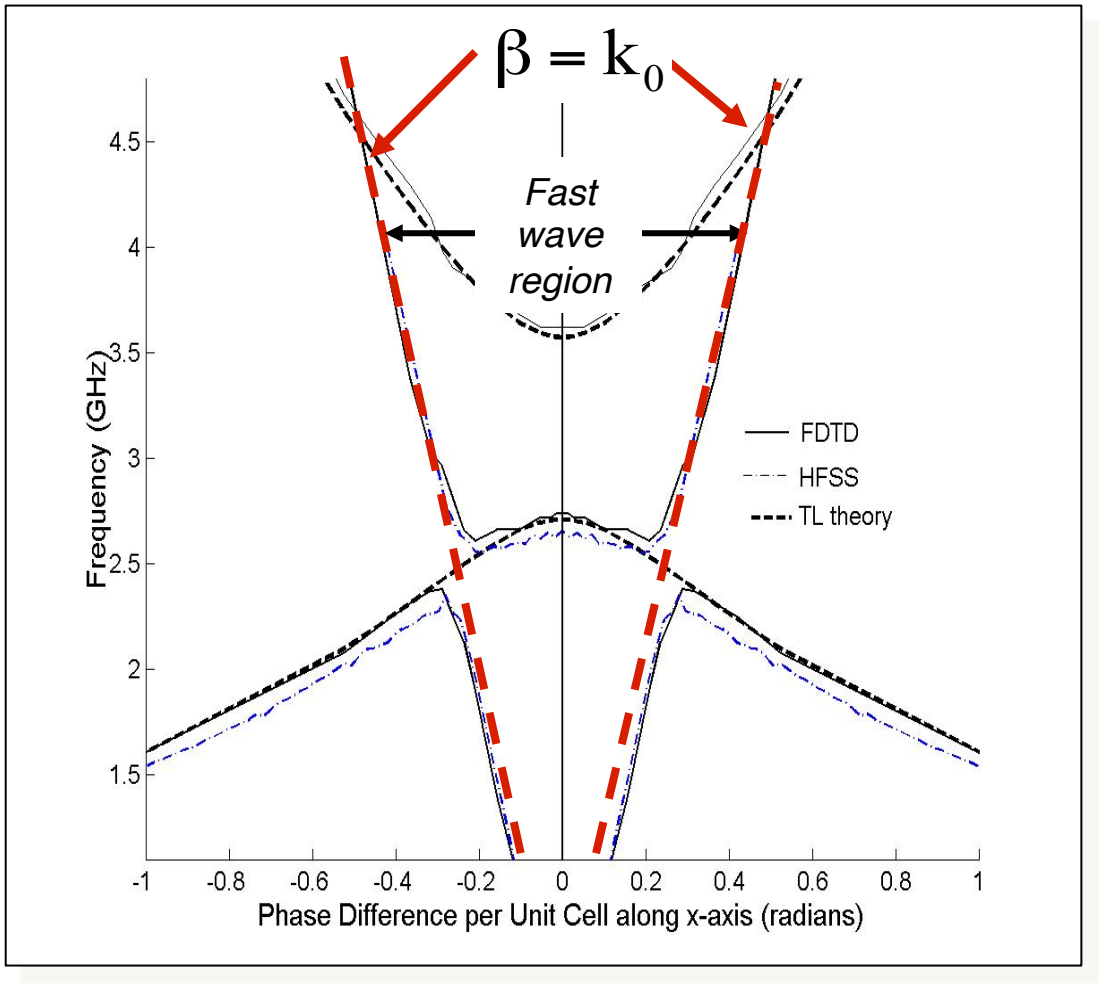

G.V. Eleftheriades et al, IEEE Trans. MTT, vol. 50, Dec. 2002.
T. Kokkinos et al., IEEE Trans. MTT, Apr. 2005.

Fast and slow waves: resonances

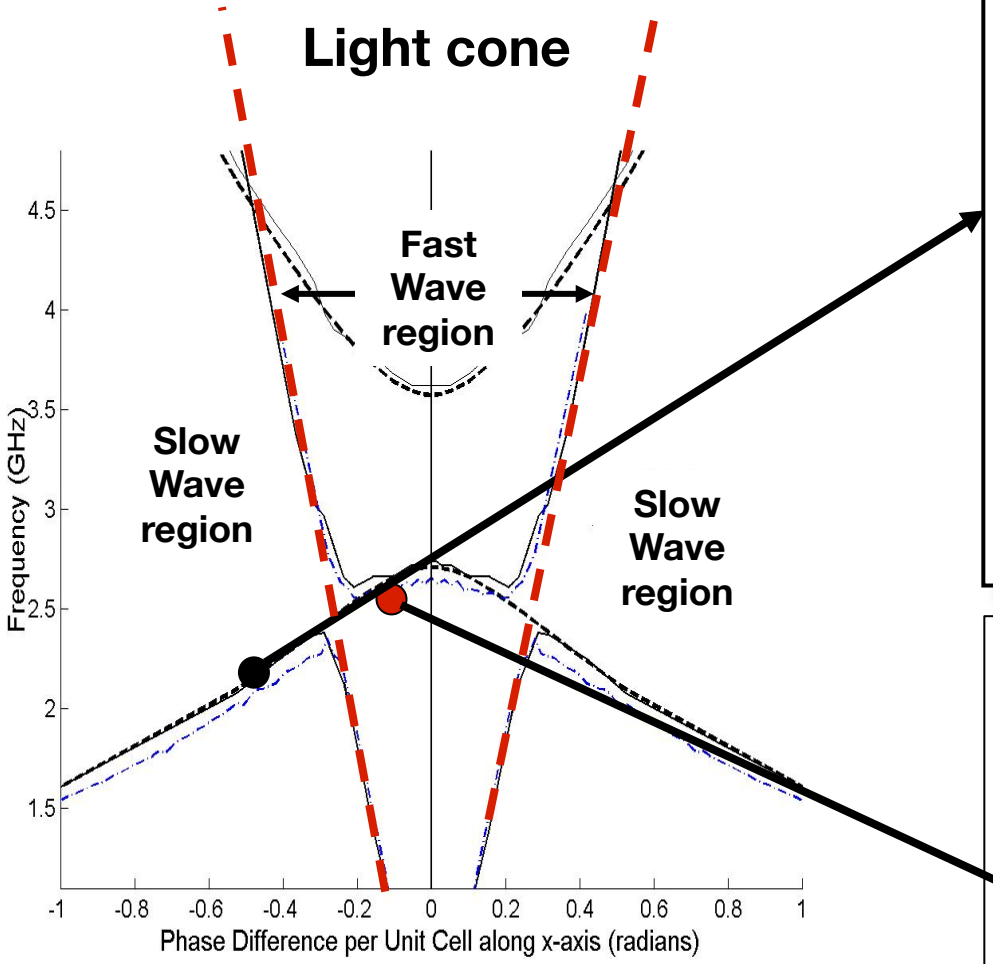

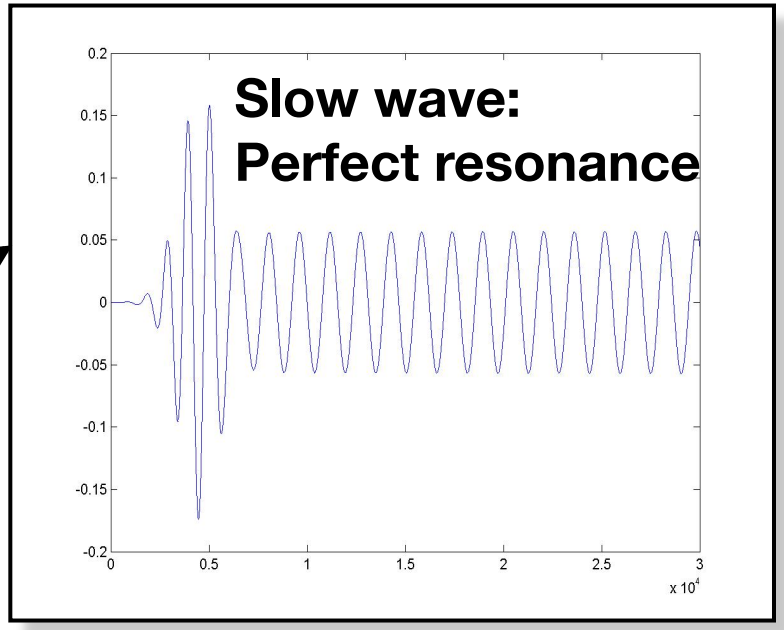

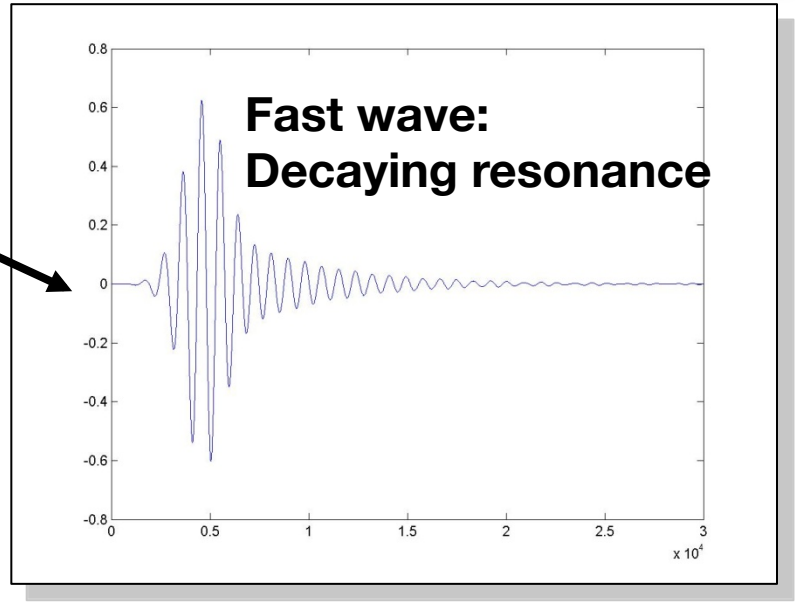

- In both cases, the real part of the Floquet wavenumber was enforced.

Leaky-waves and PBCs

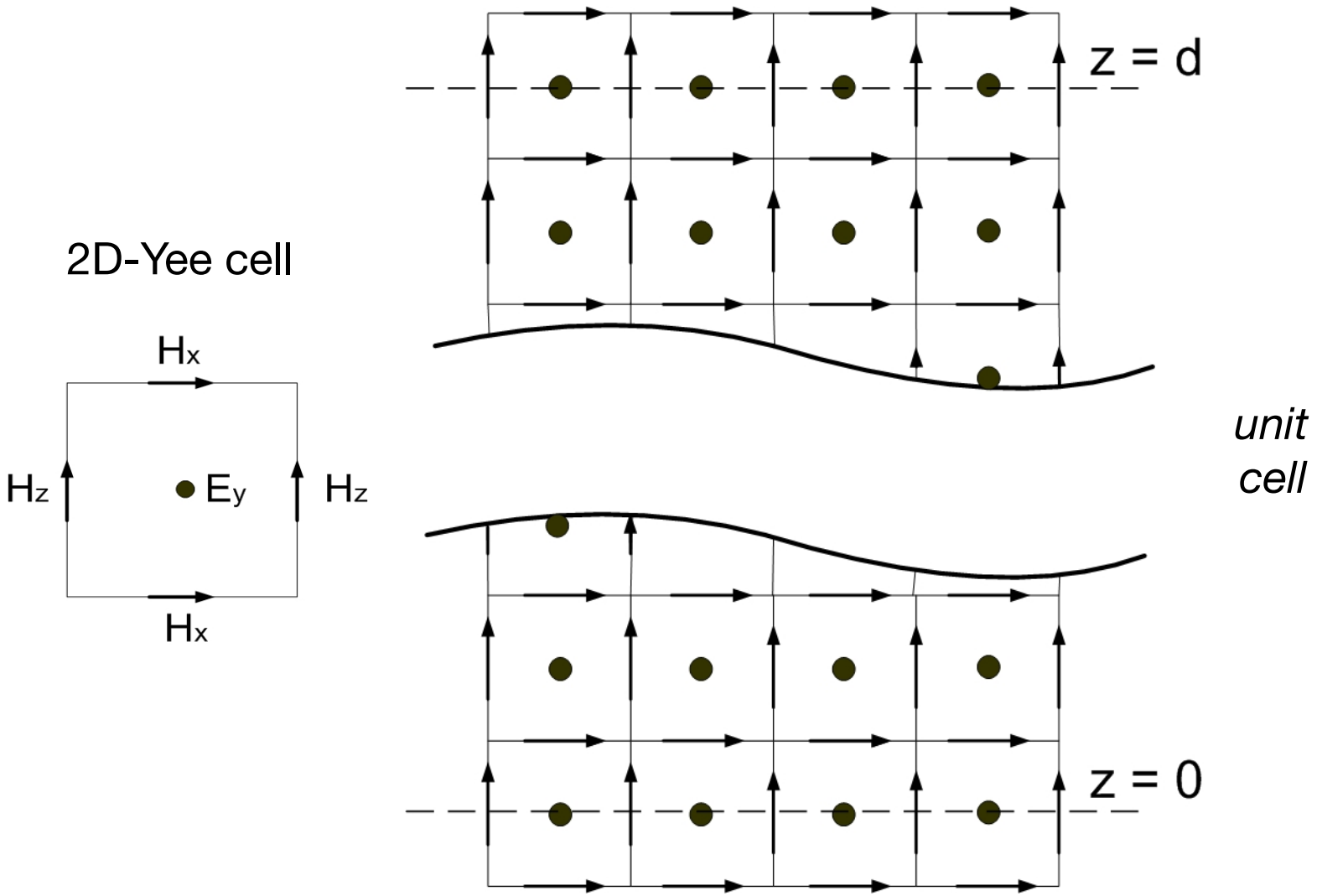

Leaky-waves and PBCs

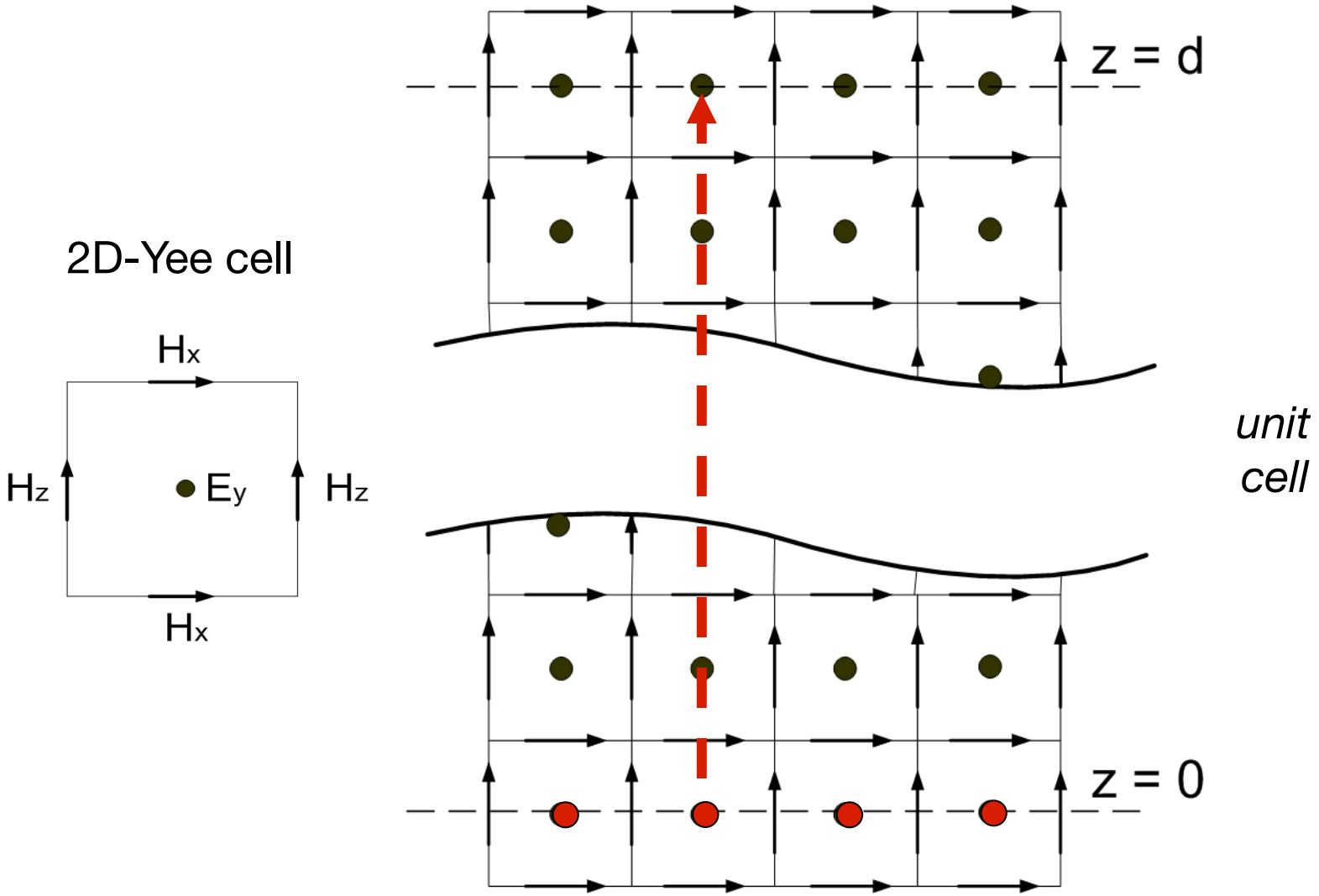

Leaky-waves and PBCs

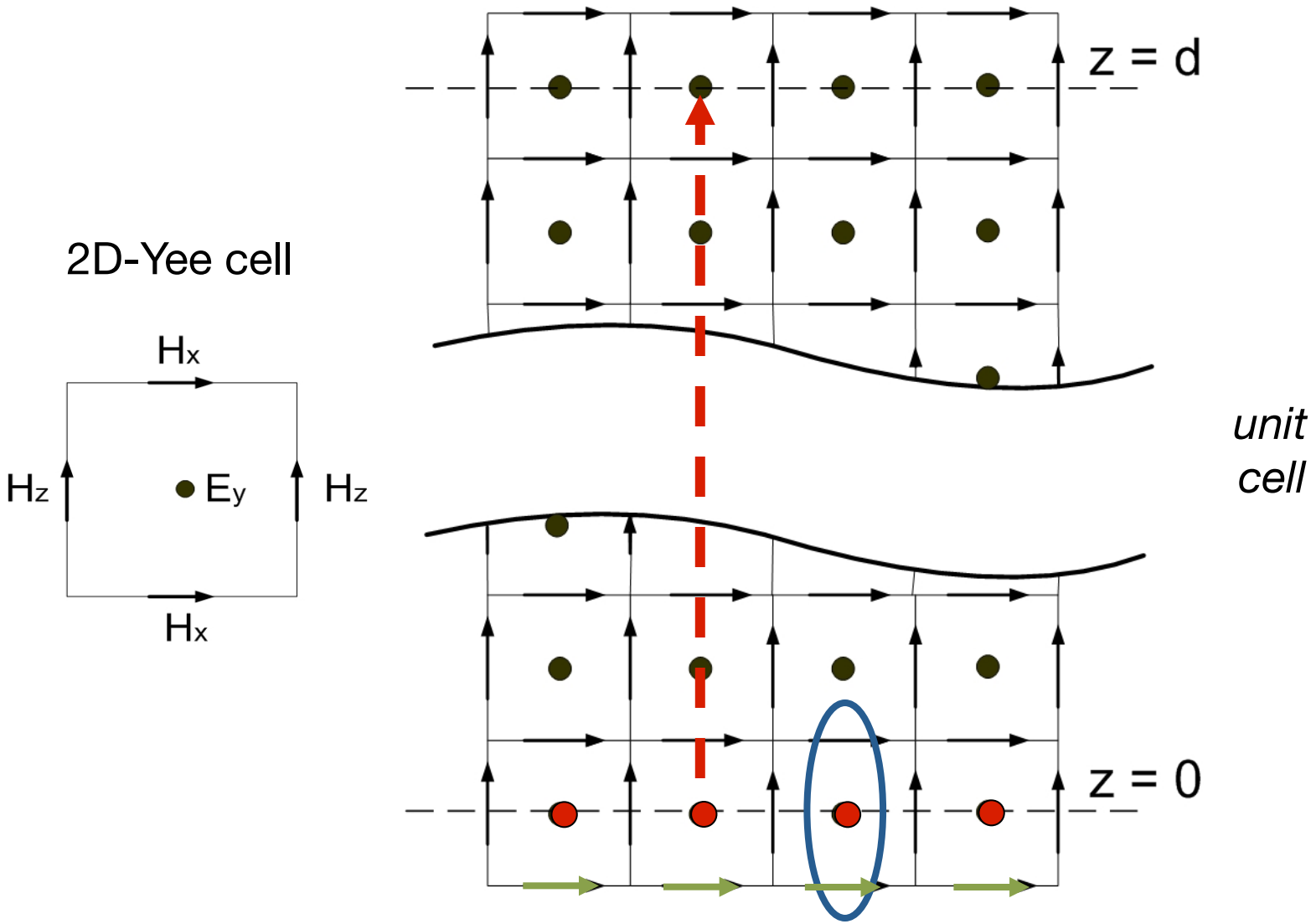

Leaky-waves and PBCs

2D-Yee cell

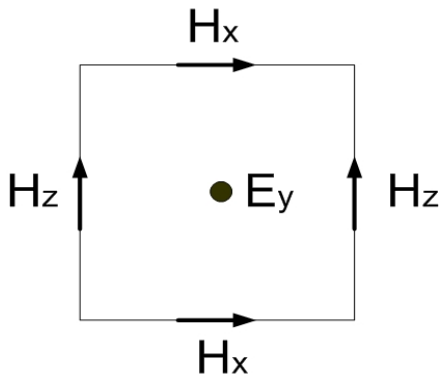

PBC updates are

bi-directional !

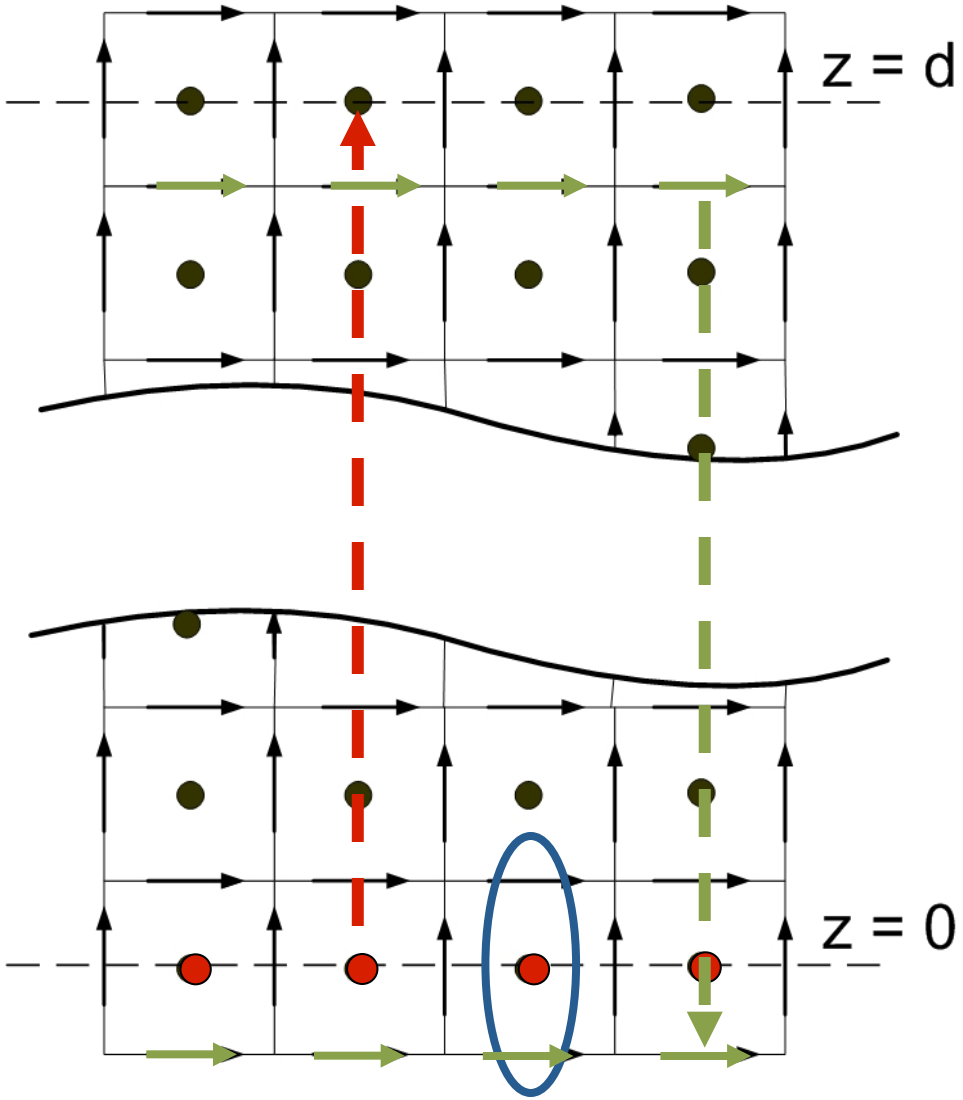

unit cell

Leaky-waves and PBCs

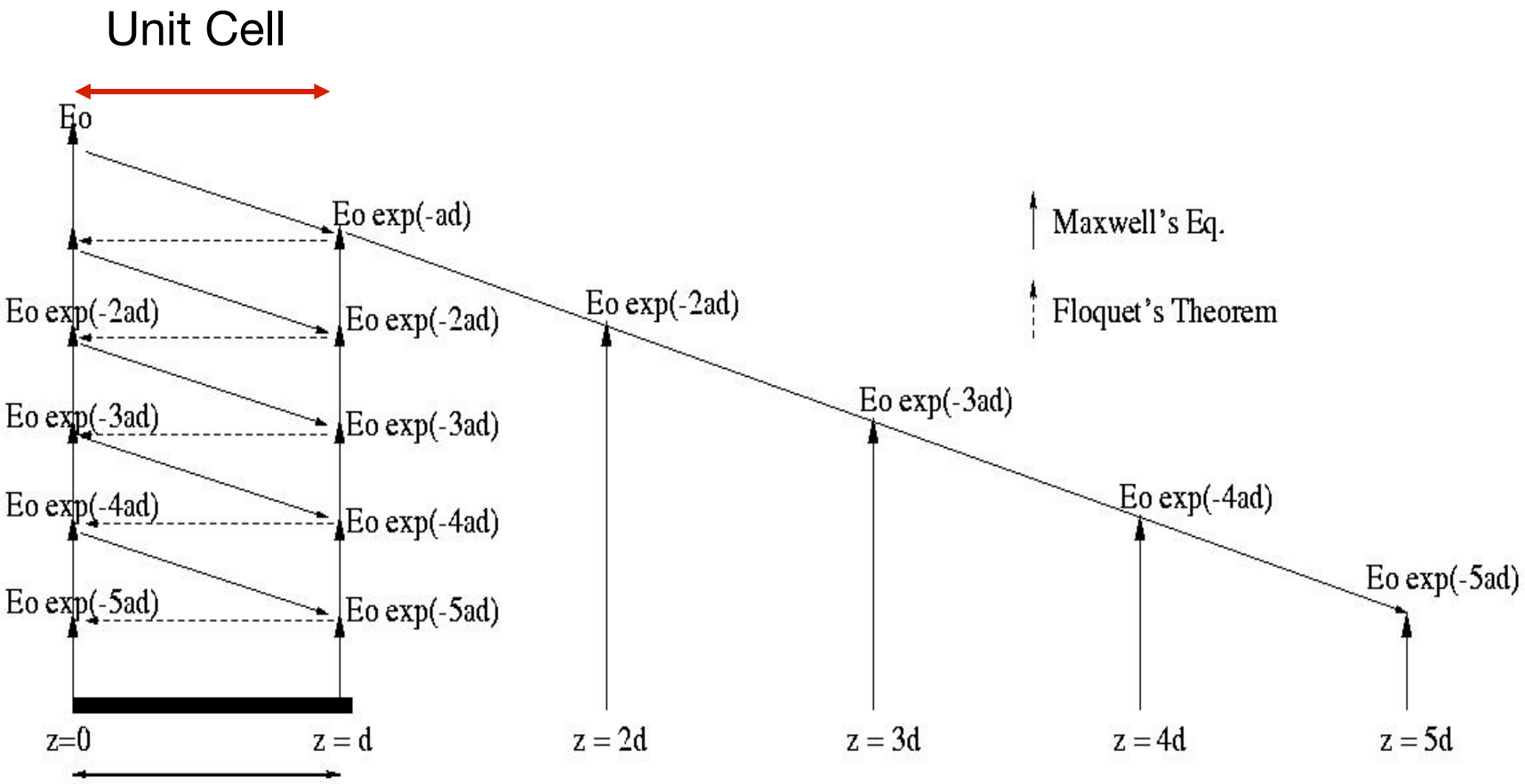

Truncated Lossy/Radiating Structure

NRI-TL at Optical Frequencies

- Lattices of plasmonic noble metal nanorods/spheres may provide optical analogs to NRI-TLs

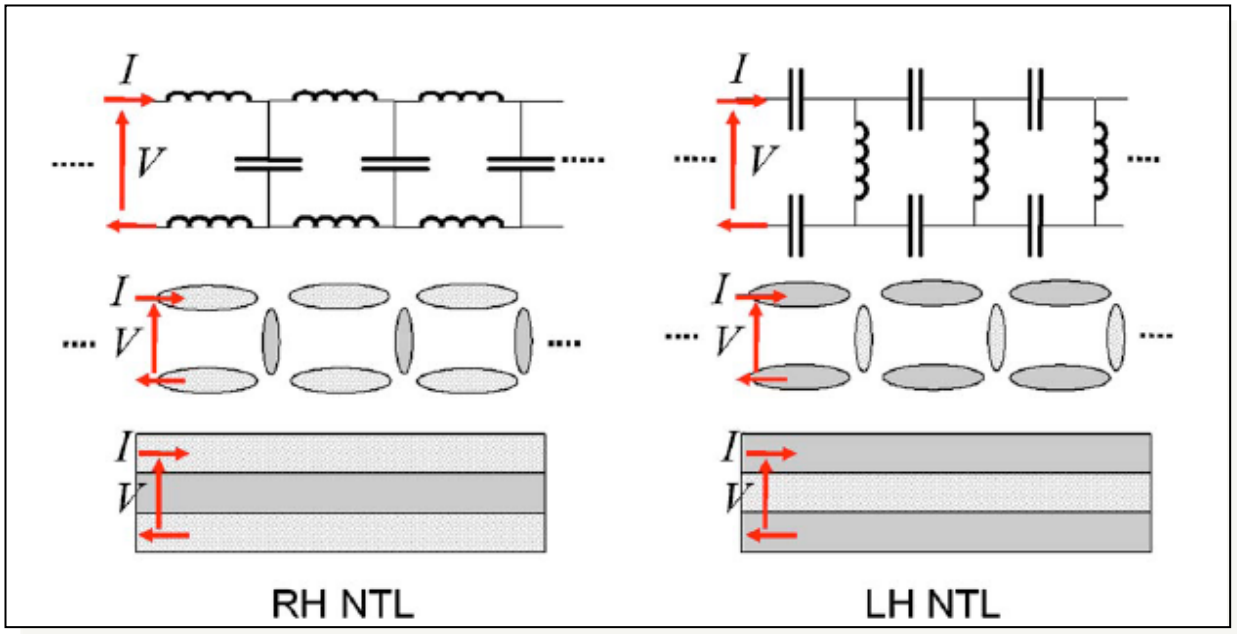

1. N. Engheta, A. Salandrino, and A. Alù, "Circuit elements at optical frequencies: nanoinductors, nanocapacitors and nanoresistors," Phys. Rev. Lett. 95, 095504 (2005).
2. A. Alù, N. Engheta, "Optical nanotransmission lines: synthesis of planar left-handed metamaterials in the infrared and visible regimes", JOSA B, vol. 23, no. 3, March 2006.

NRI-TL at Optical Frequencies (cont-d)

Backward waves in plasmonic nanosphere lattices

Silver nanoparticle waveguides

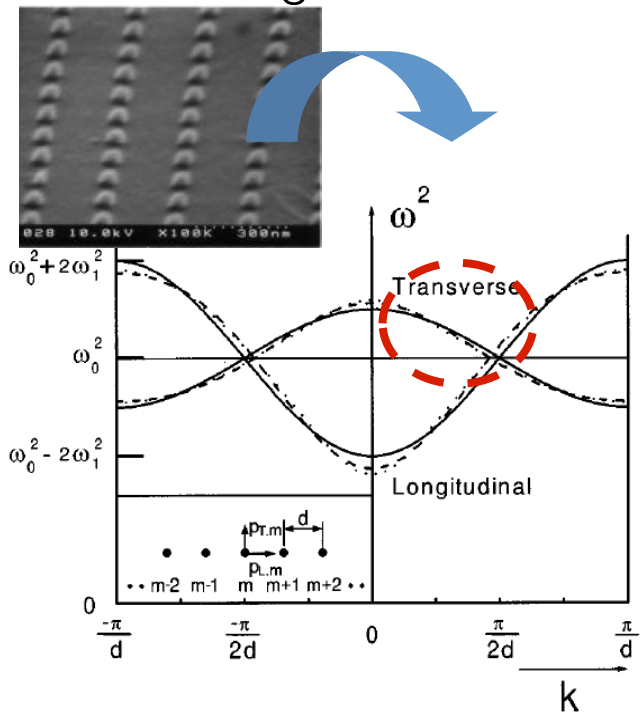

Sub-wavelength Photonic Crystals (SPC)

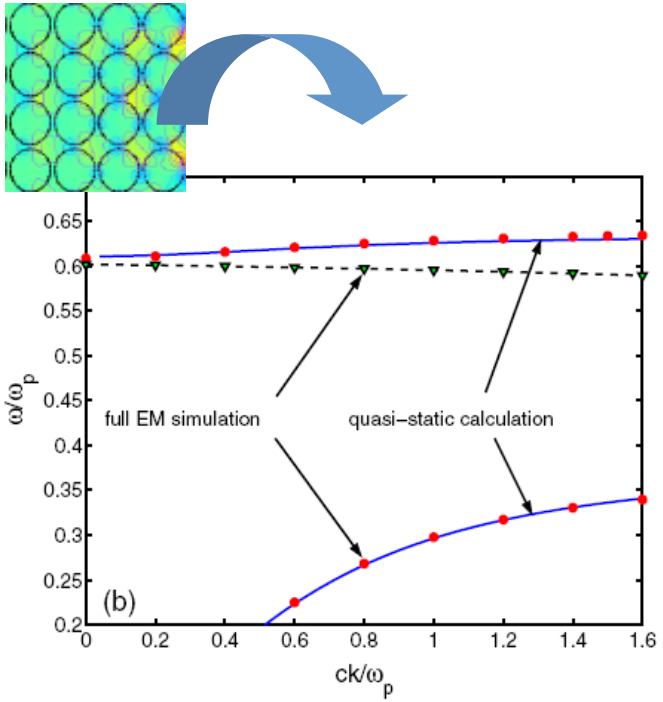

S.Maier et al, "Electromagnetic energy transport below the diffraction limit in periodic metal nanostructures", Proc. SPIE, vol. 4456.

G.Shvets, Y. Urzhumov, "Engineering the Electromagnetic Properties of Periodic Nanostructures Using Electrostatic Resonances", PRL **93,**243902 (2004)

SPC Lattice as a "Perfect Lens"

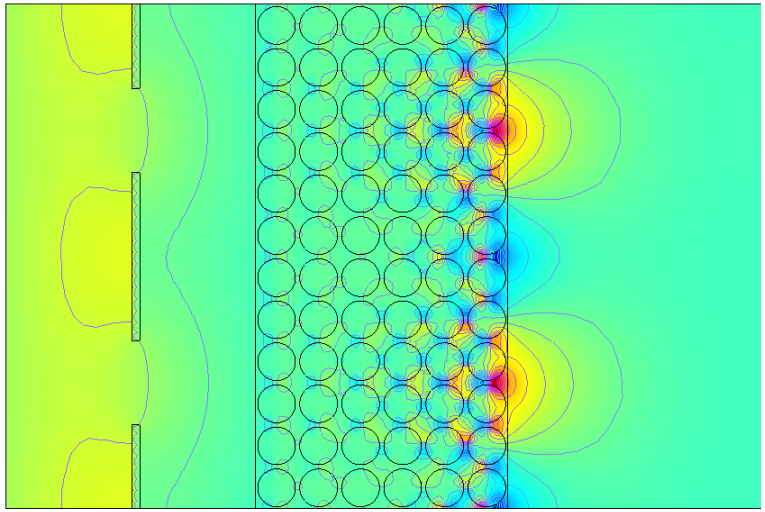

$\omega/\omega_p=0.5988$

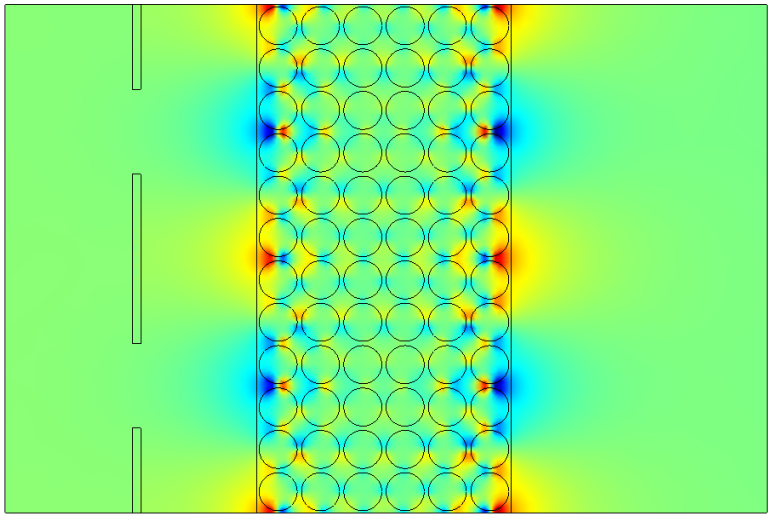

$\omega/\omega_p=0.599$

An SPC slab was successfully used to image two slits at a sub-wavelength distance (0.4λ); yet, this behavior was very narrowband (~0.01% bandwidth).

G.Shvets, Y. Urzhumov, "Engineering the Electromagnetic Properties of Periodic Nanostructures Using Electrostatic Resonances", PRL **93,**243902 (2004)

FDTD analysis of Plasmonic Metamaterials

- The use of a cartesian mesh induces dispersion errors that become significant when plasmonic resonances are considered.

- Example: Electric field in a silver sphere at 385 THz.

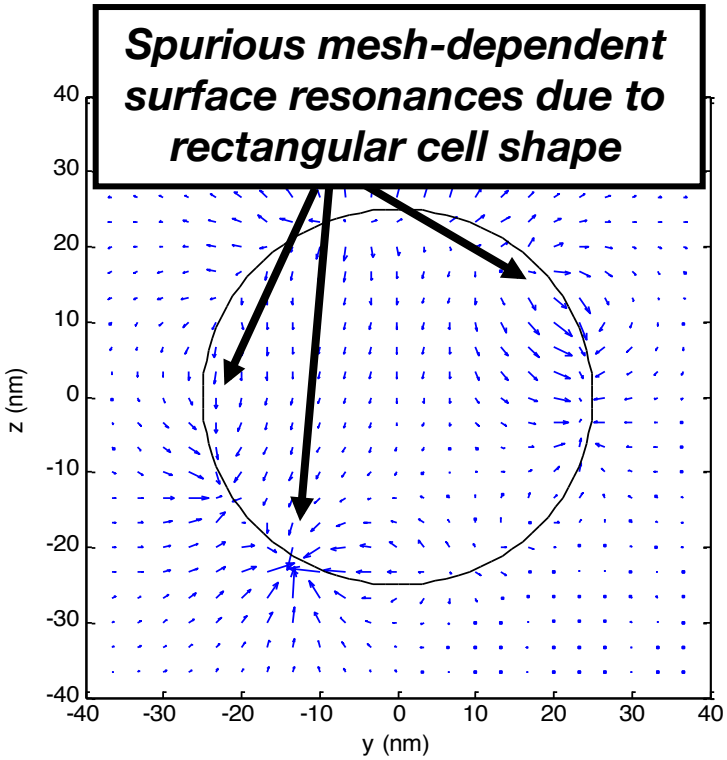

Triangular Mesh FDTD

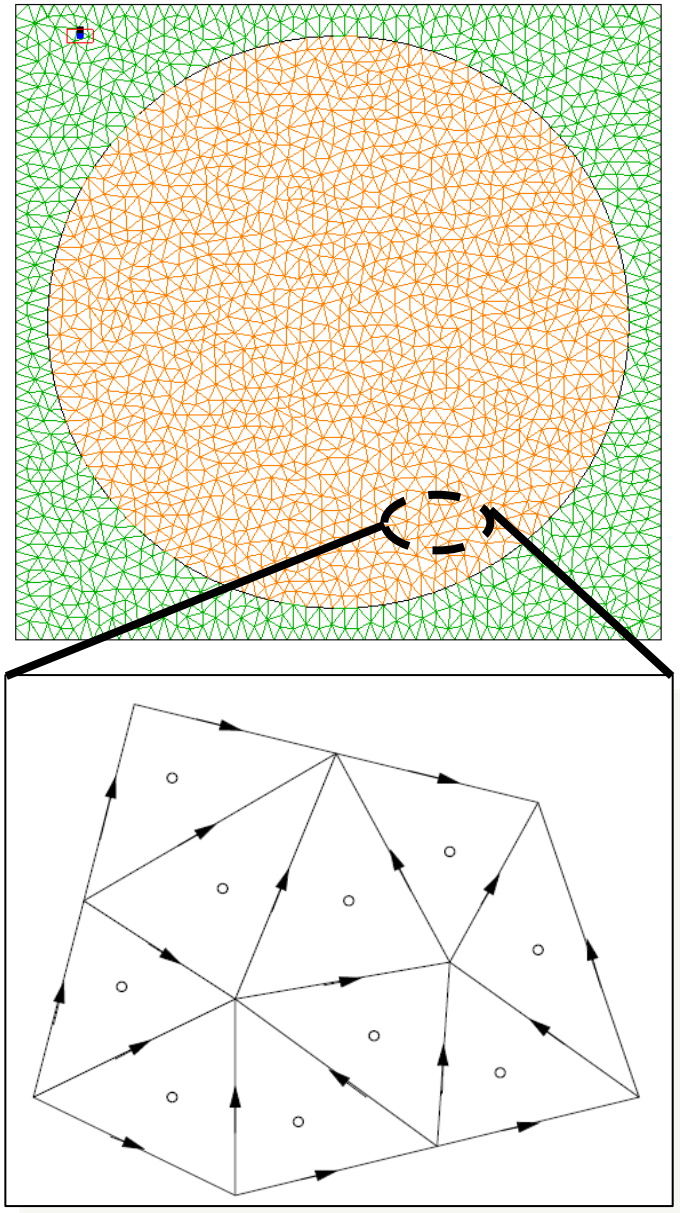

- The computational domain is meshed in triangular elements.
- Tangential electric field components are sampled at edge centers.
- Magnetic field components are sampled at the barycenter of each triangle.

1. C.F. Lee, B.J. Martin, R.T. Shin, J.A. Kong, “A triangular-grid FDTD method for electromagnetic scattering problems”, J. Electromagnetic Waves and Appl., vol. 8, no. 4, 449-470, 1994.
2. S.D. Gedney, F. S. Lansing, D. L. Rascoe, “Full wave Analysis of Microwave/Monolithic
Circuit Devices Using a Generalized Yee-Algorithm Based on an Unstructured Grid”,
IEEE Trans. MTT, vol. 44, no.8, Aug. 1996.

Triangular Mesh FDTD: Update Equations

Magnetic Field Components

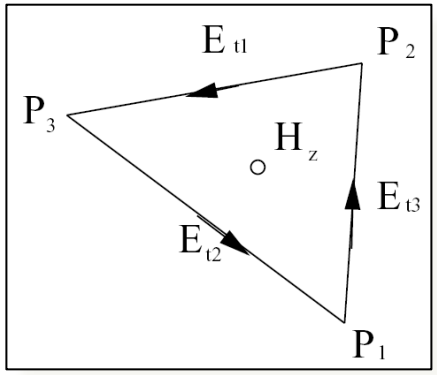

$$\frac{d}{dt}\int_{\Delta}\mu\overline{H}\cdot d\overline{s}=\oint_{\Delta}\overline{E}\cdot d\overline{l}$$

$$\mu\frac{H_z^{n+1}-H_z^n}{\Delta t}A=E_{t1}|\overline{P_2P_3}|+E_{t2}|\overline{P_3P_1}|+E_{t3}|\overline{P_1P_2}|$$

Electric Field Components

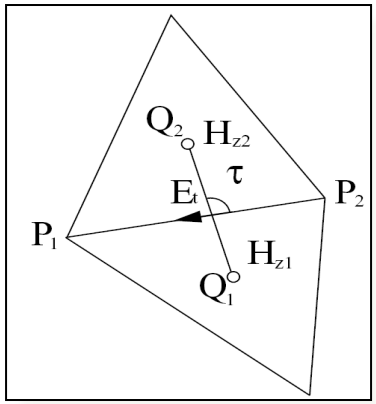

$$\frac{d}{dt}\int_{S}\epsilon\overline{E}\cdot d\overline{s}=\oint_{S}\overline{H}\cdot d\overline{l}$$

$$\epsilon\frac{E_t^{n+1}-E_t^n}{\Delta t}|\overline{Q_1Q_2}|\sin\tau=H_{z1}-H_{z2}$$

Triangular Mesh FDTD: PBCs

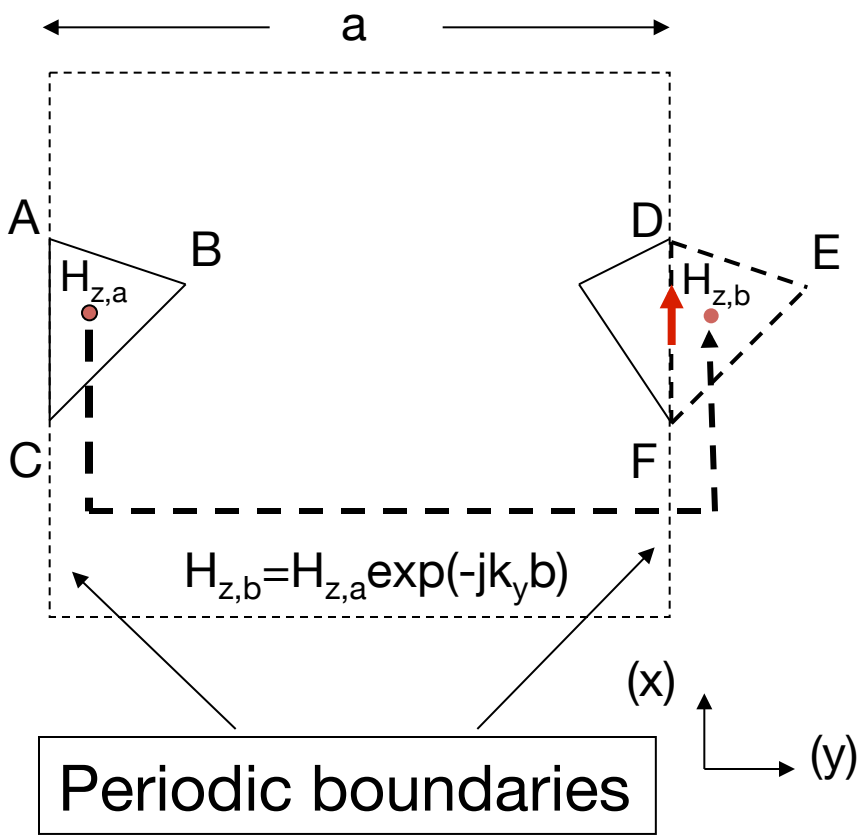

- The periodic boundaries are discretized in the same way (e.g. triangle ABC is identical to DEF).
- Periodic boundary conditions (PBCs) are implemented with the sine-cosine method.
- Boundary electric fields are updated after PBC updates.

Periodic FDTD analysis of 2-D SPC

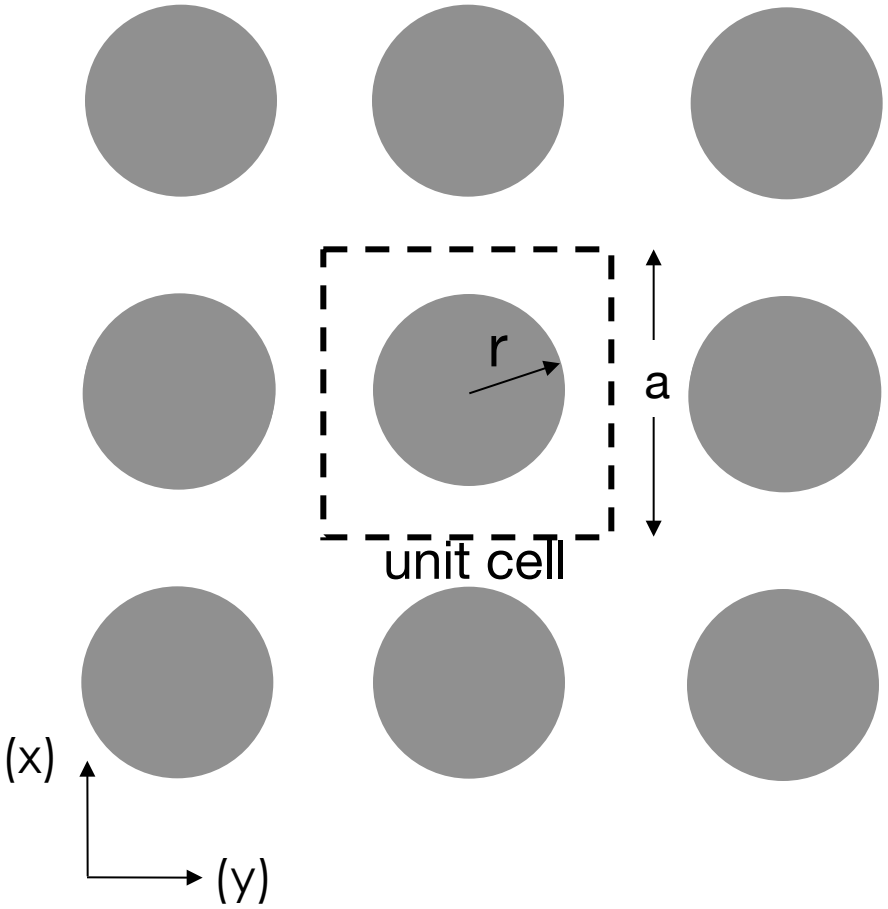

- Infinite rectangular array of plasmonic rods.
- $r/a=0.45$, $a=c/\omega_p$
- $\varepsilon(\omega)=1-(\omega_p/\omega)^2$
- Surrounding medium is air
- TE case (Hz, Ex, Ey) is considered.

For each wavevector in the Brillouin zone, field resonances indicate the corresponding mode frequencies.

2-D SPC Resonant Frequencies (0-0.4 PHz)

Rectangular FDTD Mesh

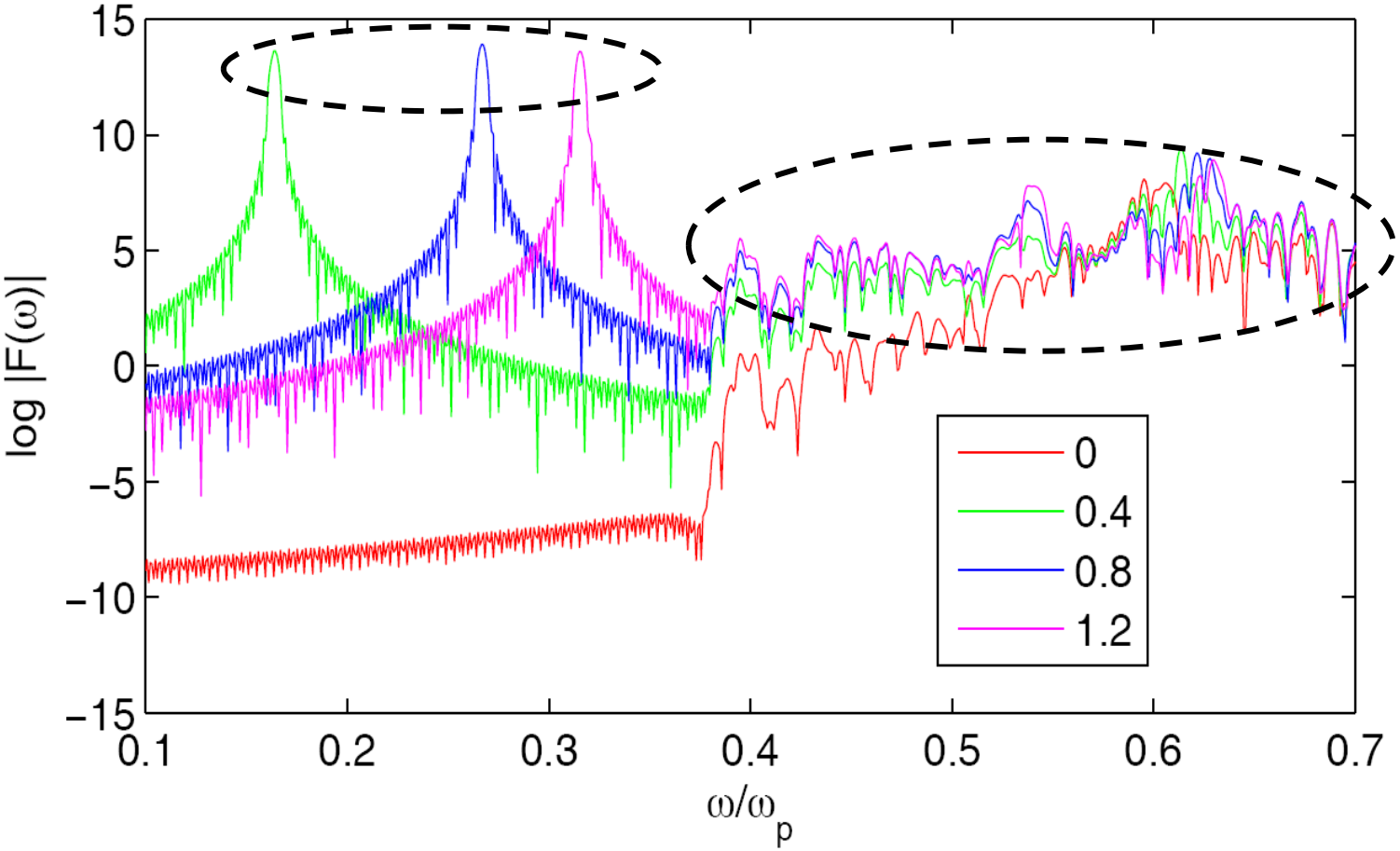

Poor convergence of higher order mode frequencies,
Lower order mode resonances clearly determined
despite mesh refinement

2-D SPC Resonant Frequencies (0-0.4 PHz)

Triangular FDTD Mesh

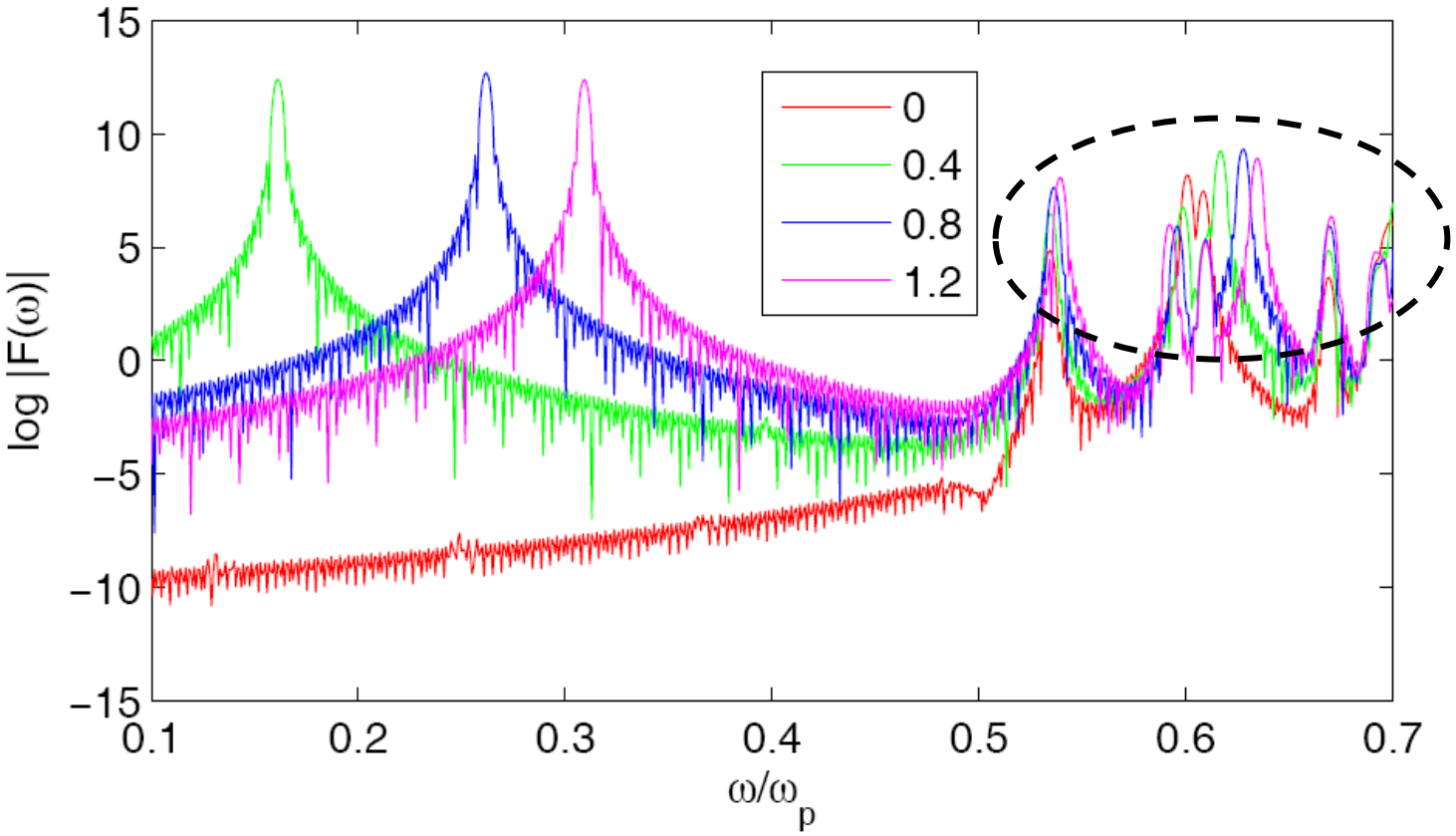

Dramatically improved convergence for higher order mode frequencies; even coarse mesh FDTD is reasonably accurate

triangle size ~ a/200

Modal Field Patterns

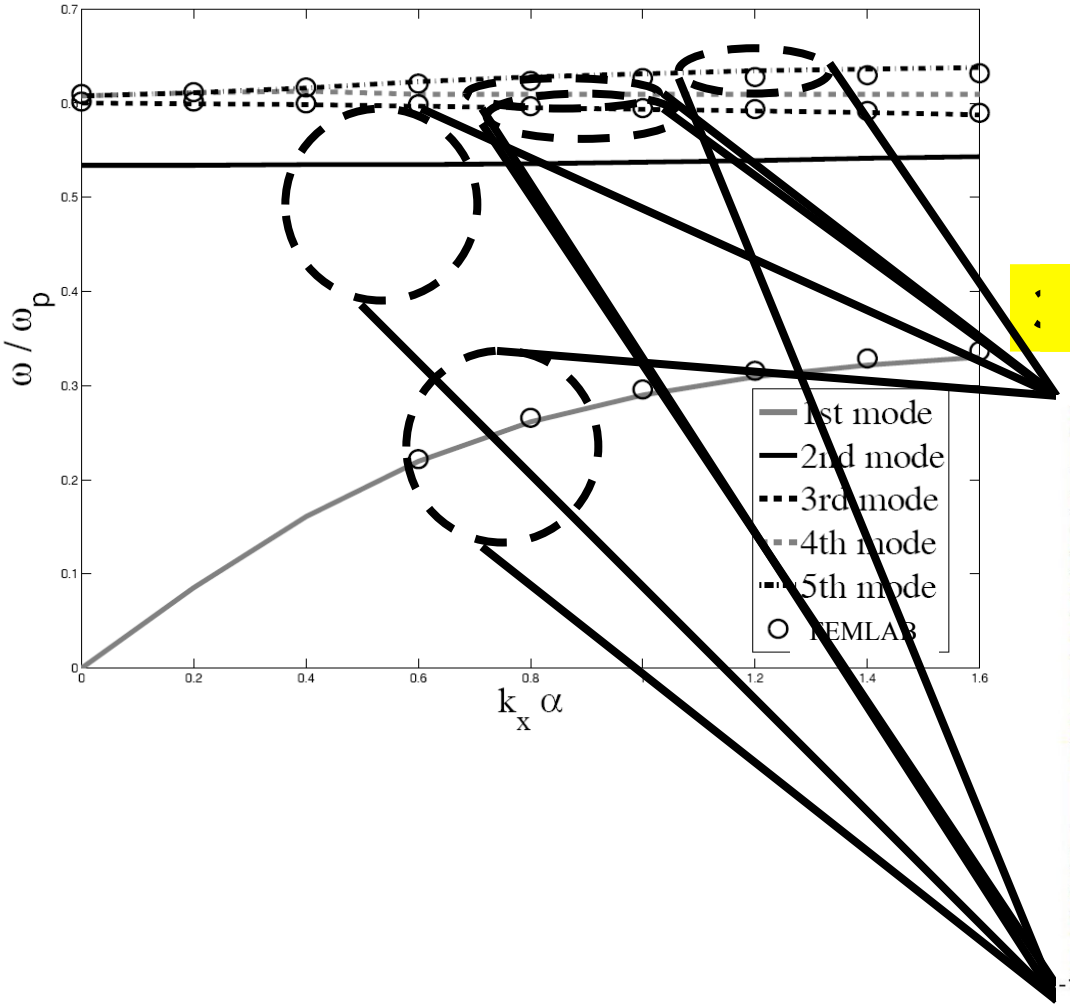

: 5th band: forward wave

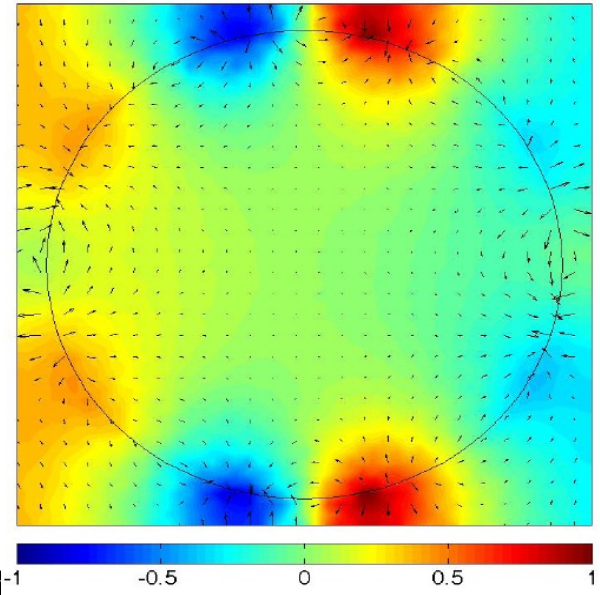

Brillouin Diagram (Γ−X) for the 2D-SPC lattice

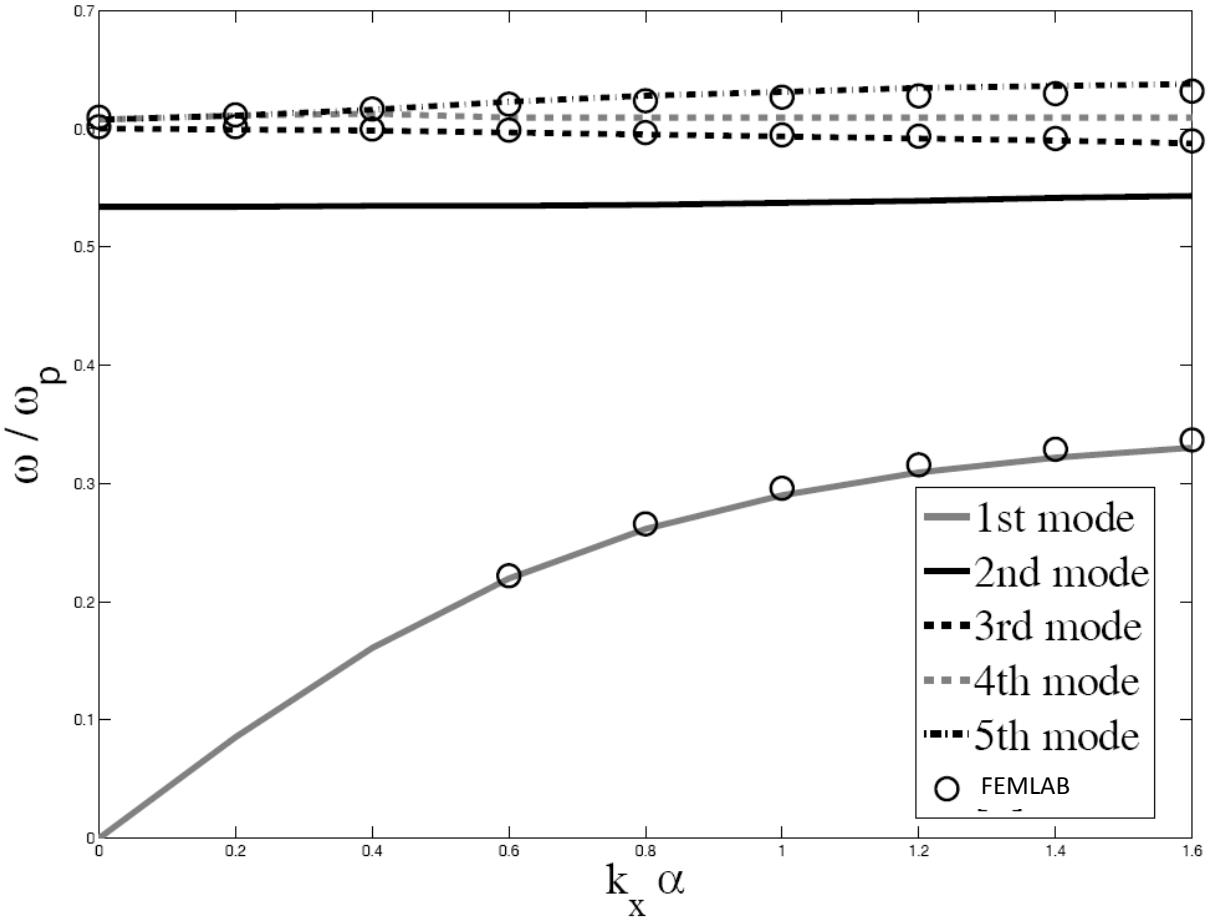

•This rich band structure explains the very narrowband behavior of the SPC lattice as a “perfect lens”.

Full Brillouin Diagram of the 2D-SPC lattice

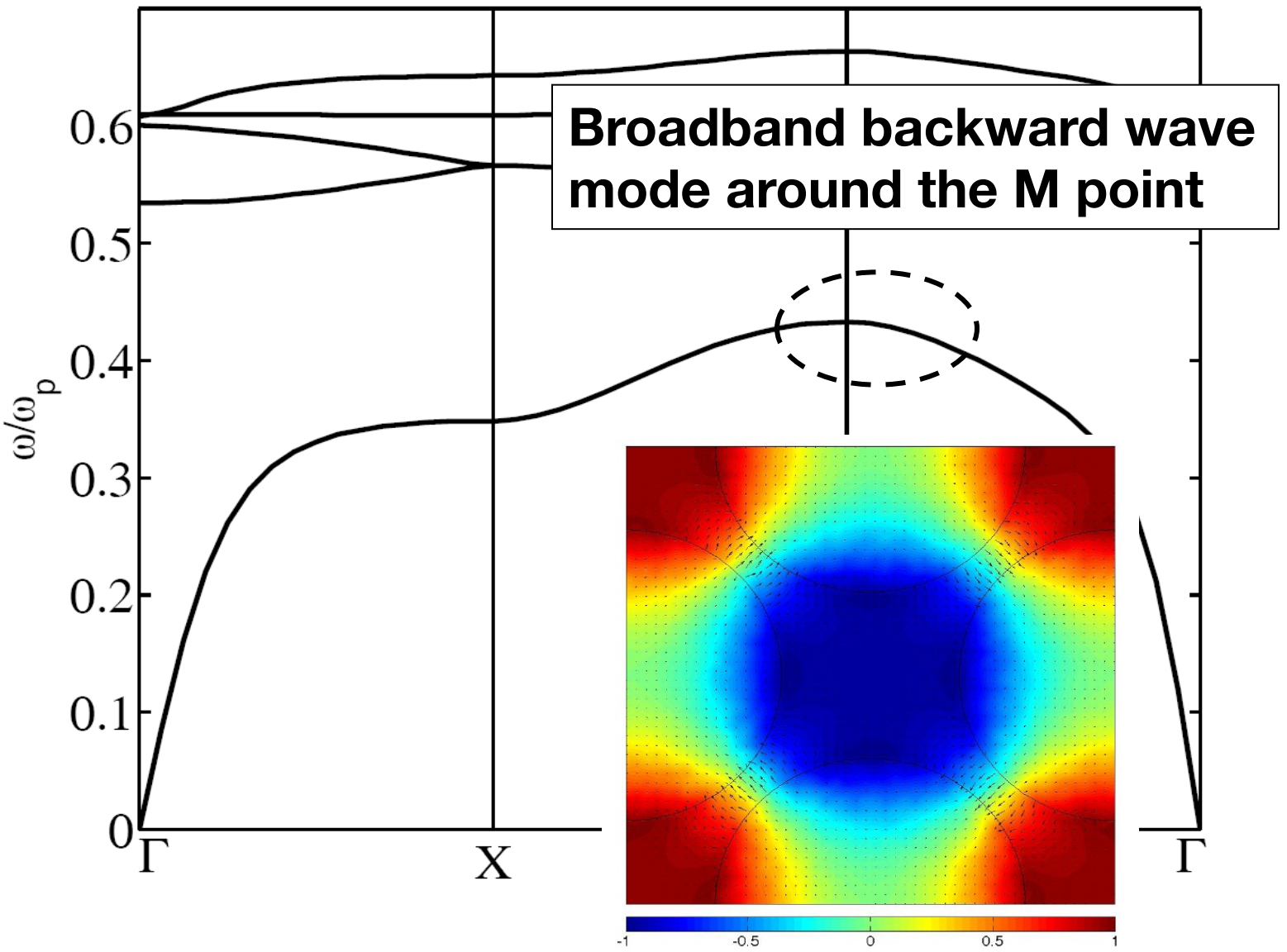

Super-directive Plasmonic Slot Antenna Array

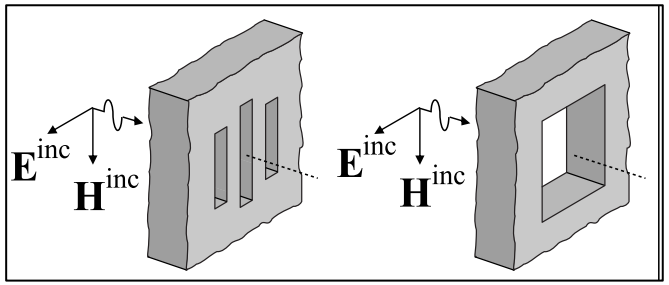

- Goal: Use a combination of three slots on a silver slab to achieve antenna directivity that surpasses that of a single slot occupying the same area.

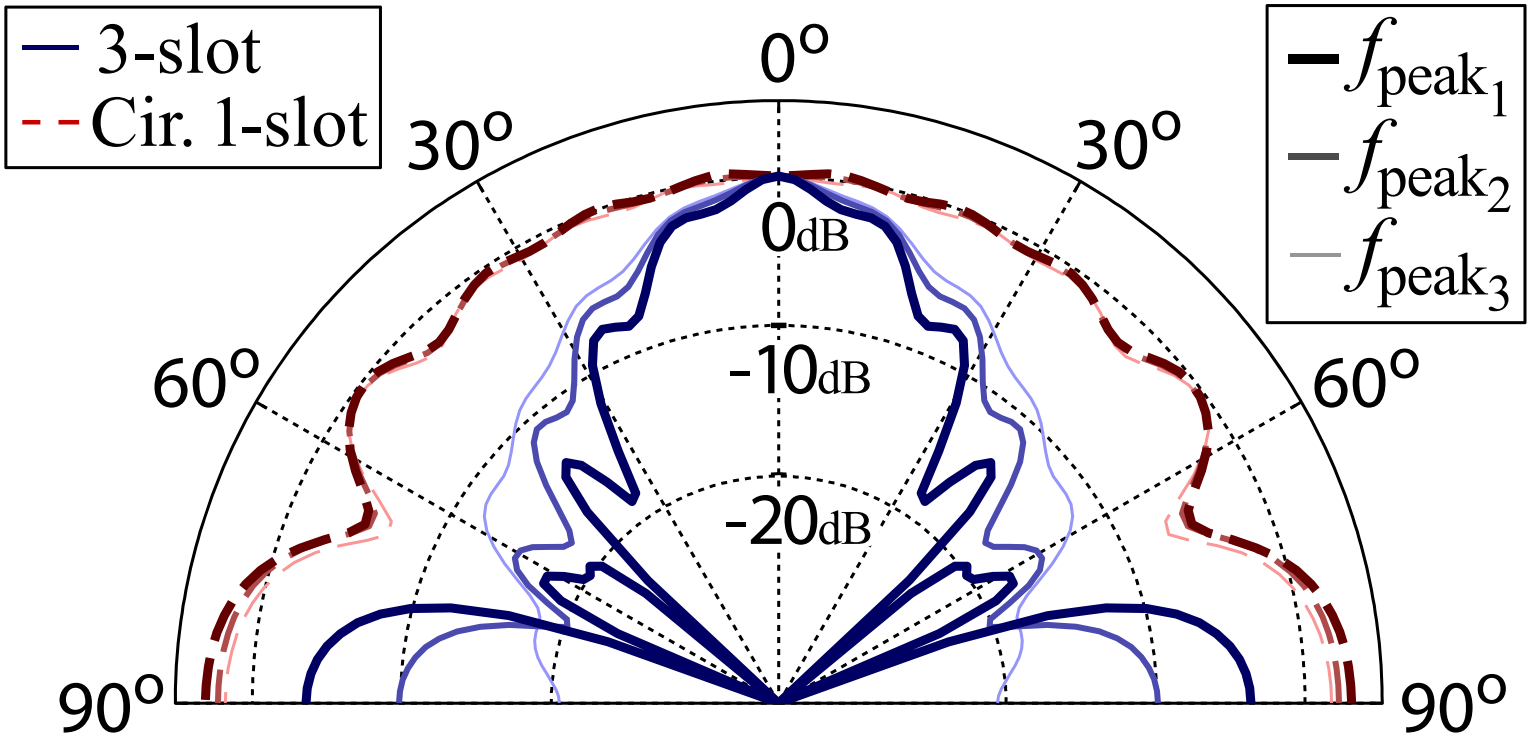

A. Ludwig, C.D. Sarris, G.V. Eleftheriades, "Metascreen-Based Superdirective Antenna in the Optical Frequency Regime", PRL, Nov. 2012.

Super-directive Plasmonic Slot Antenna Array

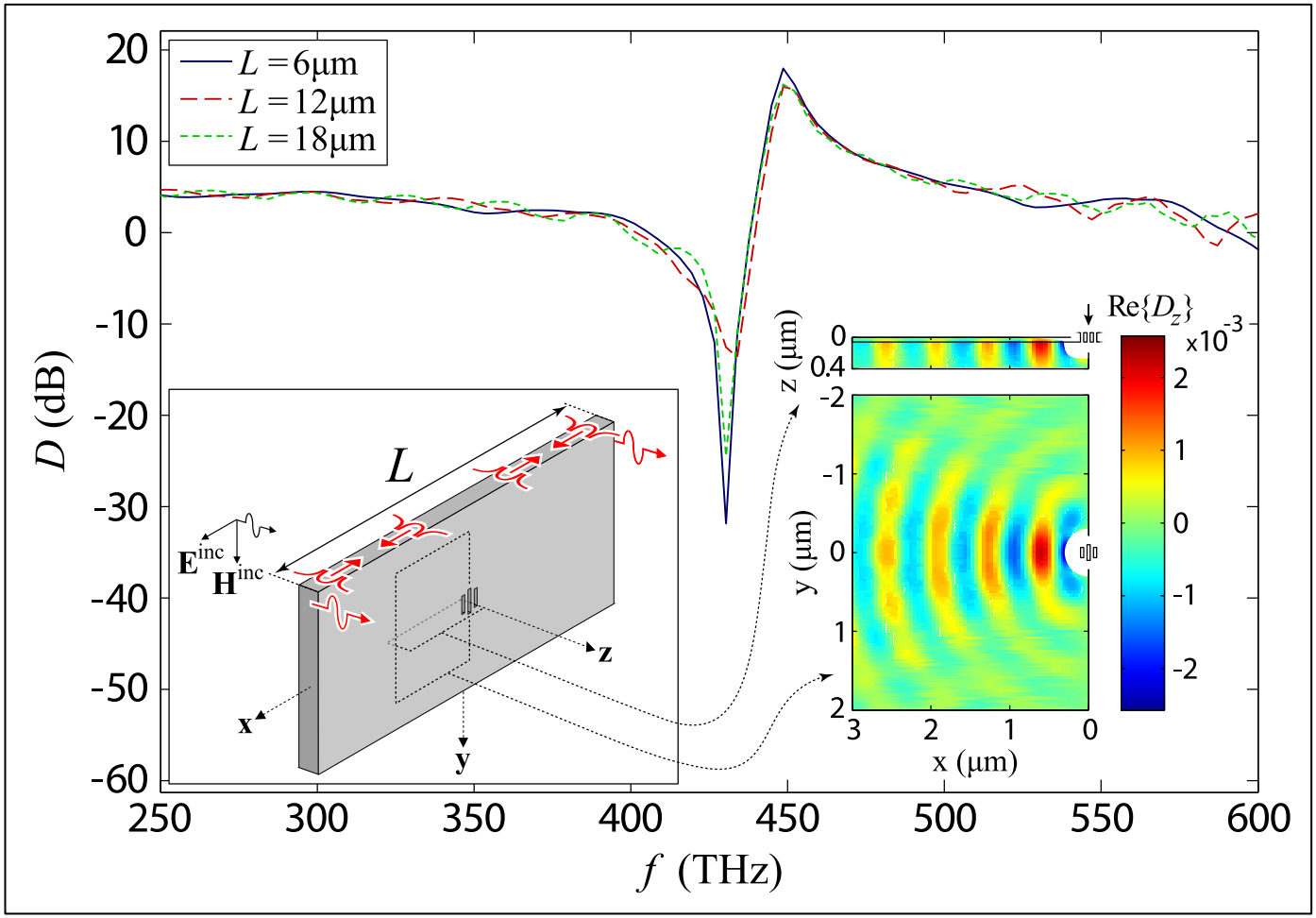

- Multiscale problem
- Strong lateral waves impinging on the PML right at the frequency of superdirectivity.

Modeling of Driven Periodic Structures

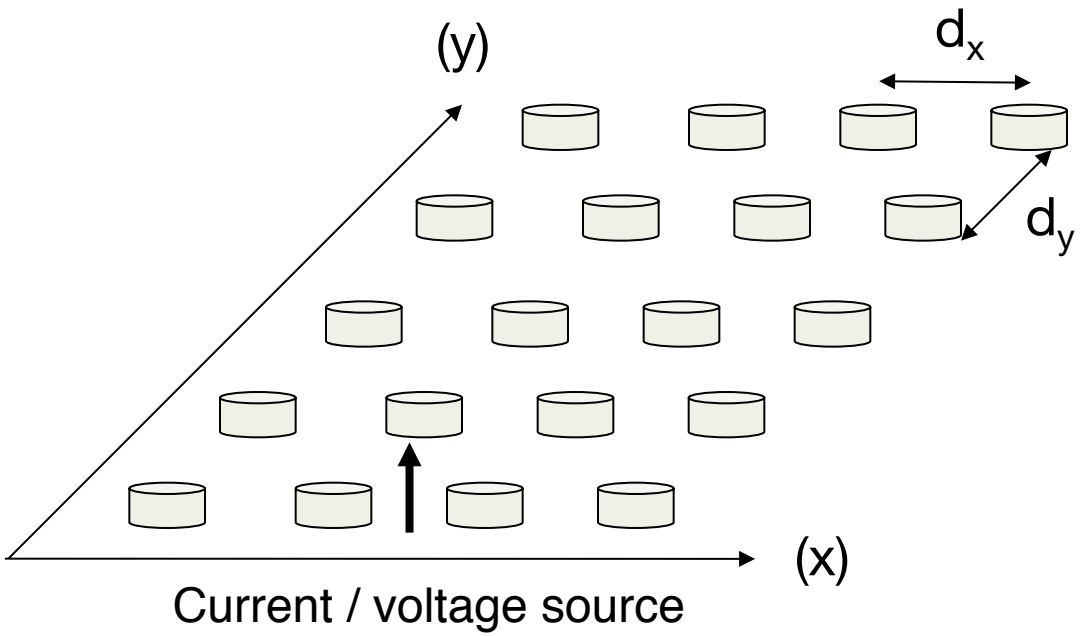

- Objective
  - Obtain driven periodic structure response using periodic FDTD analysis

Modeling of Driven Periodic Structures

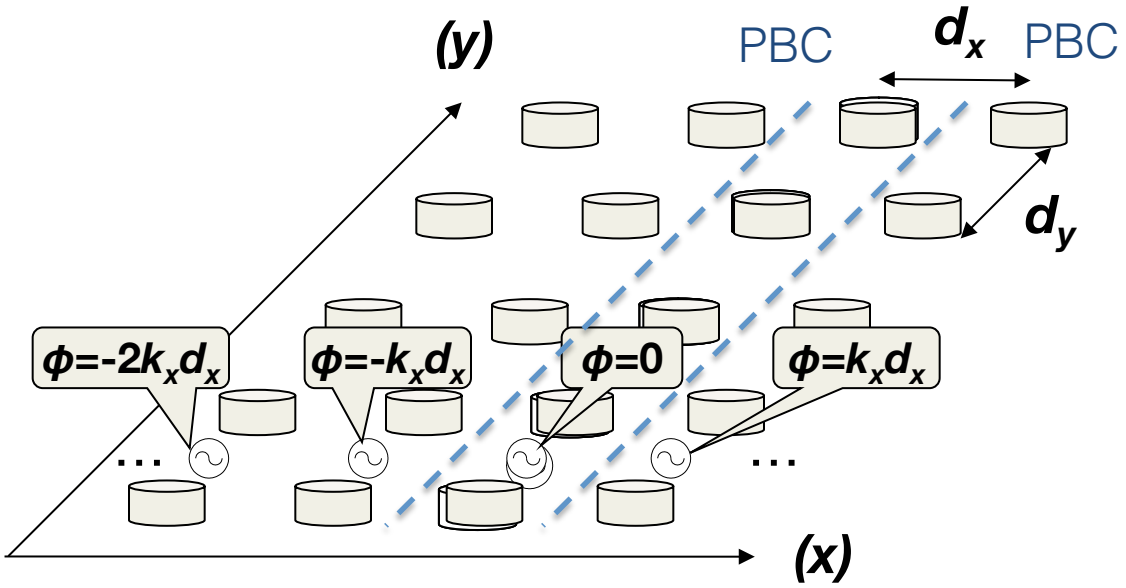

- Problem: Periodic boundary conditions implicitly convert the source to an array of sources.

- Solution: The **Array Scanning method** [Munk and Burrell, *IEEE T-AP*, 1979] isolates the effect of the original source.

Periodic FDTD with Array Scanning (1)

- Example: 1-D periodic Structure along x-axis, with periodicity d_x

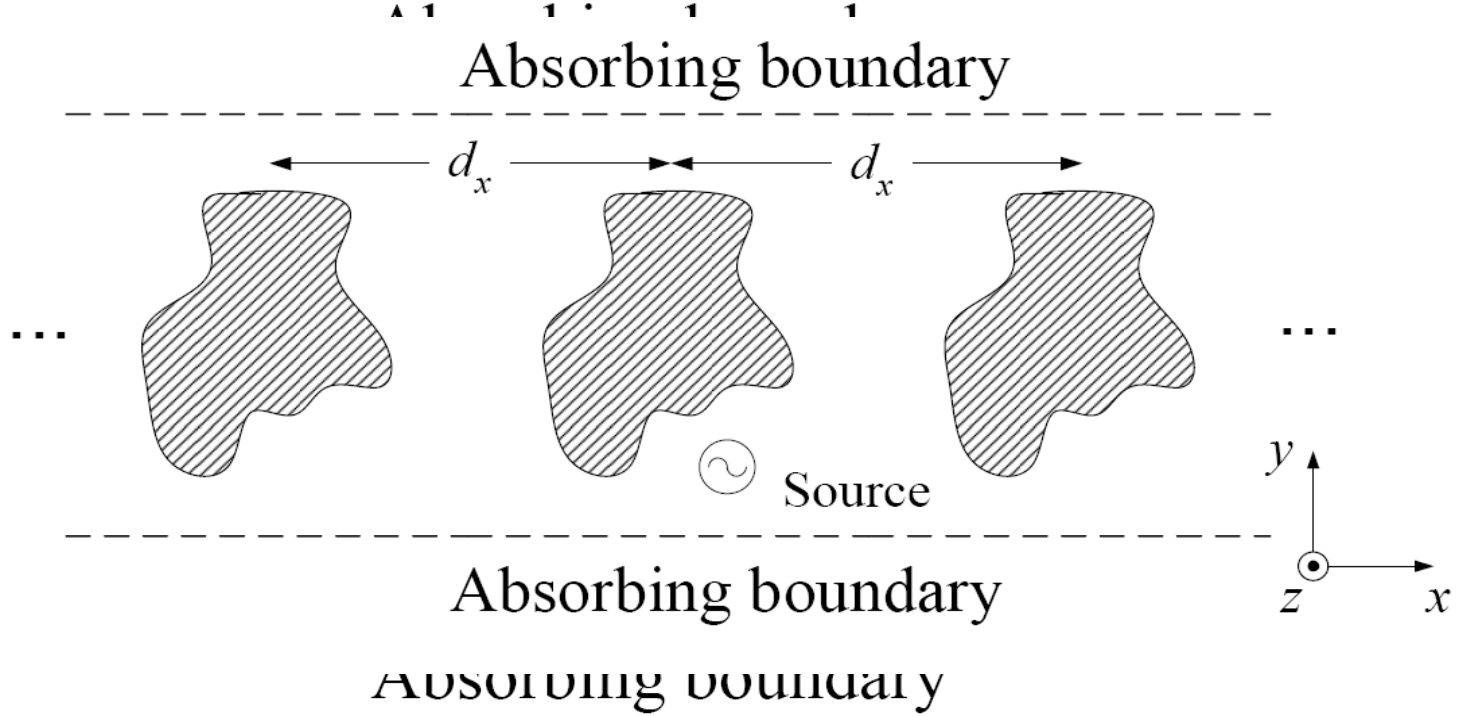

Computational domain for sine-cosine method, applied for N wave-numbers $-\pi/d_x < k_x < \pi/d_x$

Periodic FDTD with Array Scanning (2)

- Let $\bar{E}_{array}(\bar{r}_0, k_x, t)$ be the electric field determined by the sine-cosine method at $\bar{r}_0$ inside the unit cell for a certain k_x. Enforced via PBCs.

- Then, the field excited by the source in the infinite structure is:

$$\bar{E}(\bar{r}_0, t) = \frac{d_x}{2\pi} \int_{-\pi/d_x}^{\pi/d_x} \bar{E}_{array}(\bar{r}_0, k_x, t)\, dk_x$$

$$\approx \frac{1}{N} \sum_{n=-\frac{N}{2}}^{n=\frac{N}{2}} \bar{E}_{array}\left(\bar{r}_0, \frac{2\pi n}{N d_x}, t\right)$$

N=10-20 points typically needed for convergence

Periodic FDTD with Array Scanning : Results

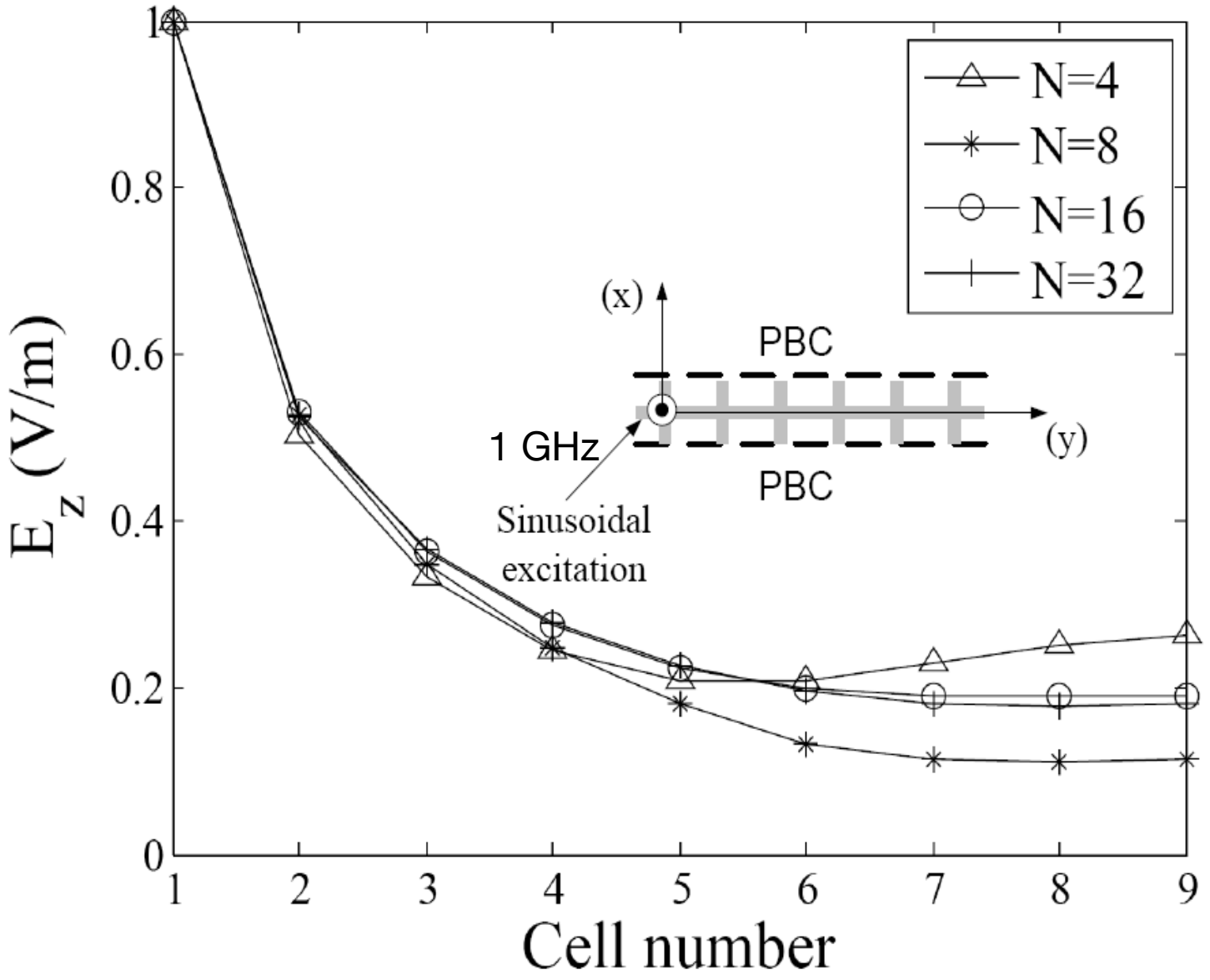

Periodic FDTD with Array Scanning : Results

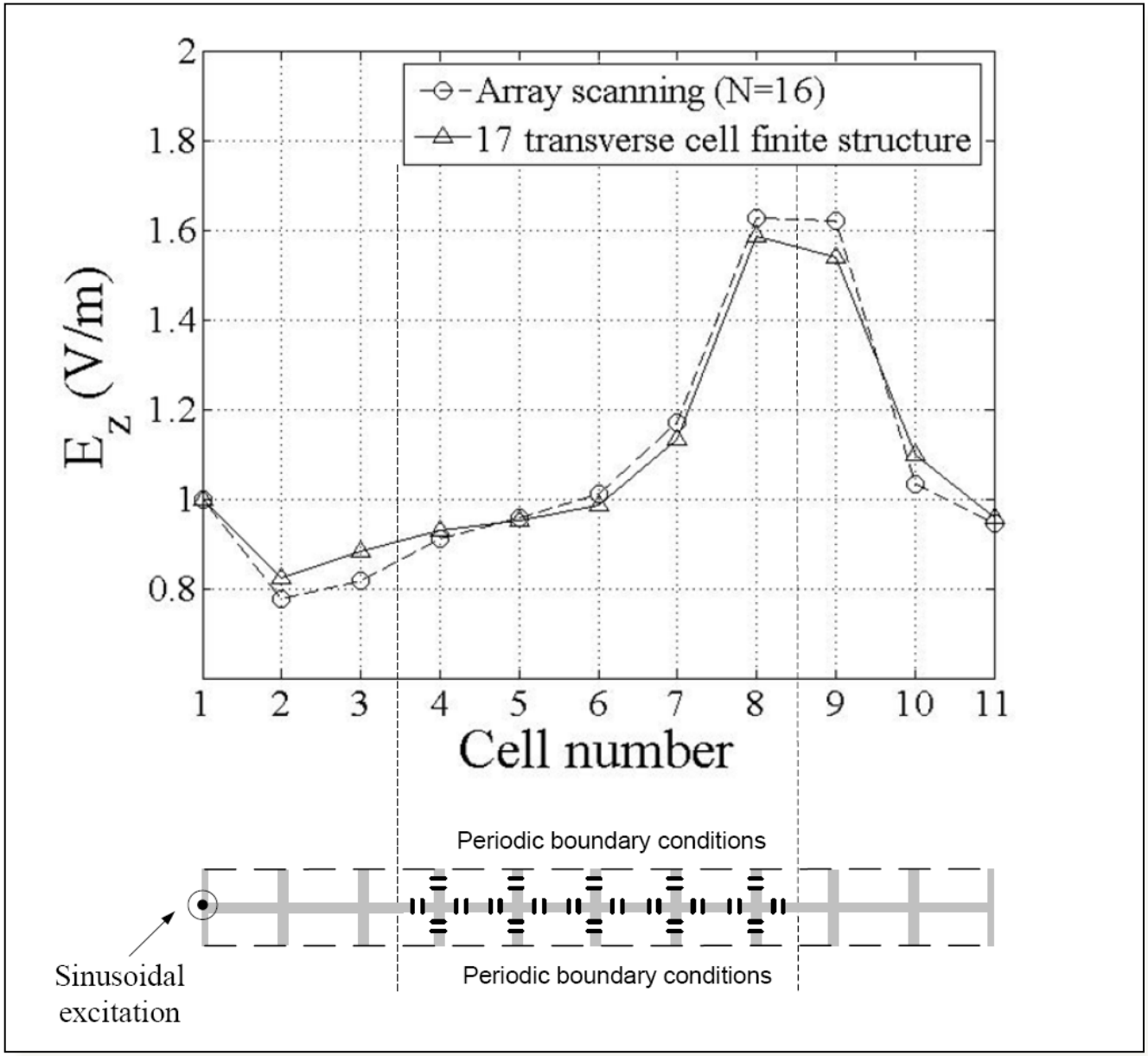

Periodic FDTD with Array Scanning : Results

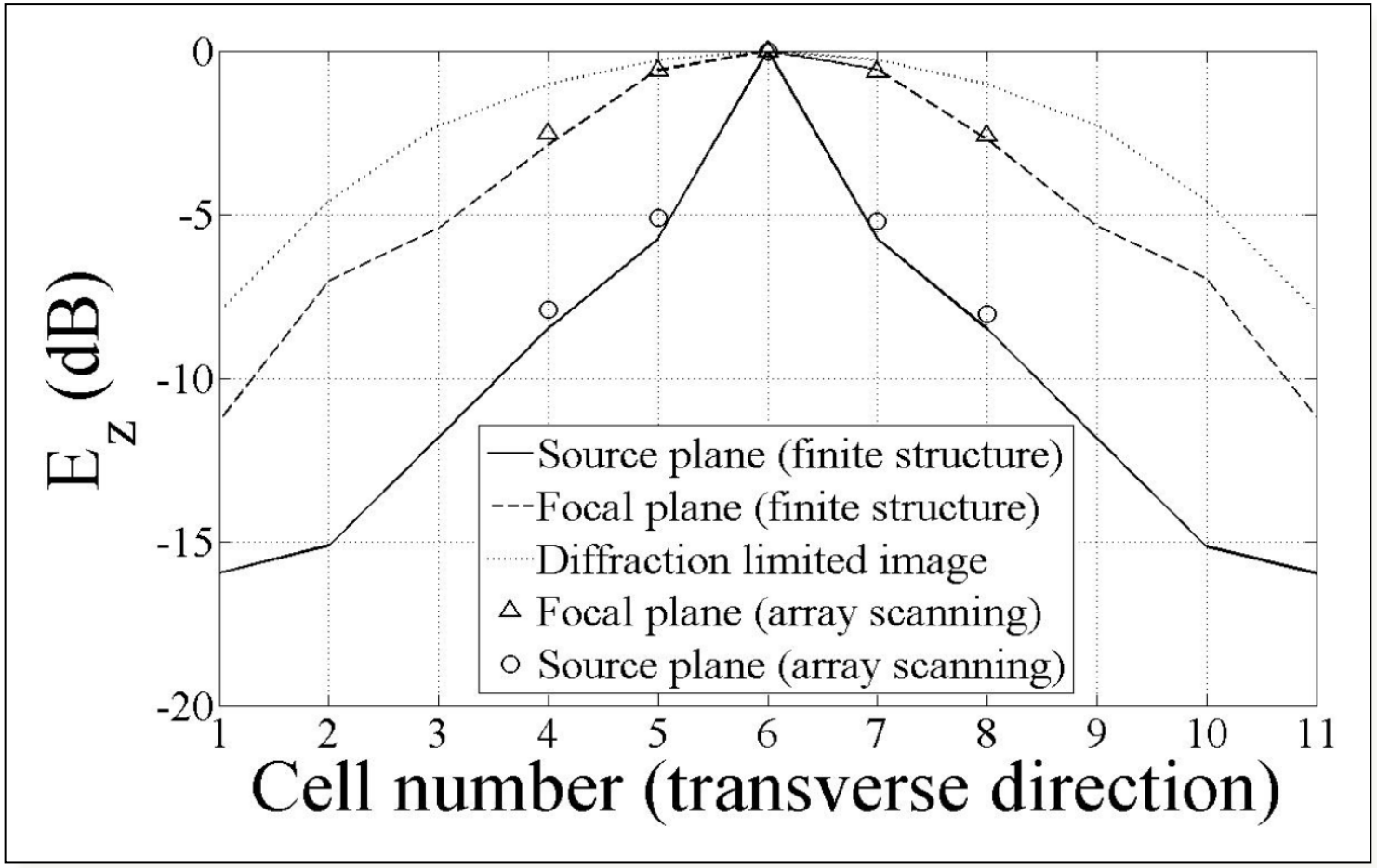

Finite structure simulation time: 20,513 sec
Array-scanning FDTD with PBCs: 2,454 sec

Non-periodic structures on periodic substrates

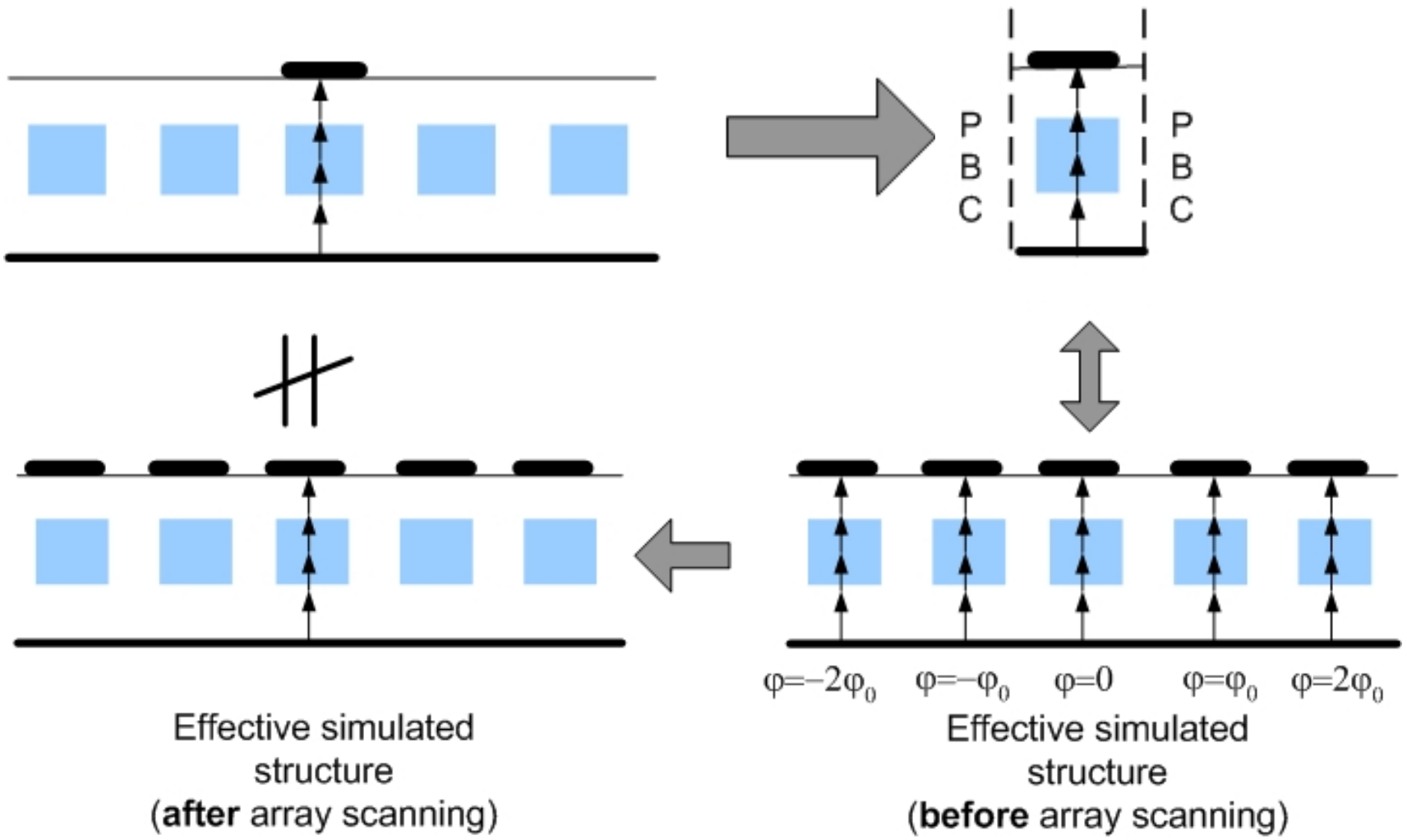

Non-periodic structures on periodic substrates

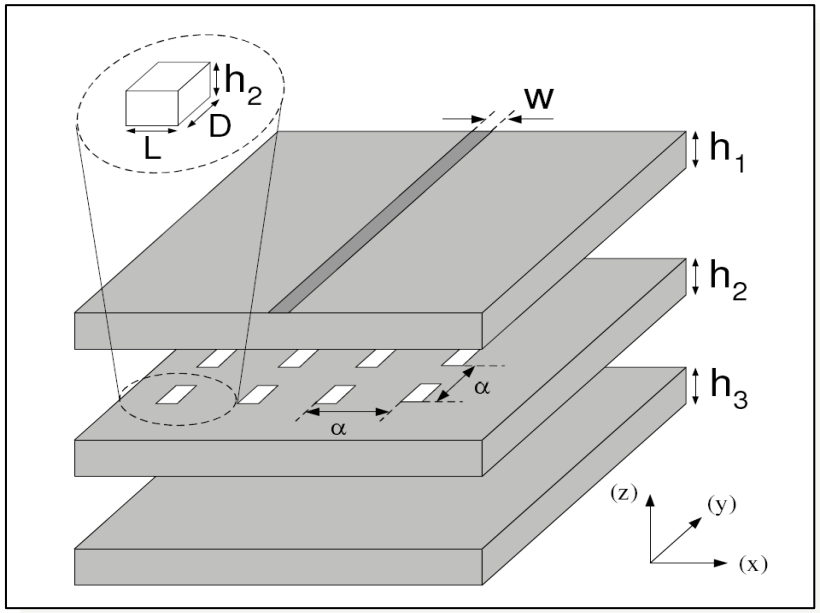

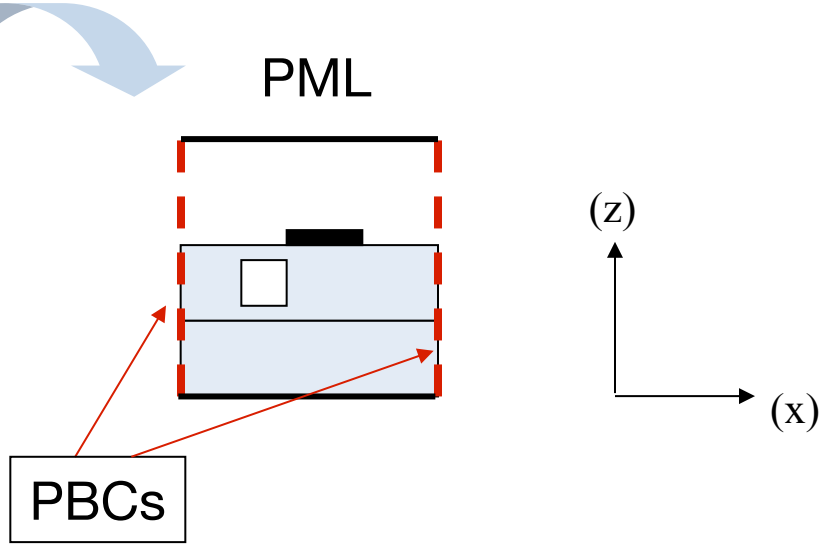

$h_1 = h_2 = h_3 = 0.635\,\text{mm}$, $w = 3\,\text{mm}$, $\alpha = 14\,\text{mm}$

$\varepsilon_{r,1} = \varepsilon_{r,3} = 9.8;\ \varepsilon_{r,2} = 3.2$

$L = D = 6.5\,\text{mm}$

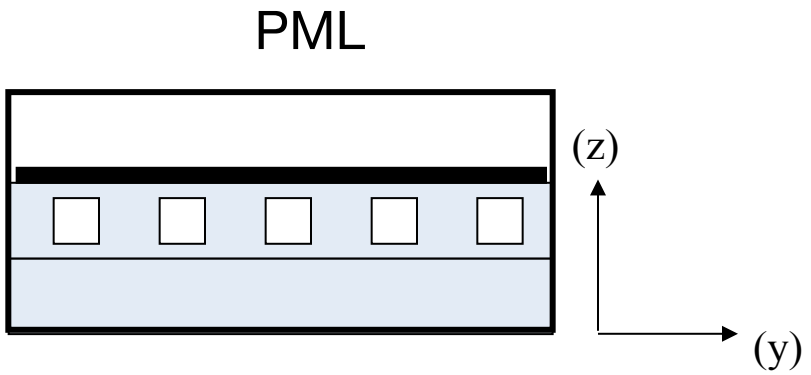

*H.-Y. D. Yang, "Theory of microstrip lines on artificial periodic substrates," *IEEE Trans. Microwave Theory Tech.*, vol. 47, no. 5, pp. 629-635, May 1999.

Non-periodic structures on periodic substrates

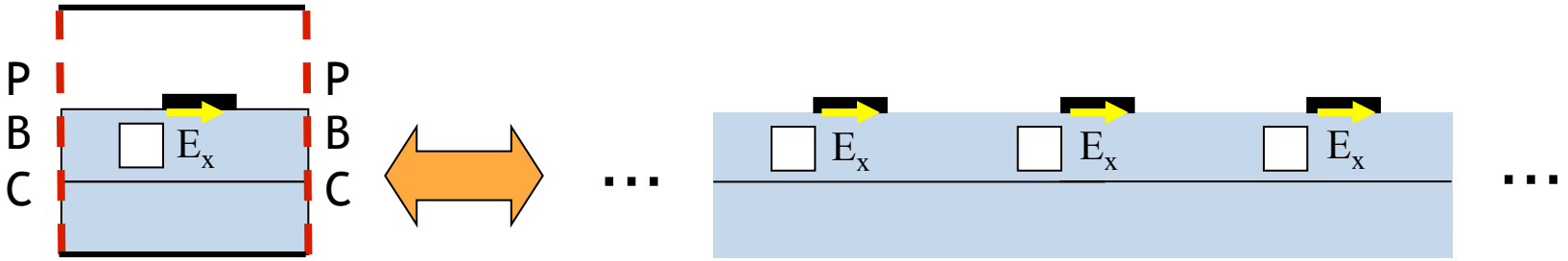

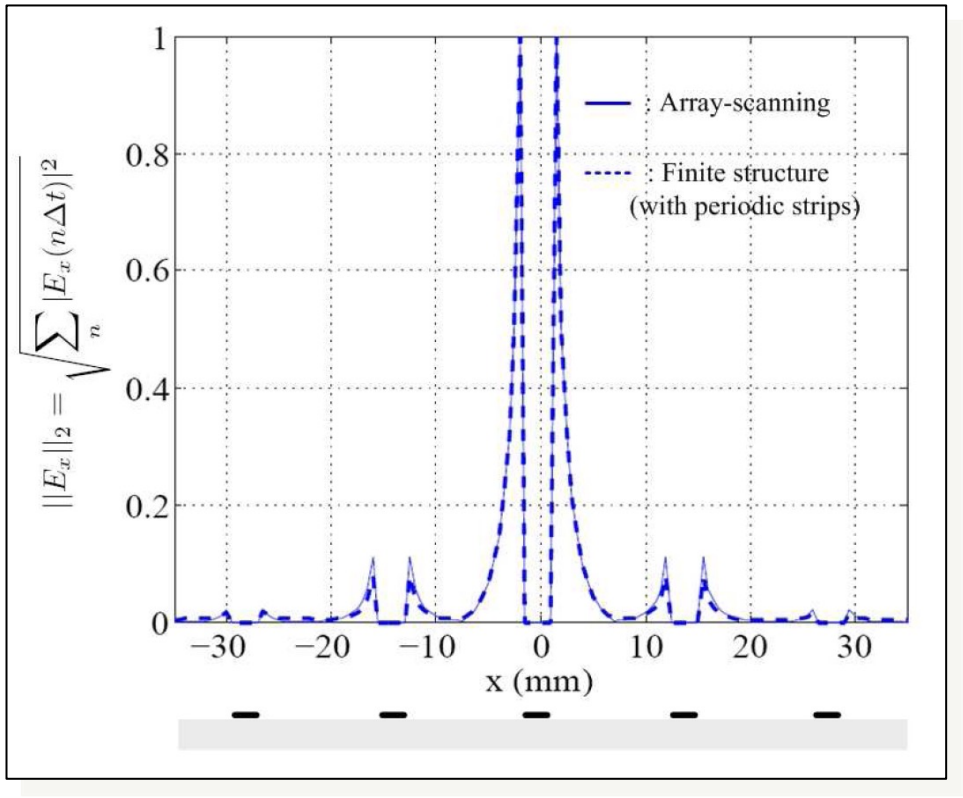

Simulated geometry is equivalent to an array of microstrips

Mixed periodic/absorbing boundaries

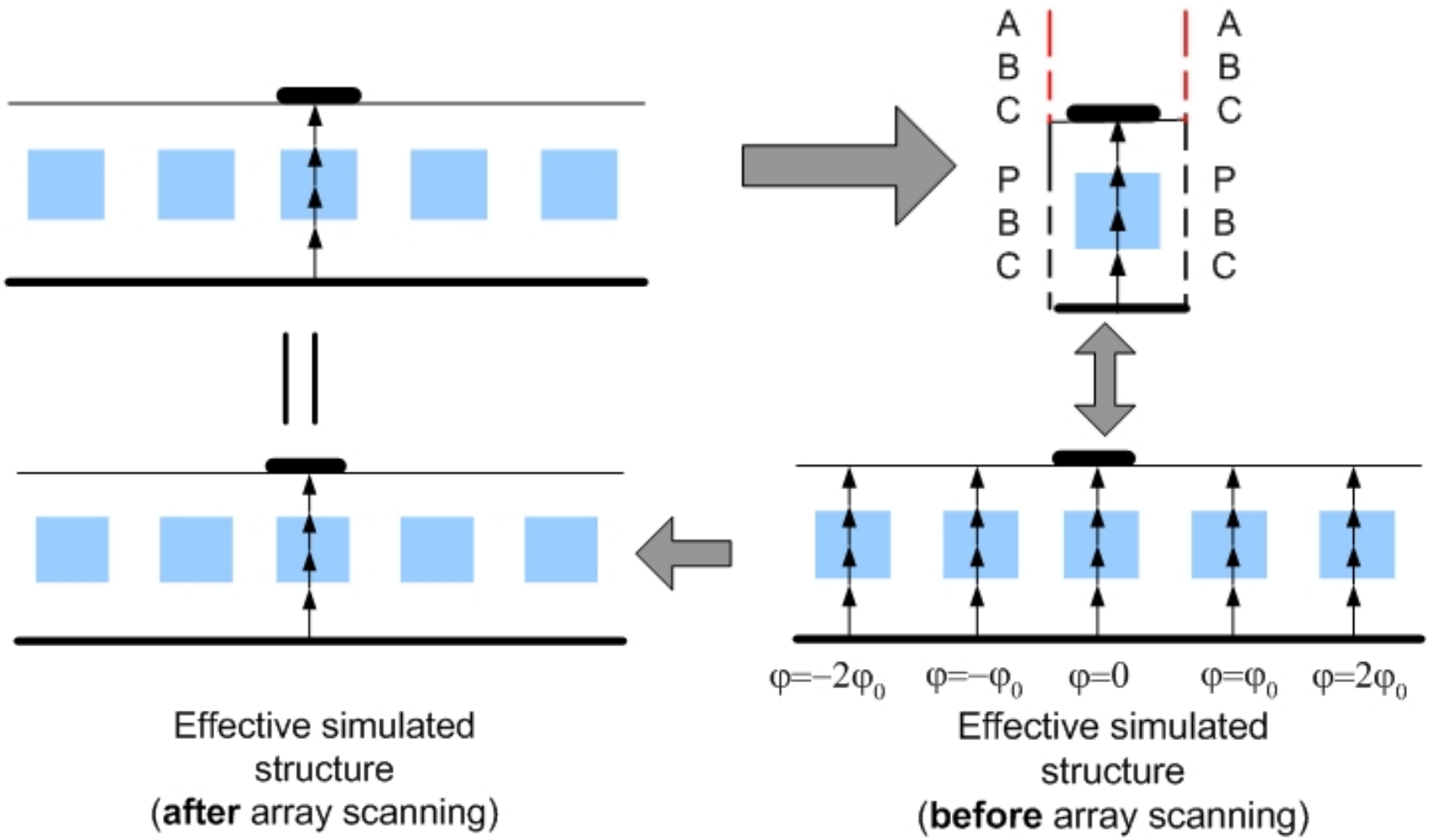

Mixed periodic/absorbing boundaries: Updates

Updates at the PML/PBC interface

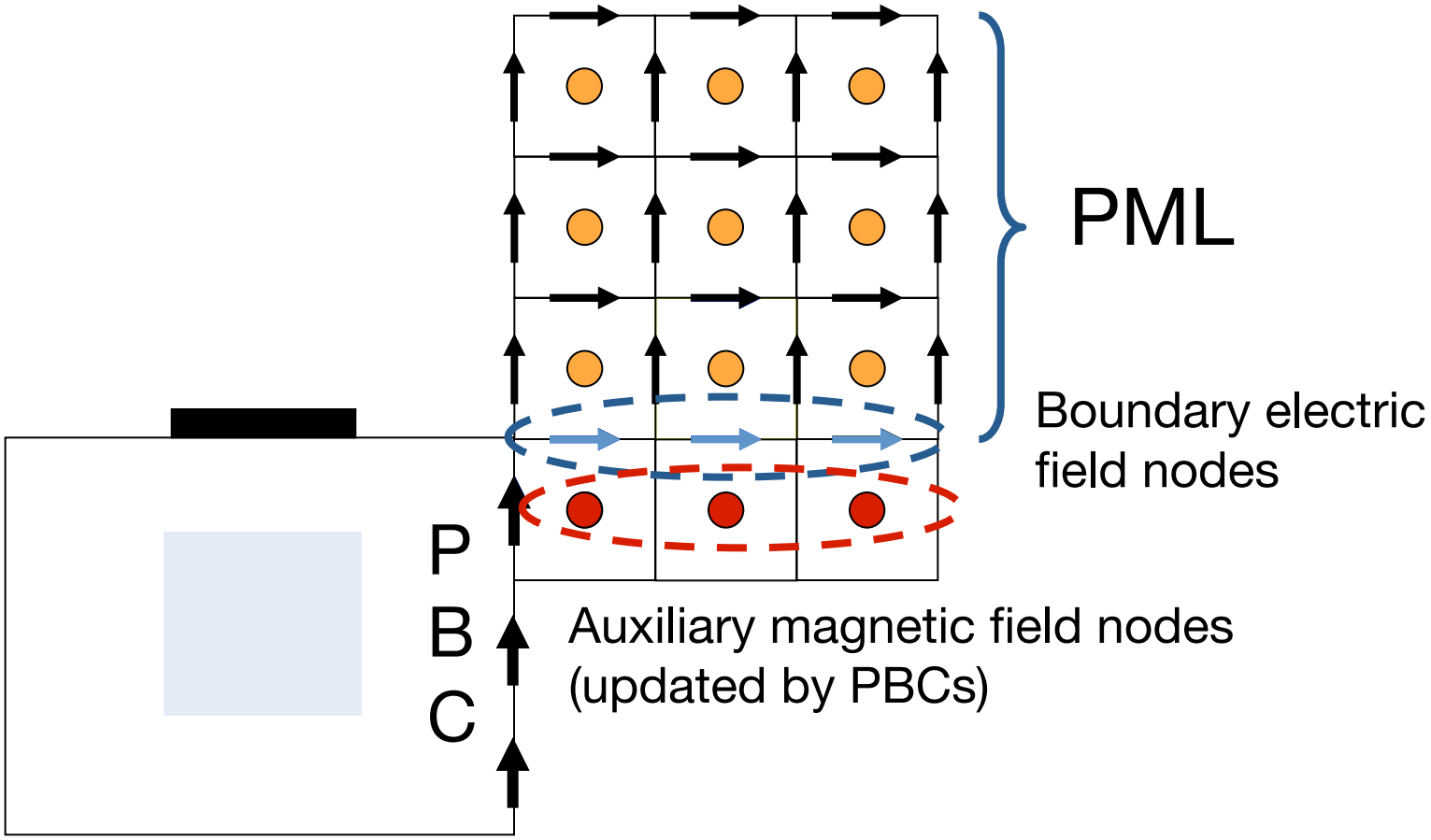

Mixed periodic/absorbing boundaries: Results

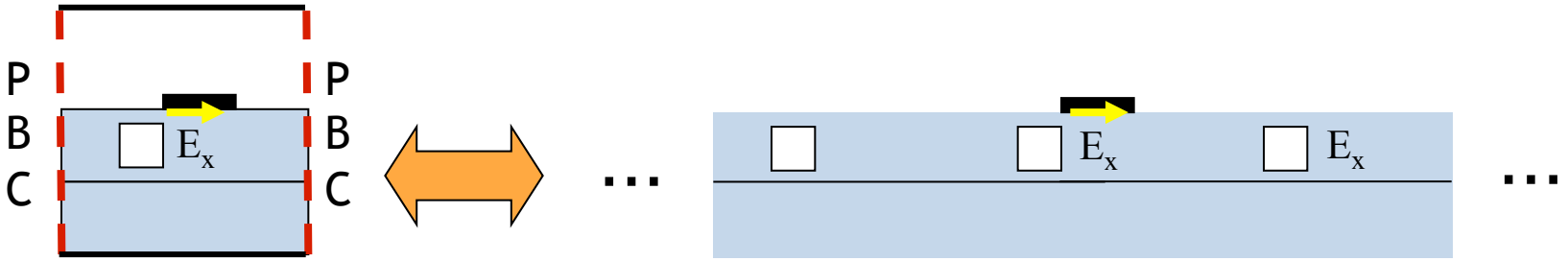

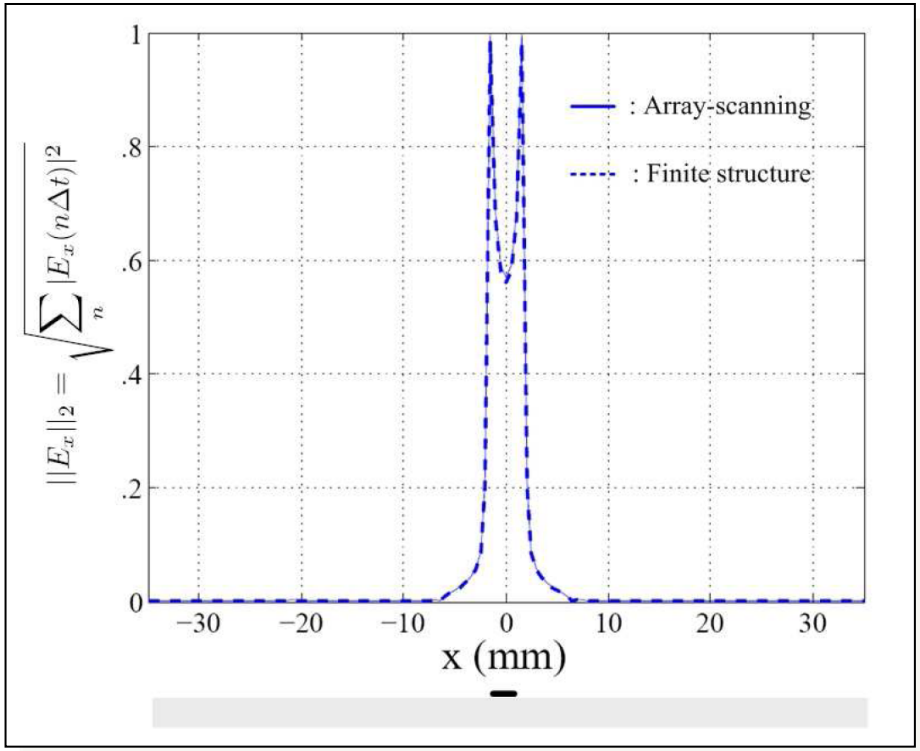

The spurious presence of periodic strips has been eliminated.

Mixed periodic/absorbing boundaries: Results

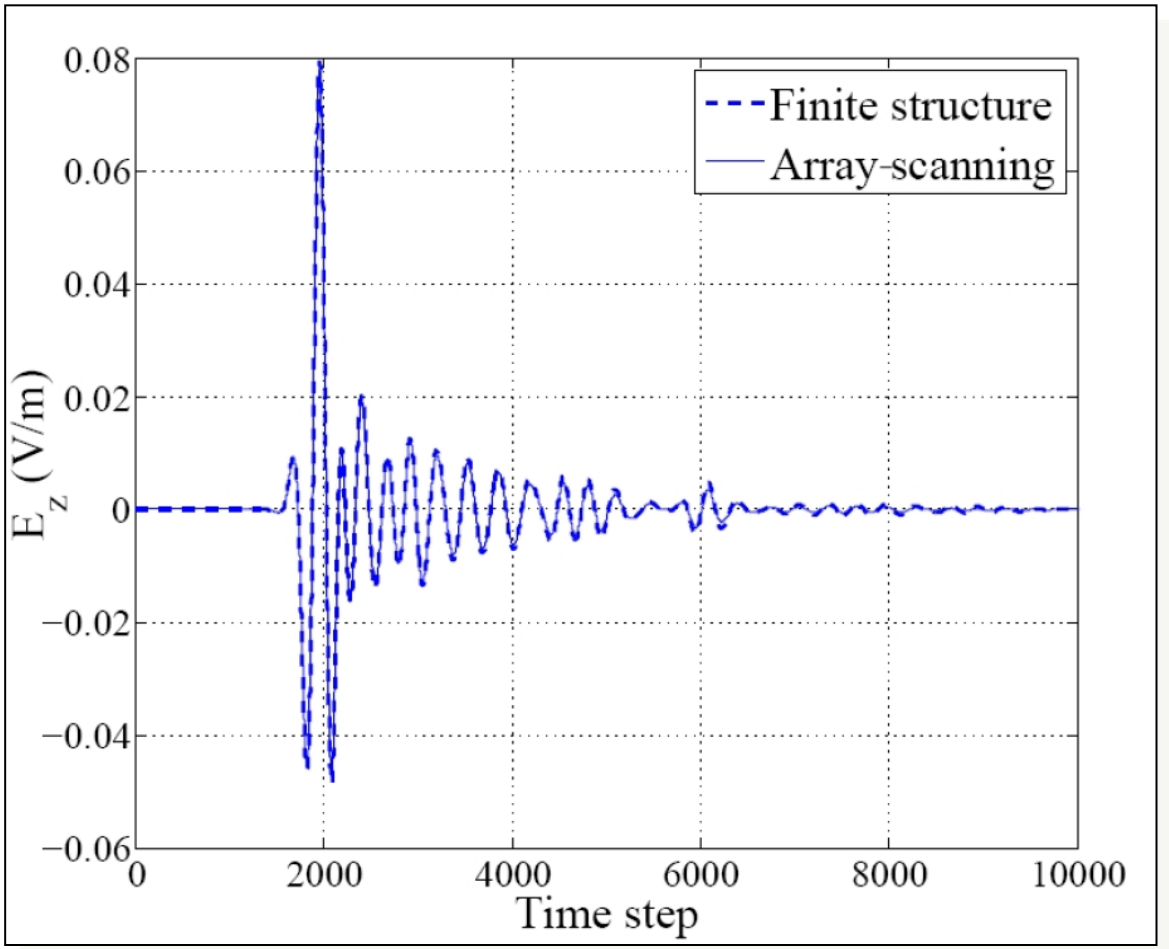

Vertical field component below the microstrip, five cells along the direction of propagation.

Mixed periodic/absorbing boundaries: Results

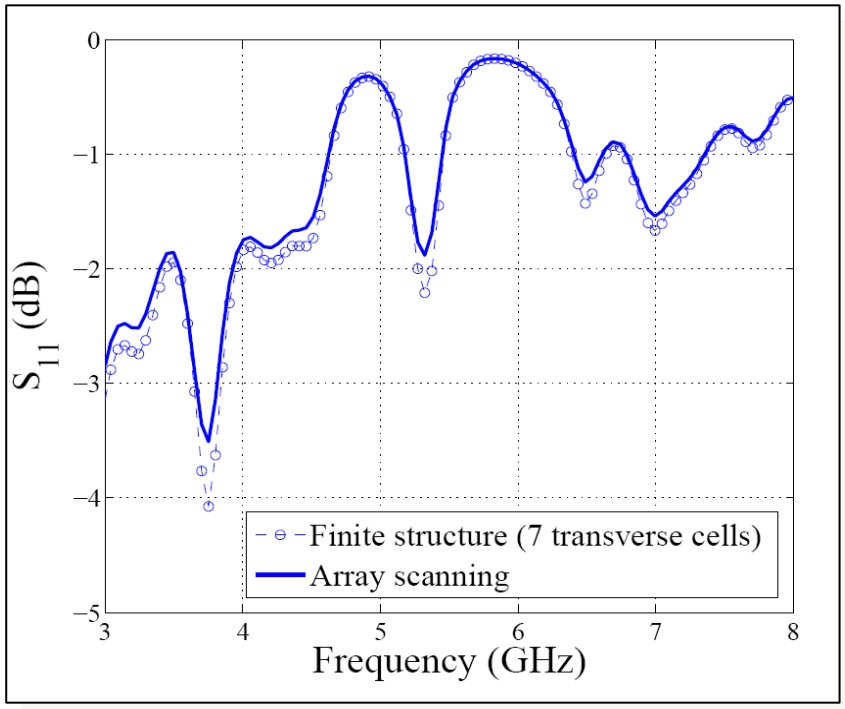

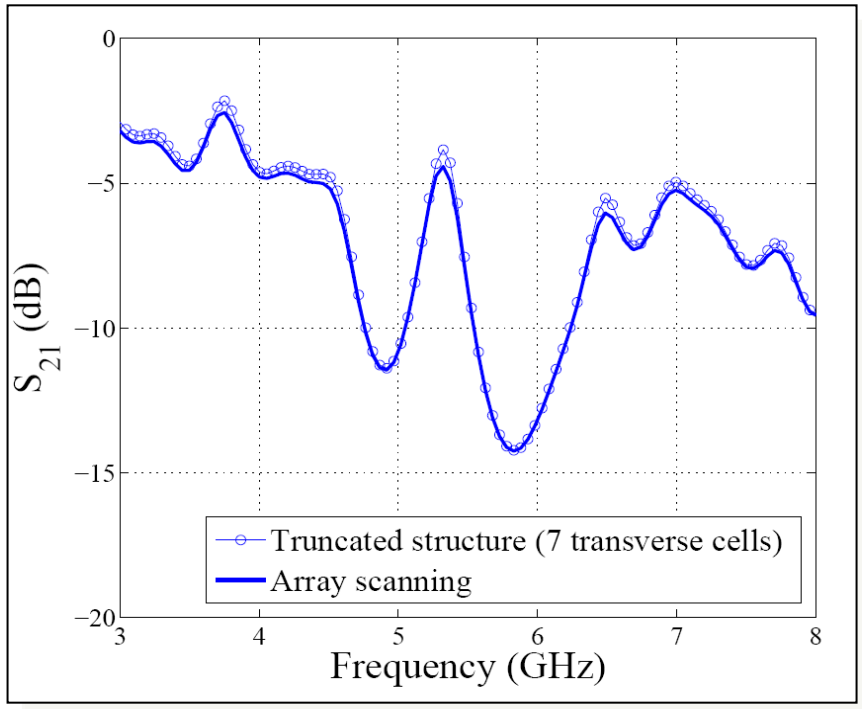

Execution time: 863 sec (proposed method, 16 k-points)
vs. 4017 (conventional FDTD, 7 transverse cells)

Mixed periodic/absorbing boundaries: Results

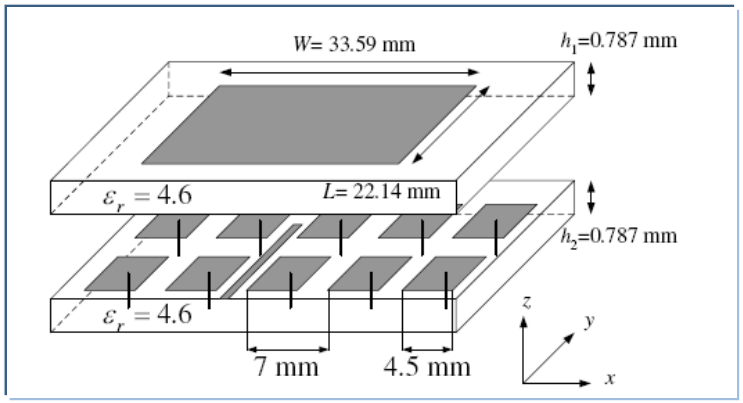

- S_{11}, radiation pattern at 2.5 GHz (32 kx-points); 38.35 mins
- Finite structure (6x8 unit cells); 374.63 mins

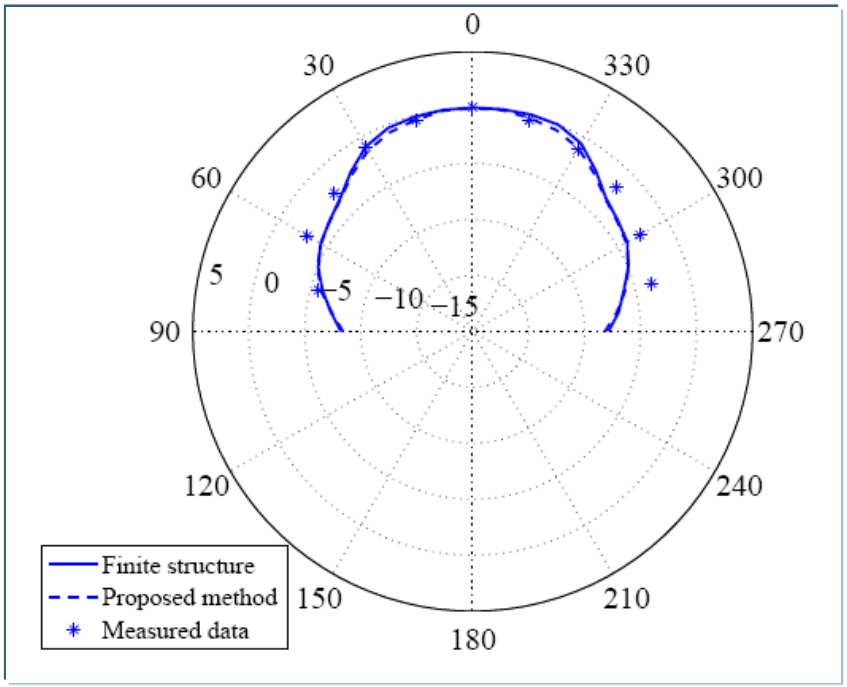

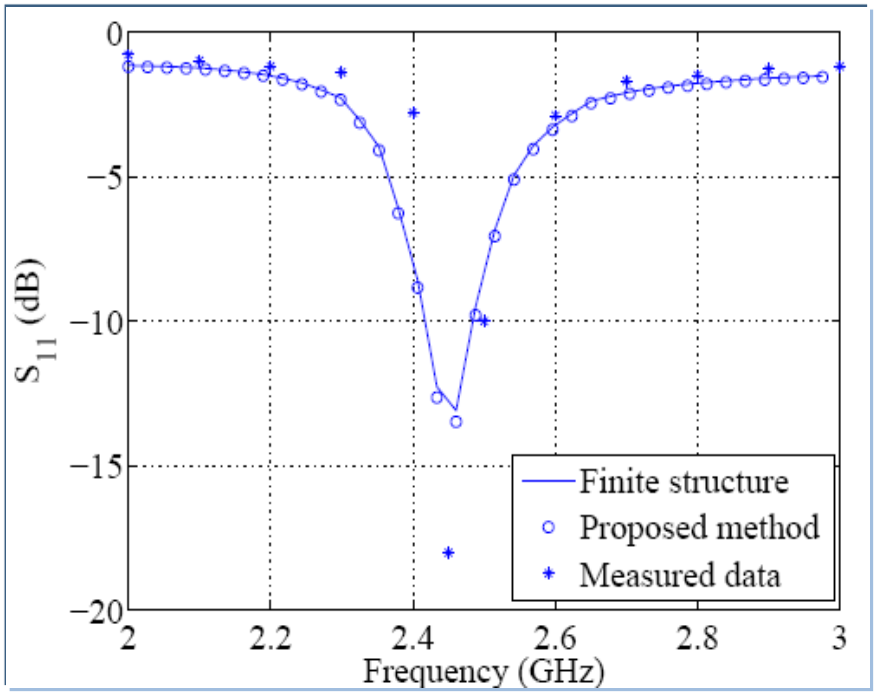

* J. Liang and H.-Y. D. Yang, “Radiation characteristics of a microstrip patch over an EBG surface,” *IEEE Trans. Microwave Theory Tech., vol. 55, no. 6, pp. 1691–1697, June 2007.*

Transformation optics

- Consider a coordinate transformation $q_x = q_x(x,y,z)$, $q_y = q_y(x,y,z)$:

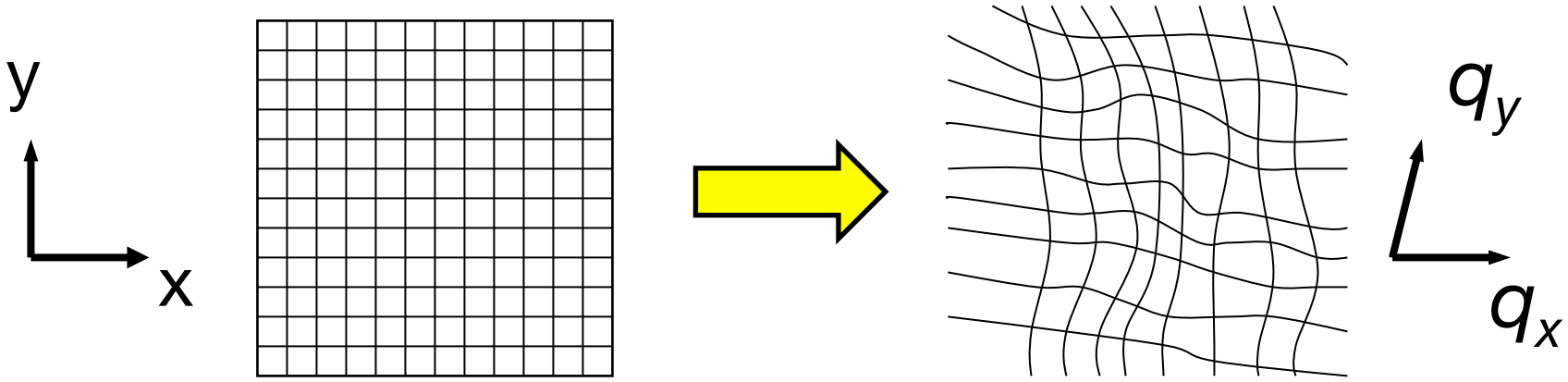

- In the new coordinate system, free-space Maxwell's equations become:

$$\nabla_q \times \overline{E}_q = -\mu_0 \overline{\overline{\mu}} \frac{\partial \overline{H}_q}{\partial t} \qquad \nabla_q \times \overline{H}_q = \varepsilon_0 \overline{\overline{\varepsilon}} \frac{\partial \overline{E}_q}{\partial t}$$

Metric invariance

Pendry's Cloak

- Idea: explore a coordinate transformation that compresses the interior of a sphere $R<R_1$ into a region $R_1< R < R_2$, in order to create a "cloak" in $R<R_1$.

$$r' = R_1 + r(R_2 - R_1)/R_2$$
$$\theta' = \theta,$$
$$\phi' = \phi$$

$$\varepsilon'_{r'} = \mu'_{r'} = \frac{R_2}{R_2 - R_1}\frac{(r' - R_1)^2}{r'^2}$$
$$\varepsilon'_{\theta'} = \mu'_{\theta'} = \frac{R_2}{R_2 - R_1},$$
$$\varepsilon'_{\phi'} = \mu'_{\phi'} = \frac{R_2}{R_2 - R_1}$$

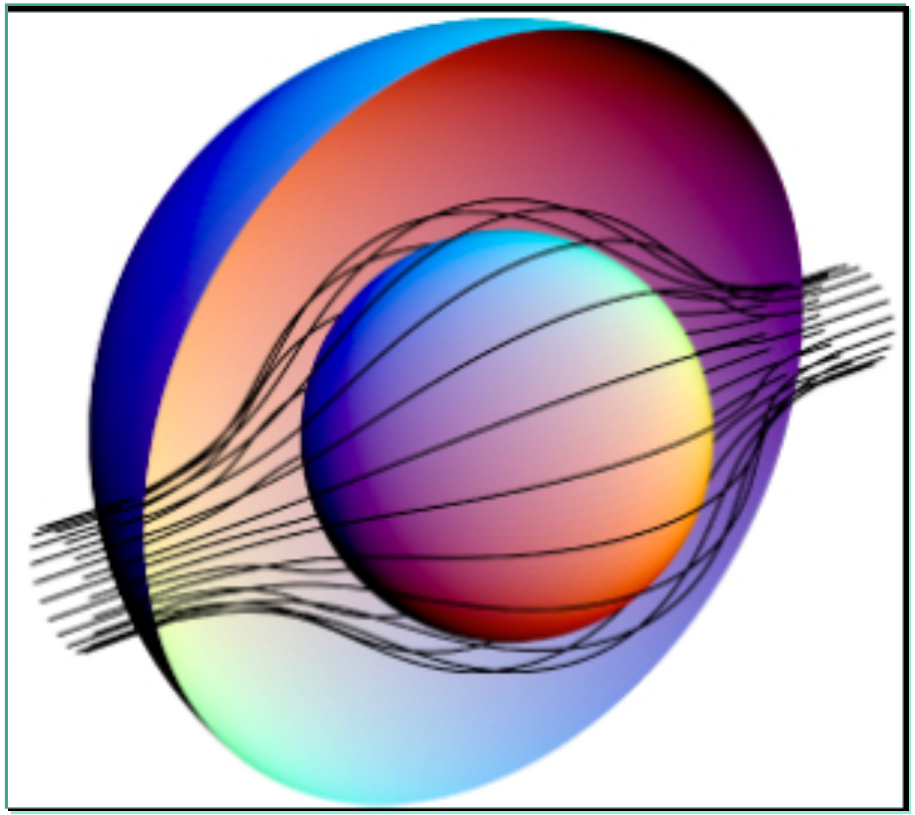

*J.B. Pendry, D. Schurig, D.R. Smith, "Controlling Electromagnetic Fields", *Science,* May 2006.

Maxwell's equations: Metric Invariance

Cartesian coordinates: $x^i \quad \text{for} \quad i = 1,2,3.$

General curvilinear coordinates: $u^j \quad \text{for} \quad j = 1,2,3.$

$$\nabla \times \mathbf{H} = \frac{\partial \mathbf{D}}{\partial t} + \mathbf{J}$$
$$\nabla \times \mathbf{E} = -\frac{\partial \mathbf{B}}{\partial t}$$
$$\mathbf{E} = \boldsymbol{\mathcal{E}}^{-1}\mathbf{D}$$
$$\mathbf{H} = \boldsymbol{\mathcal{M}}^{-1}\mathbf{B}$$

$$\frac{1}{\sqrt{g}}\left(\frac{\partial h_k}{\partial u^j} - \frac{\partial h_j}{\partial u^k}\right) = \frac{\partial d^i}{\partial t} + j^i$$
$$\frac{1}{\sqrt{g}}\left(\frac{\partial e_k}{\partial u^j} - \frac{\partial e_j}{\partial u^k}\right) = -\frac{\partial b^i}{\partial t}$$
$$e_j = \sum_{s=1}^{3} \varepsilon_{js}^{-1} d^s$$
$$h_j = \sum_{s=1}^{3} \mu_{js}^{-1} b^s$$

$\{i,j,k\} \rightarrow \{1,2,3\}, \{3,1,2\}, \{2,3,1\}$

Maxwell's equations: Metric Invariance

The coordinate system is customized so that all the material interfaces of the problem are described by coordinate surfaces:

$$u^i = \text{constant} \quad \text{for} \quad i = 1,2,3.$$

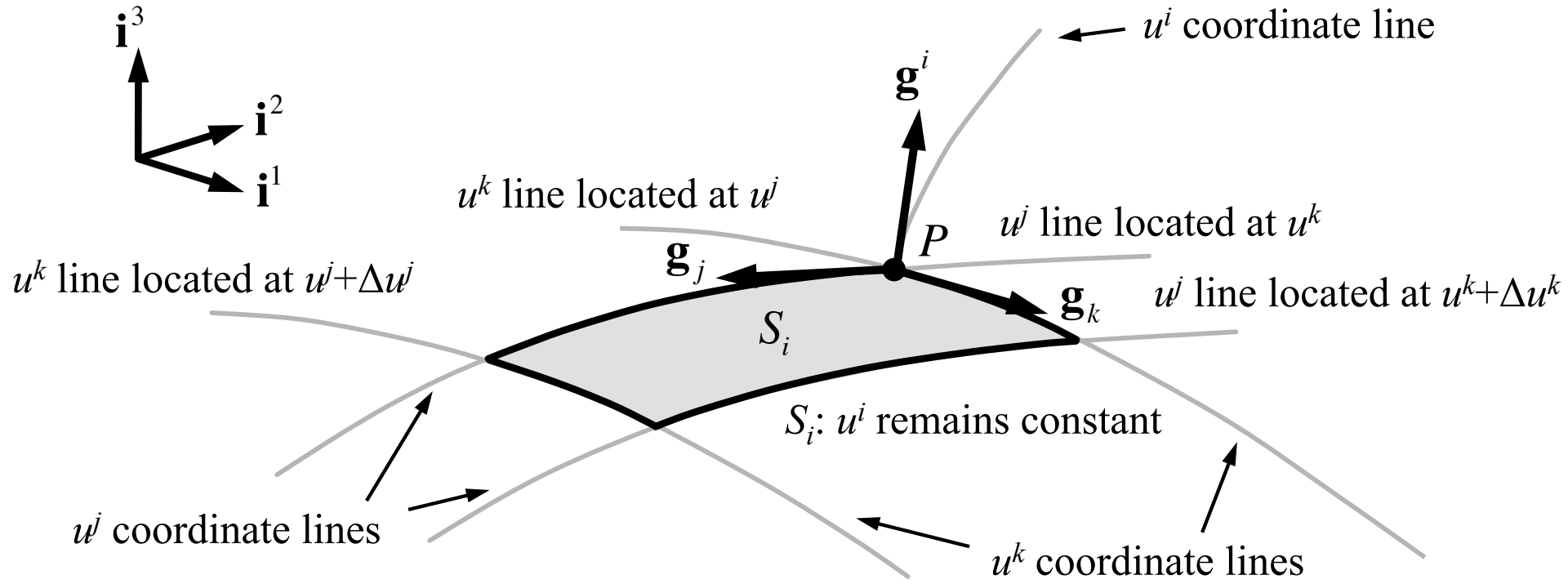

From transformation optics to FDTD

To illustrate the proposed procedure, consider the following 2-D waveguide structure:

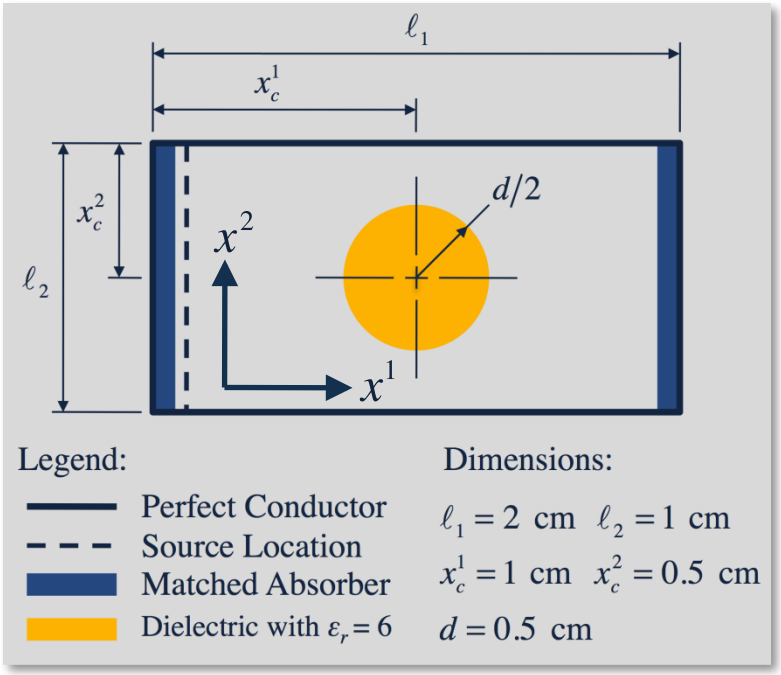

Problem Geometry in Physical Space

To implement the proposed method two spatial domains must be clearly defined:

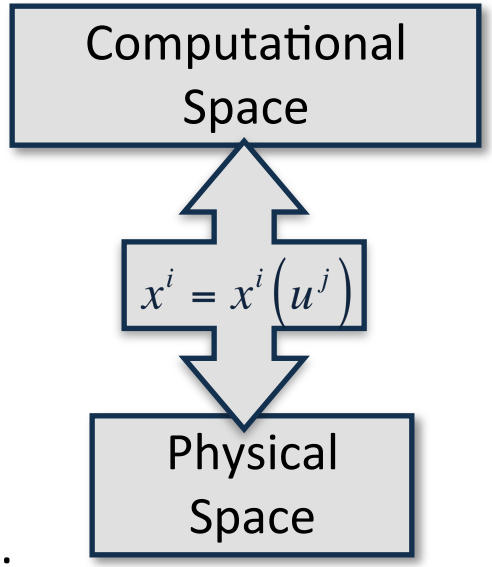

Notation:

- u^j represents curvilinear coordinates, which determine position in computational space
- x^i represents Cartesian coordinates, which determine position in physical space

From transformation optics to FDTD (II)

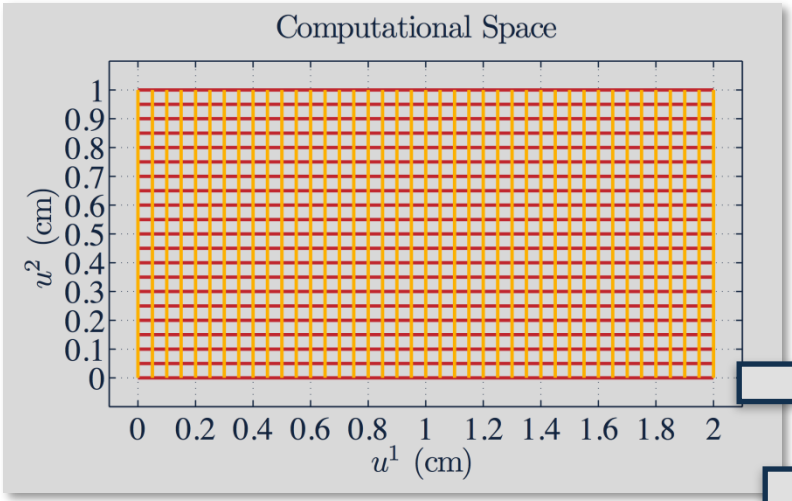

$$x^i = x^i\left(u^j\right)$$

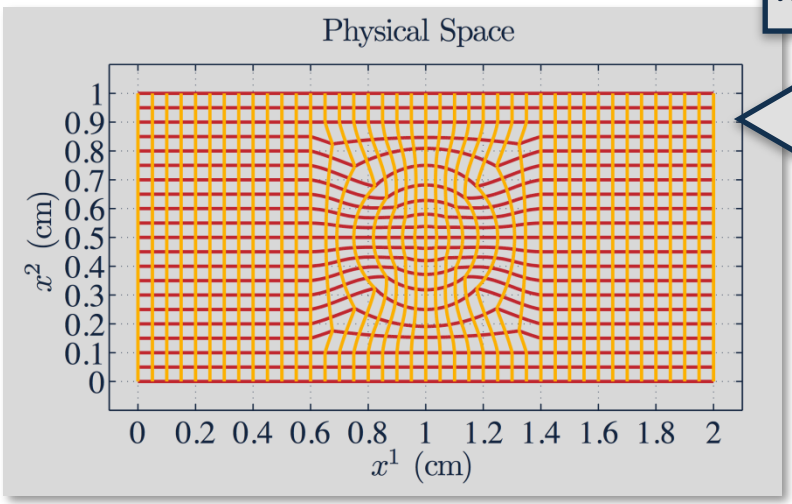

Coordinate lines:

u^1 lines are in red

u^2 lines are in yellow

Maxwell's equations must be projected into computational space using curvilinear basis vectors:

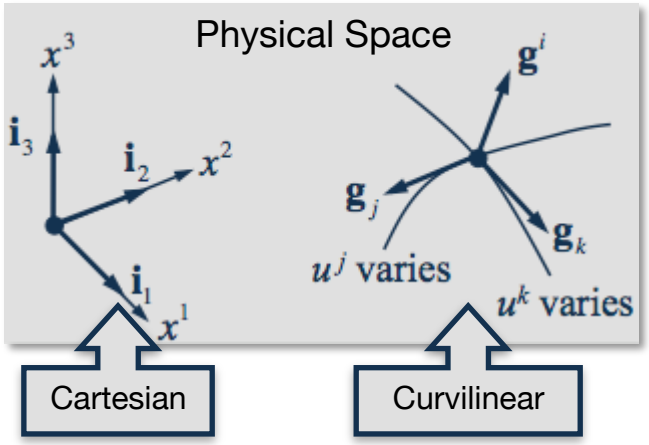

If nothing varies along the u^3-axis, Maxwell's equations split into two sets: TE^3 and TM^3. The TE^3 set was used to compute results:

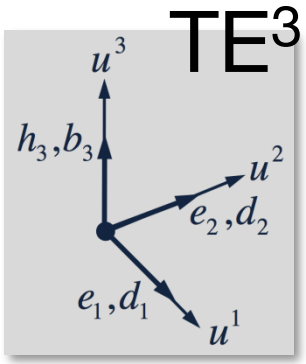

From transformation optics to FDTD (II)

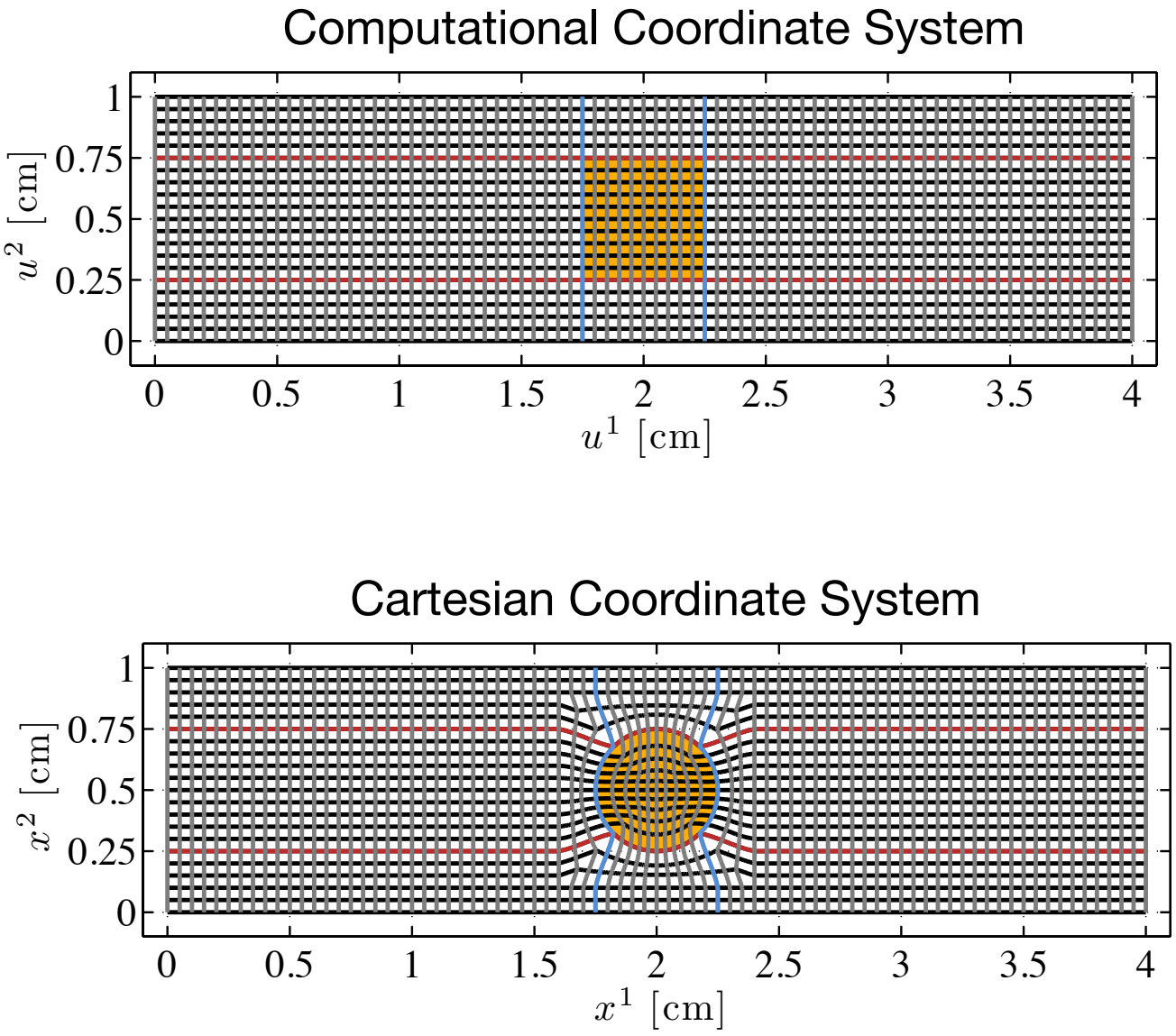

From transformation optics to FDTD (III)

Incident Field

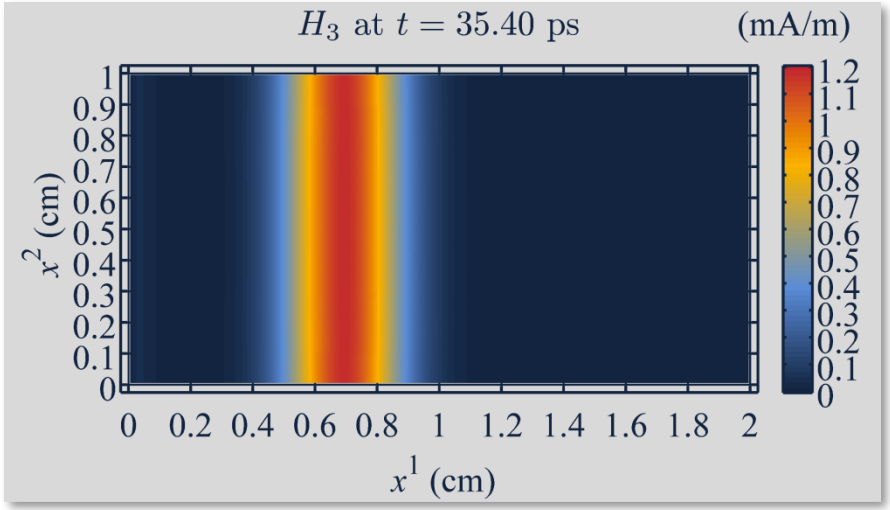

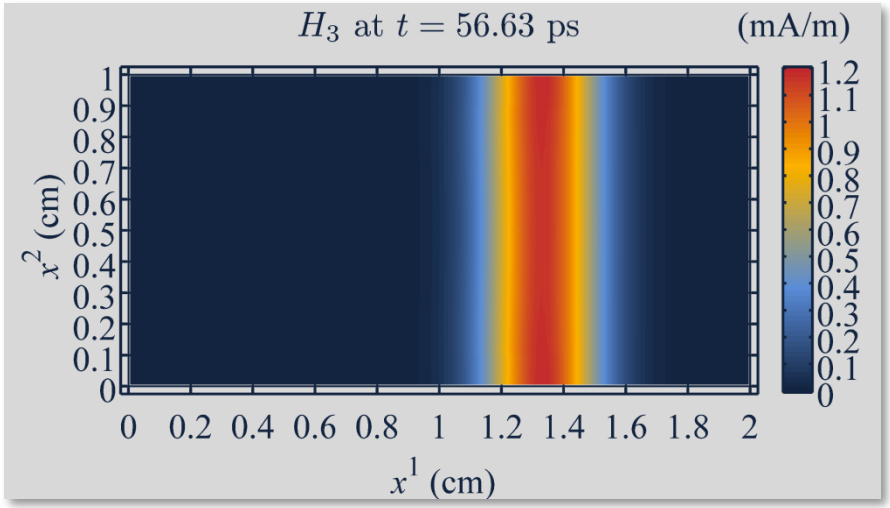

Total Field

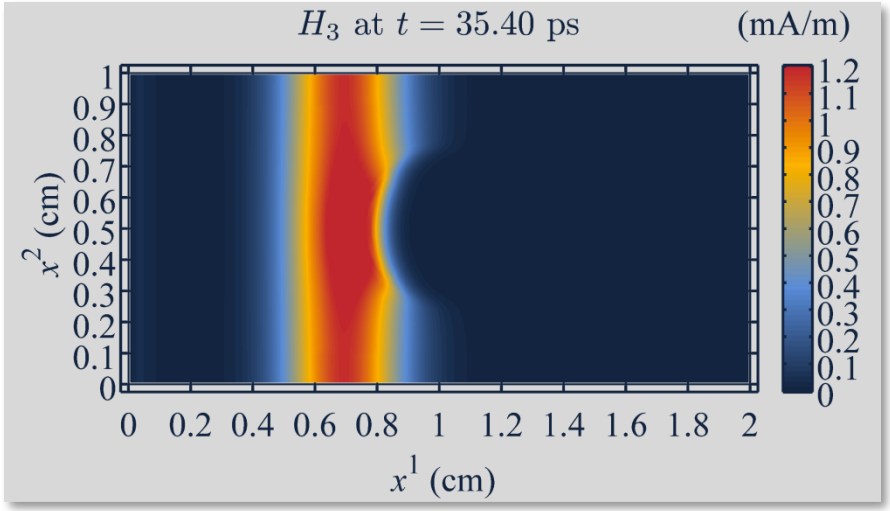

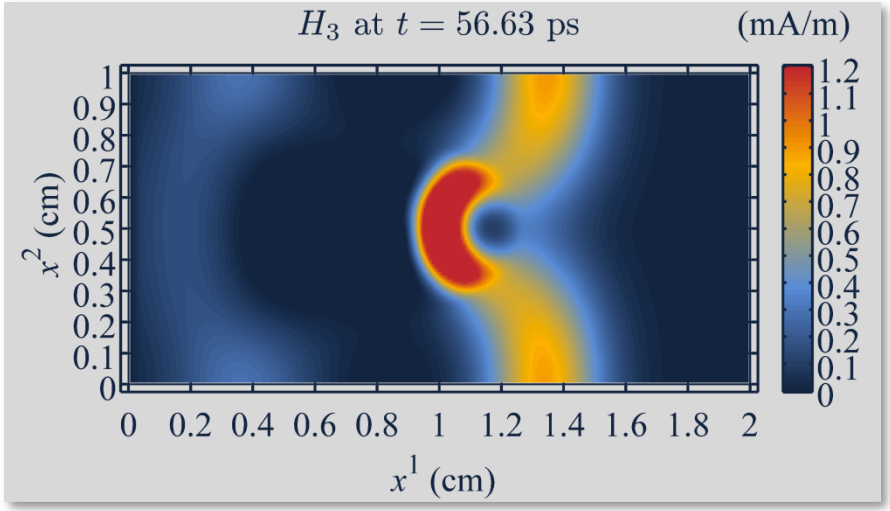

Why high order finite differences ?

Three different discretizations were used to analyze this problem:

Parameter	Grid 1	Grid 2	Grid 3
Order of Accuracy	10	2	2
# of Cells	180 x 30	180 x 30	360 x 60
# of Time Steps	10000	10000	20000
CPU Time	175.44 s	21.34 s	169.58 s
Resolution	Excellent	Poor	Poor

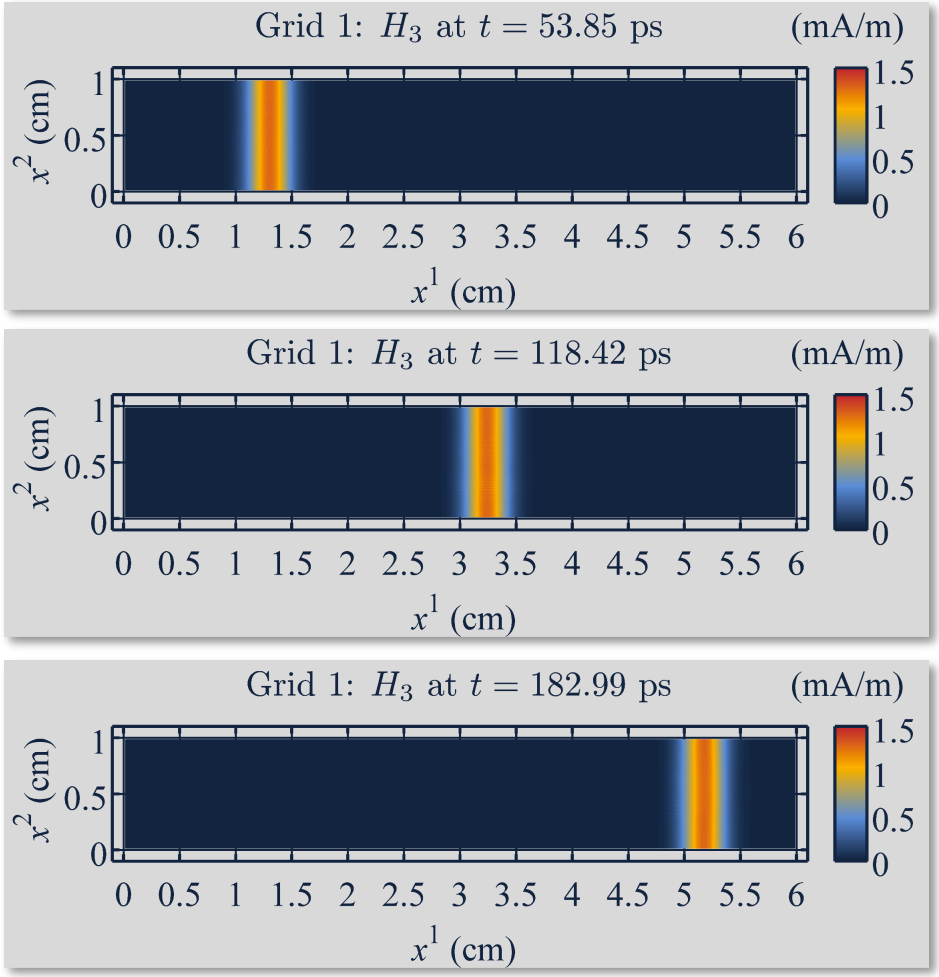

Why high order finite differences ?

Parameter	Grid 1	Grid 2	Grid 3
Order of Accuracy	10	2	2
# of Cells	180 x 30	180 x 30	360 x 60
# of Time Steps	10000	10000	20000
CPU Time	175.44 s	21.34 s	169.58 s
Resolution	Excellent	Poor	Poor

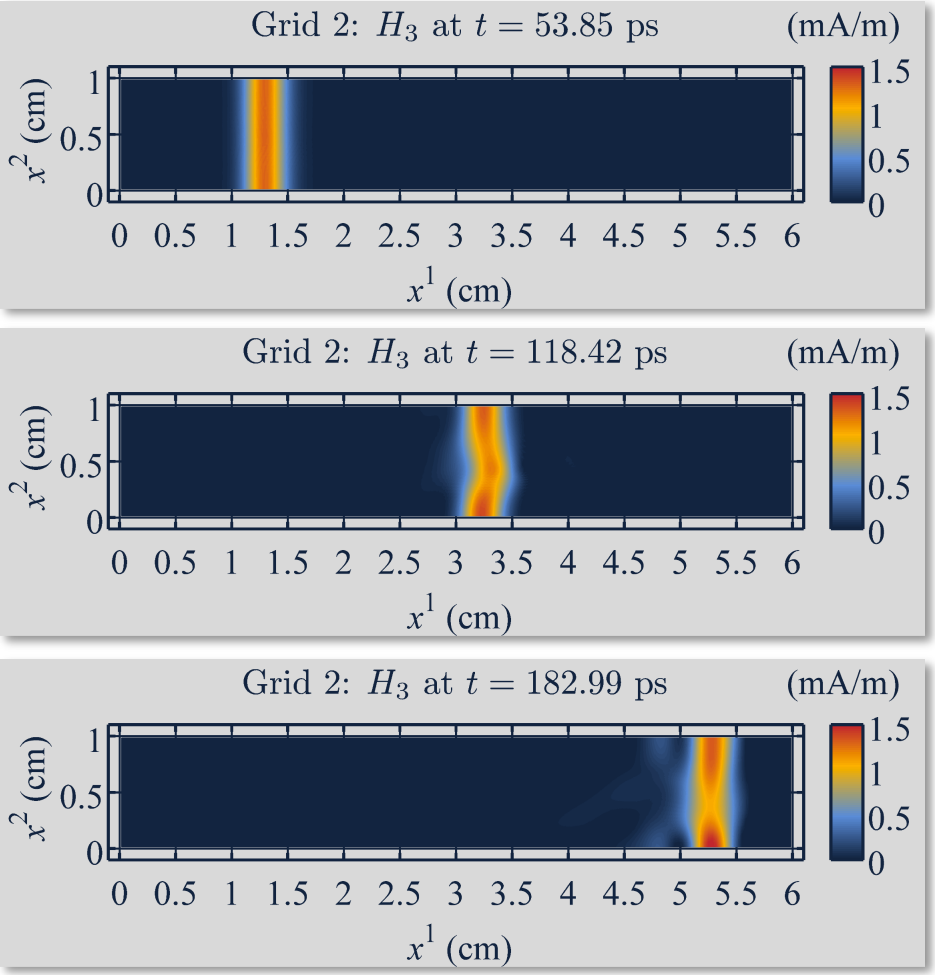

Why high order finite differences ?

Parameter	Grid 1	Grid 2	Grid 3
Order of Accuracy	10	2	2
# of Cells	180 x 30	180 x 30	360 x 60
# of Time Steps	10000	10000	20000
CPU Time	175.44 s	21.34 s	169.58 s
Resolution	Excellent	Poor	Poor

These results demonstrate that, to produce an optimal solution in the presence of a highly nonorthogonal grid, one must often resort to high-order finite differences.

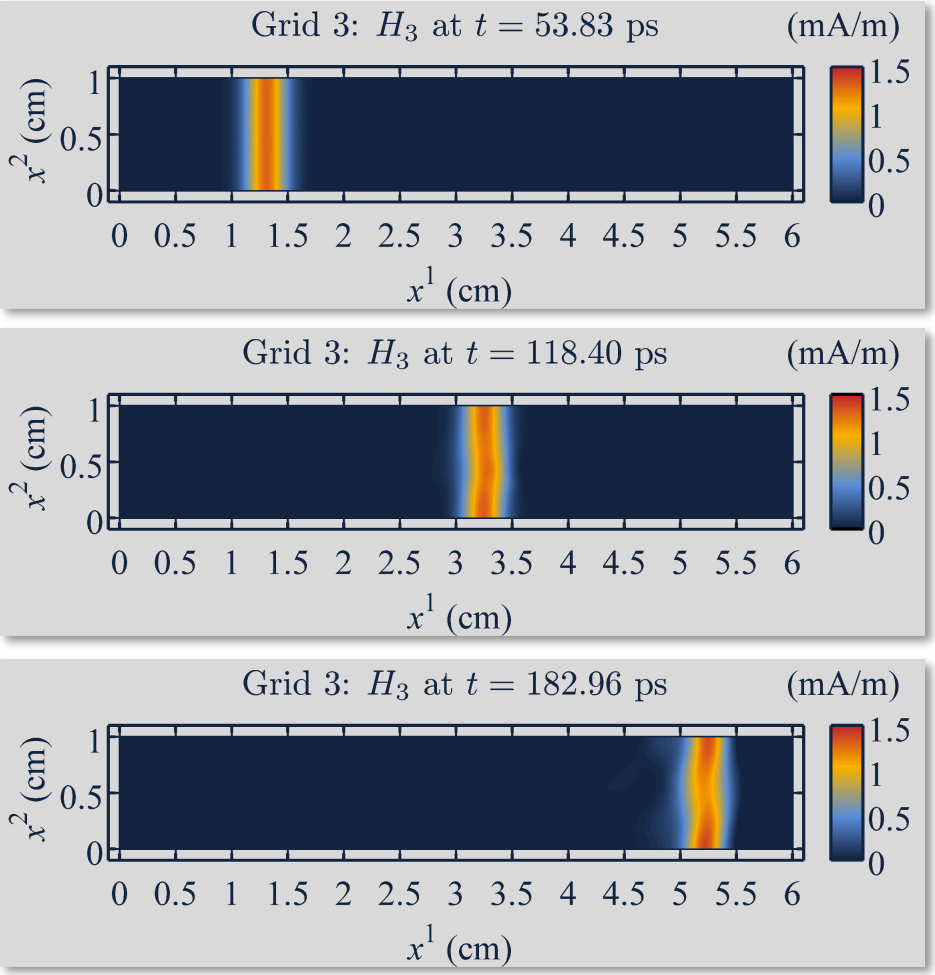

Interrelations with the design of artificial materials

The use of coordinate transformations is closely related to the design of artificial materials. To illustrate this, consider the following 2-D waveguide bend:

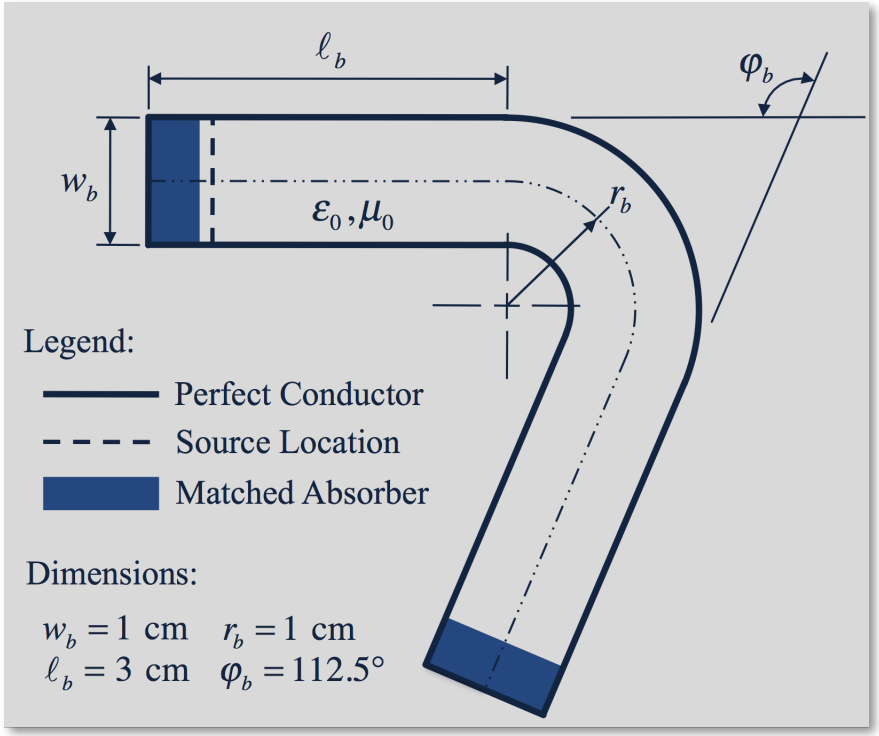

A suitable coordinate transformation for modeling this structure can be found in:

B. Donderici and F. L. Teixeira, "Metamaterial Blueprints for Reflectionless Waveguide Bends," *IEEE Microw. Wireless Compon. Lett.*, vol. 18, no. 4, pp. 233-235, April 2008.

Interrelations with the design of artificial materials

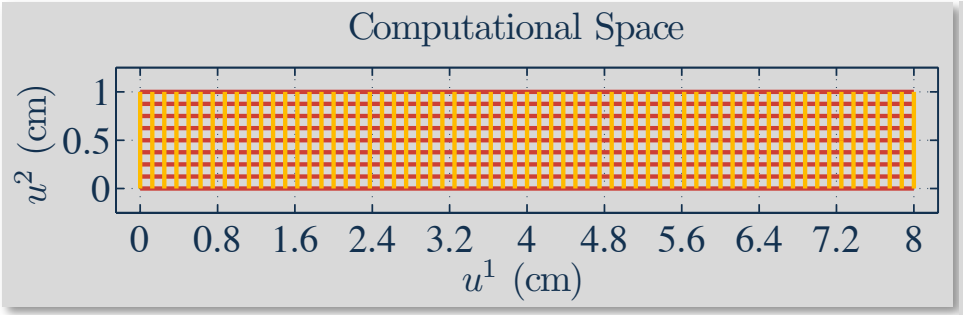

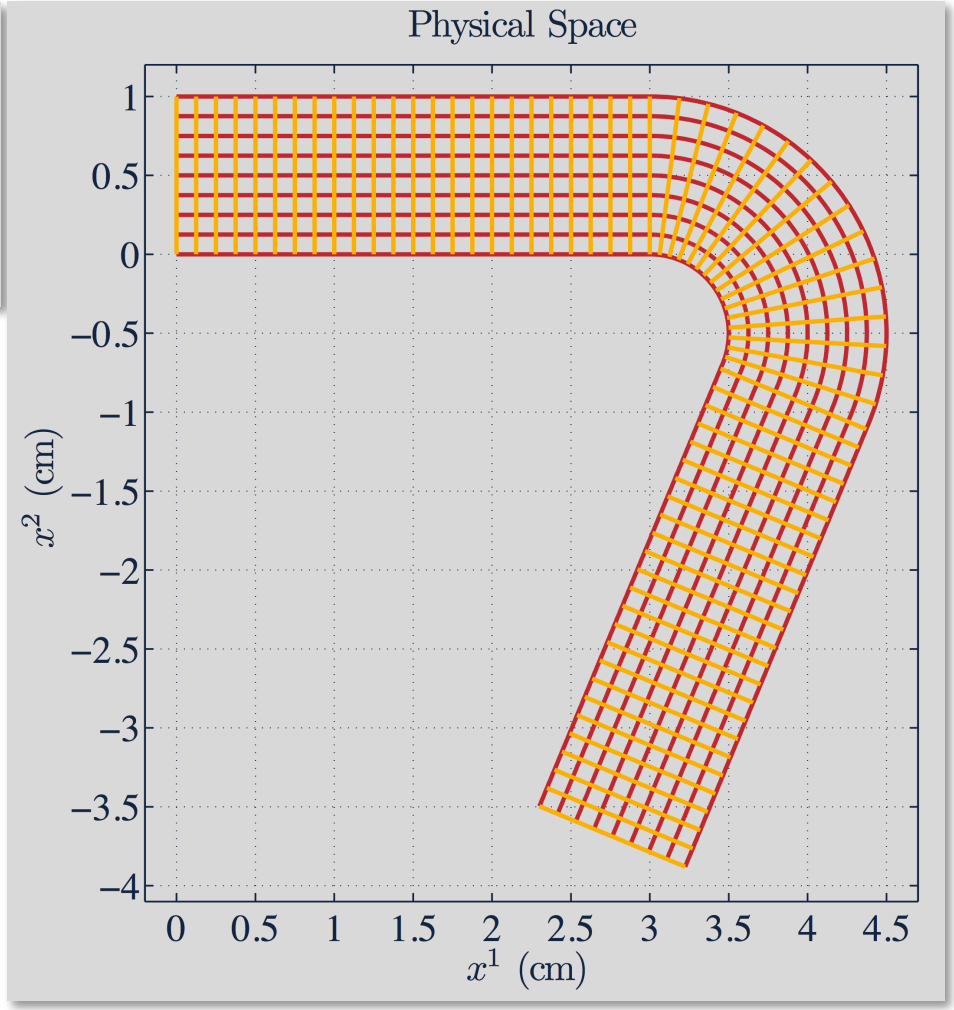

Observe that, to obtain a device that is reflectionless and distortionless, waves must travel undisturbed in computational space. The conditions to attain this are simply

$$\mathcal{M}_{is} = \frac{\partial x^q}{\partial u^i}\frac{\partial x^j}{\partial u^s}\mu_{qj} = \mu_0 g_{is}$$

$$\mathcal{E}_{is} = \frac{\partial x^q}{\partial u^i}\frac{\partial x^j}{\partial u^s}\varepsilon_{qj} = \varepsilon_0 g_{is}$$

The components of the metric tensor g_{is} are combinations of the partial derivatives of the shown coordinate transformation.

Interrelations with the design of artificial materials

Using the proposed numerical procedure, it is very easy to examine the response of the device in the presence of the artificial material:

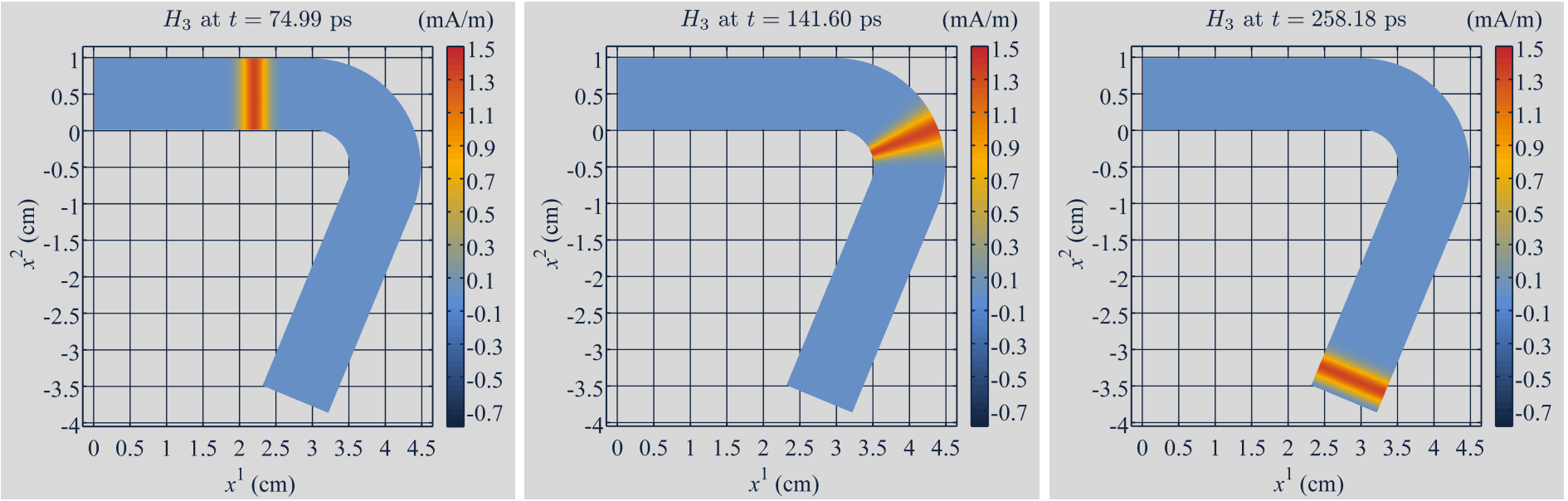

The use of coordinate transformations to design this type of artificial material is now being called transformation electromagnetics.

Interrelations with the design of artificial materials

1. Operating principle: a coordinate transformation is used to map an arbitrary non-orthogonal structured grid onto a uniform rectangular grid.

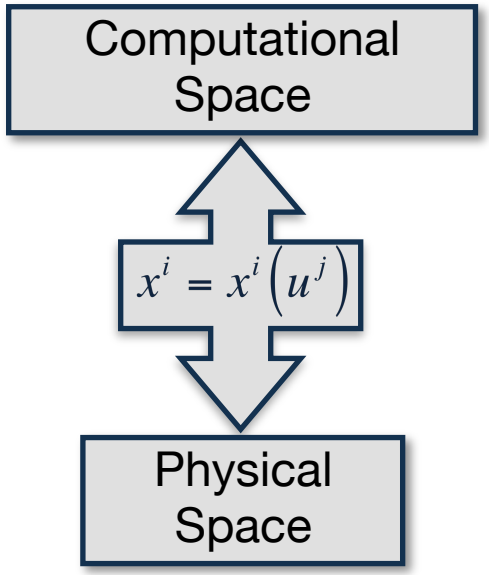

2. The use of high-order finite differences is clearly justified when a highly nonorthognal coordinate transformation is being used.

3. Coordinate transformations can have a dual purpose: designing an artificial material and introducing a structured nonorthogonal grid.

Time Dependent Coordinate Transformations

The following mapping was created to generate a moving grid that tracks a pulse propagating in vacuum along x^1:

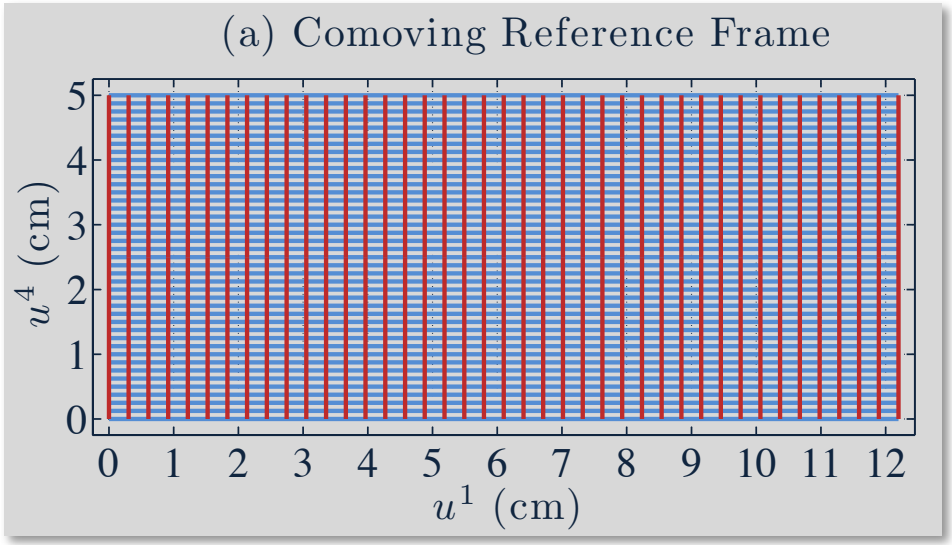

Coordinate u^4 can advance you in both time and space.

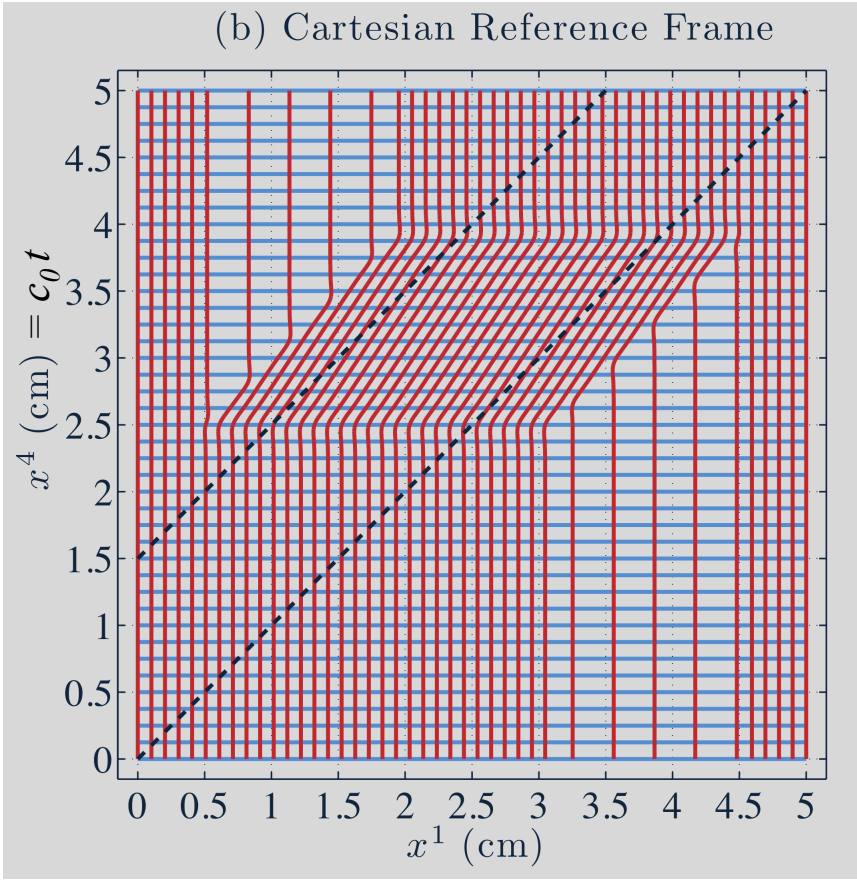

This type of coordinate transformation is not time orthogonal and is needed to introduce moving grids.

Example: Pulse Tracking in 2D

The same number of grid points are used in both space and time.

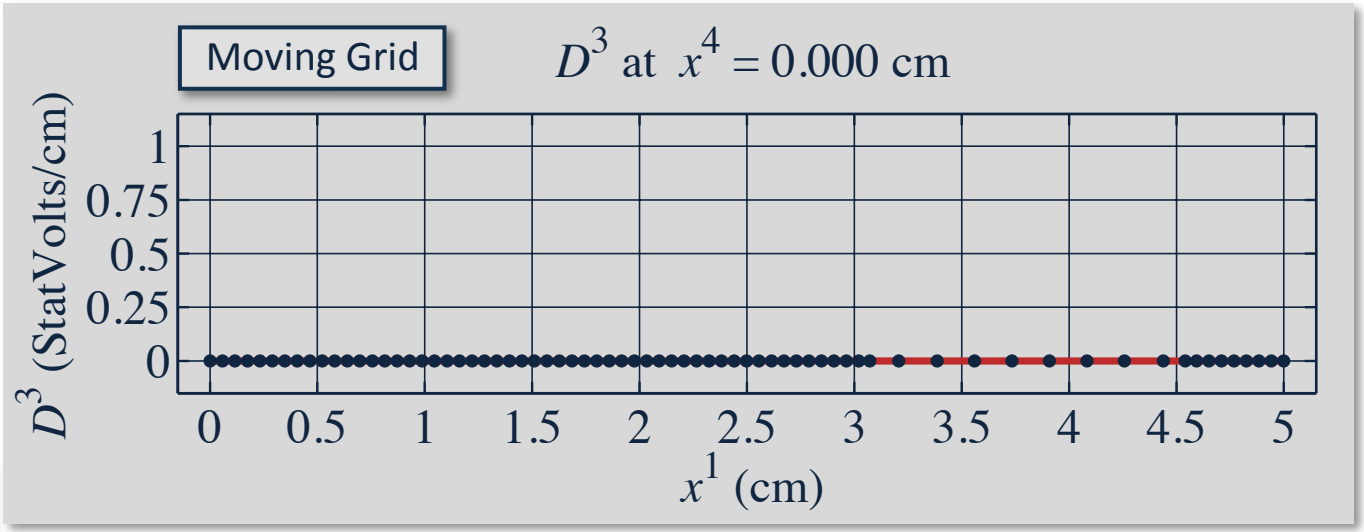

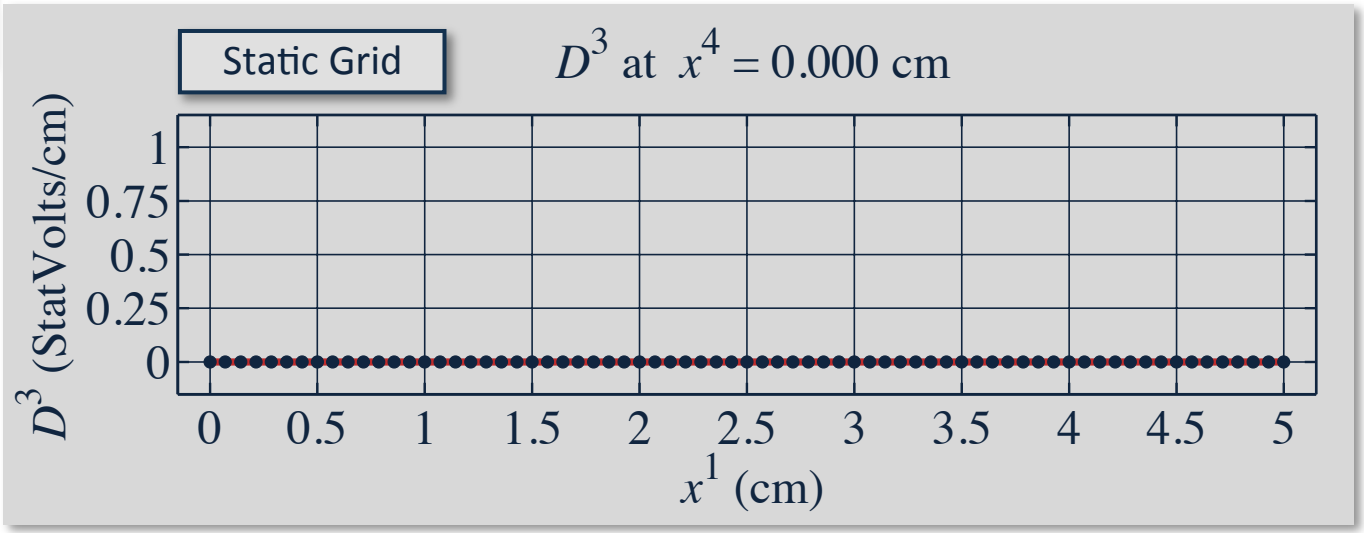

The dots show the location of the grid points.

Example: Pulse Tracking in 2D

The same number of grid points are used in both space and time.

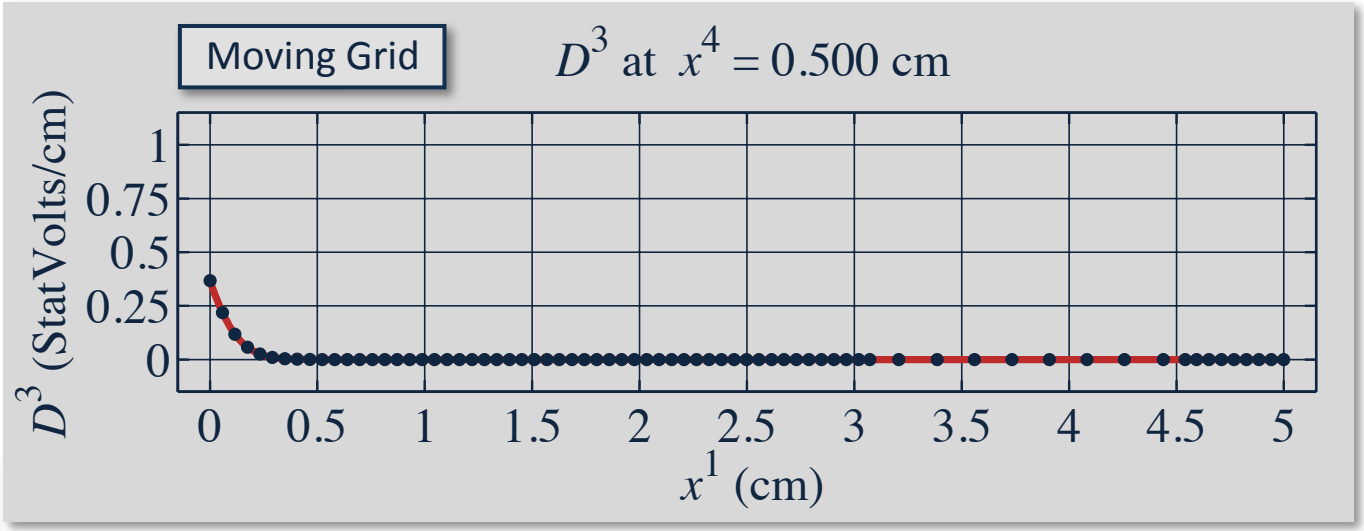

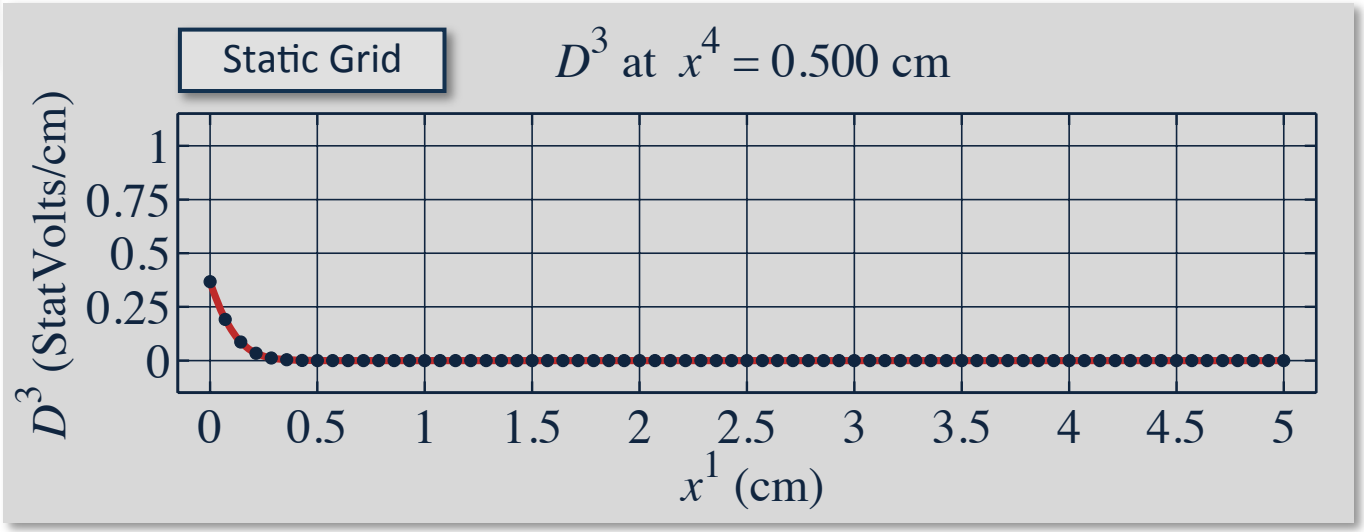

The dots show the location of the grid points.

Example: Pulse Tracking in 2D

The same number of grid points are used in both space and time.

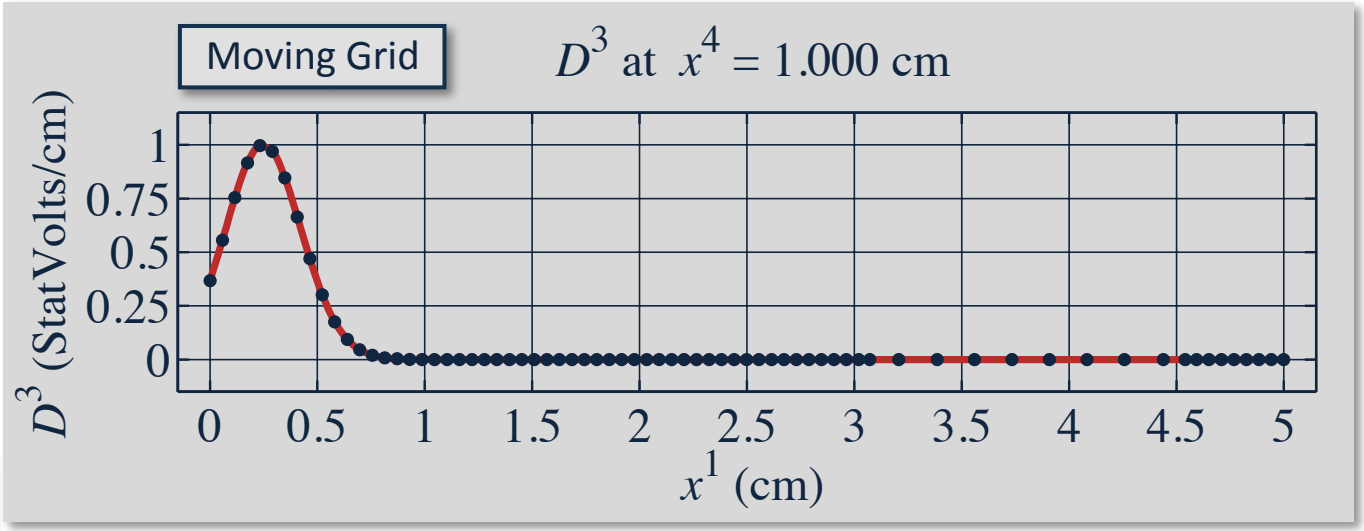

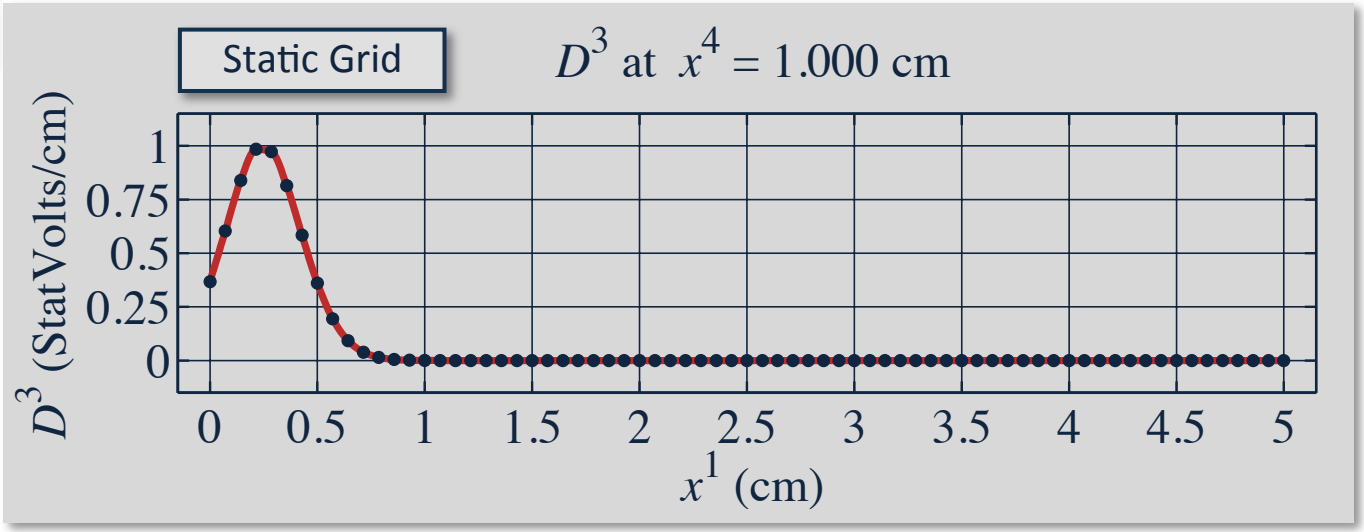

The dots show the location of the grid points.

Example: Pulse Tracking in 2D

The same number of grid points are used in both space and time.

The dots show the location of the grid points.

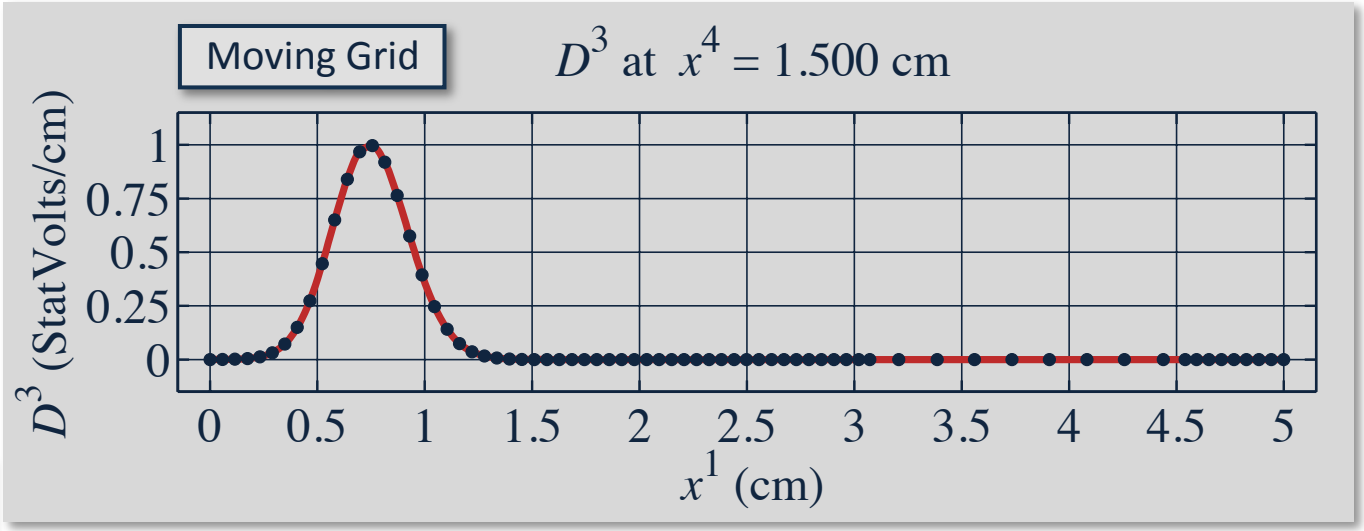

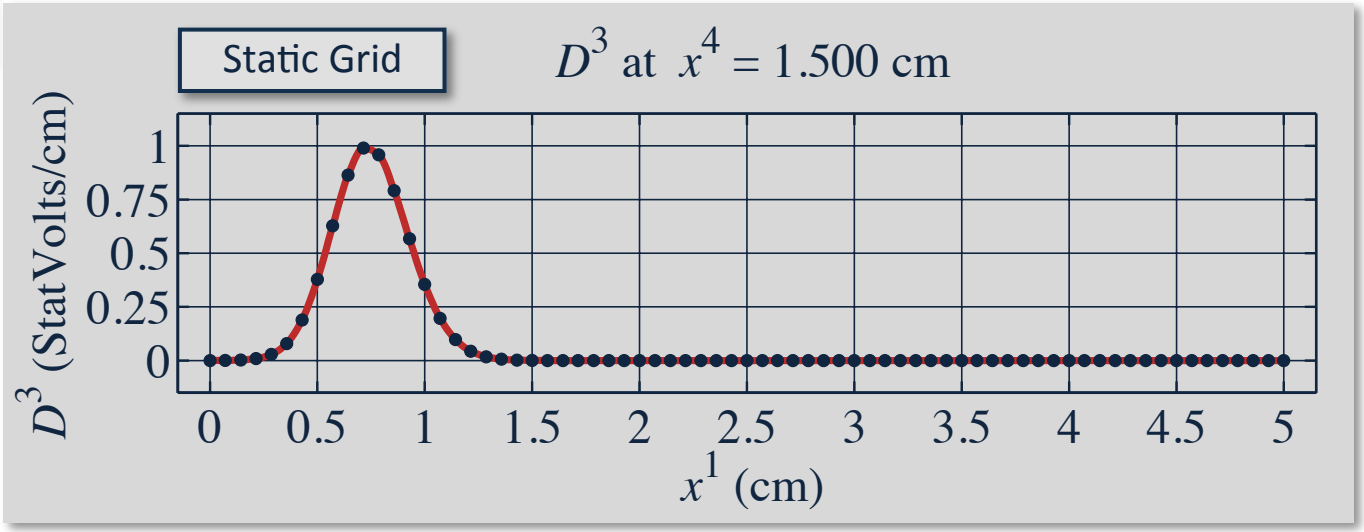

Example: Pulse Tracking in 2D

The same number of grid points are used in both space and time.

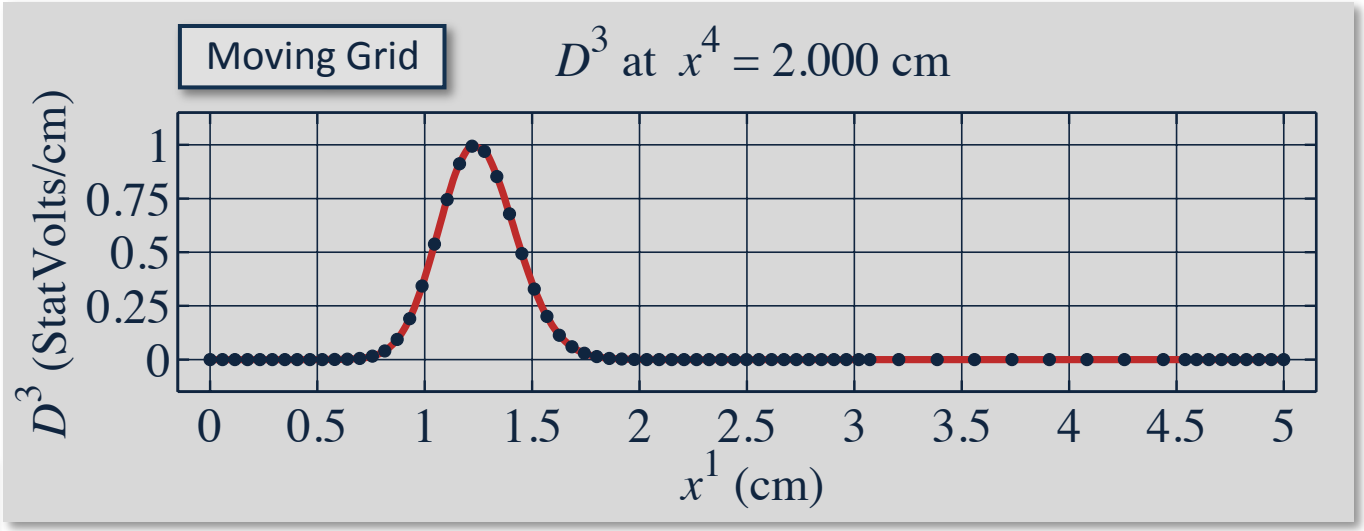

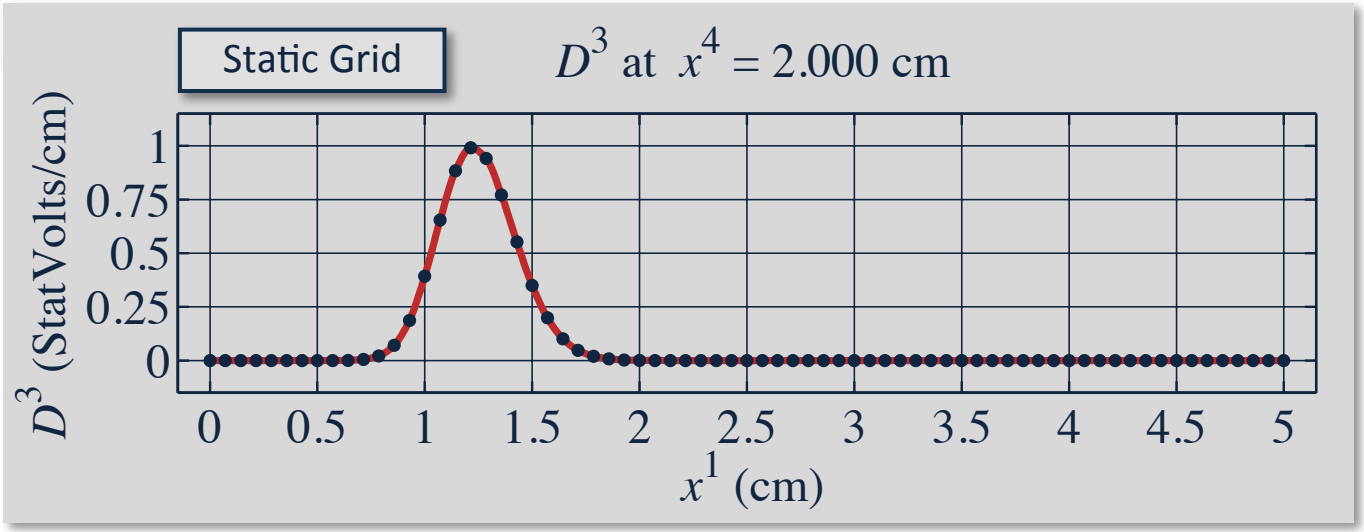

The dots show the location of the grid points.

Example: Pulse Tracking in 2D

The same number of grid points are used in both space and time.

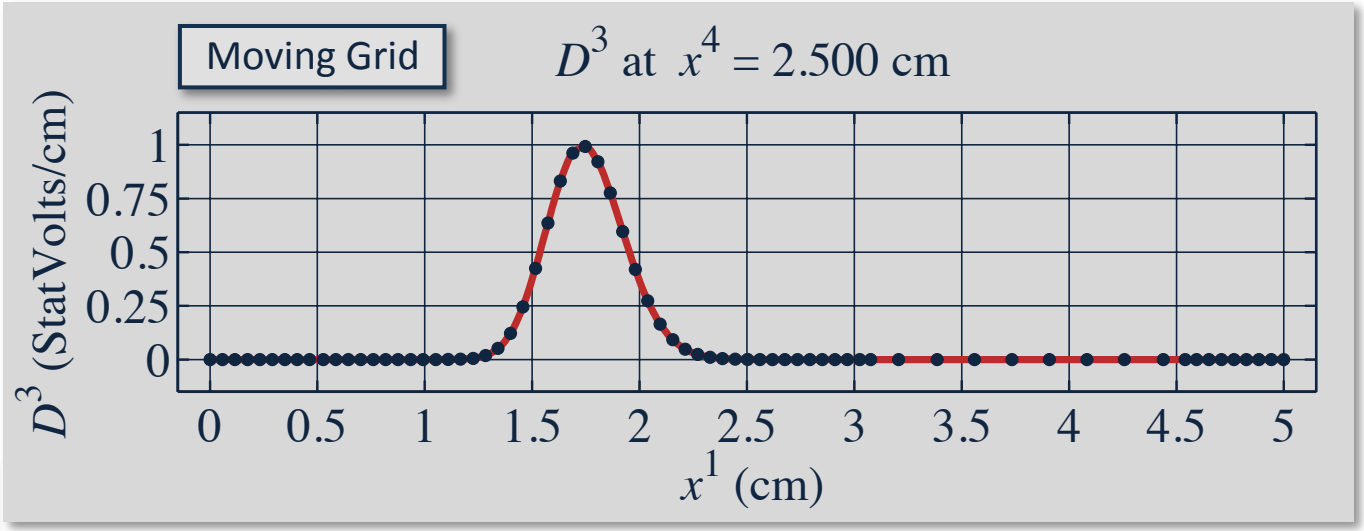

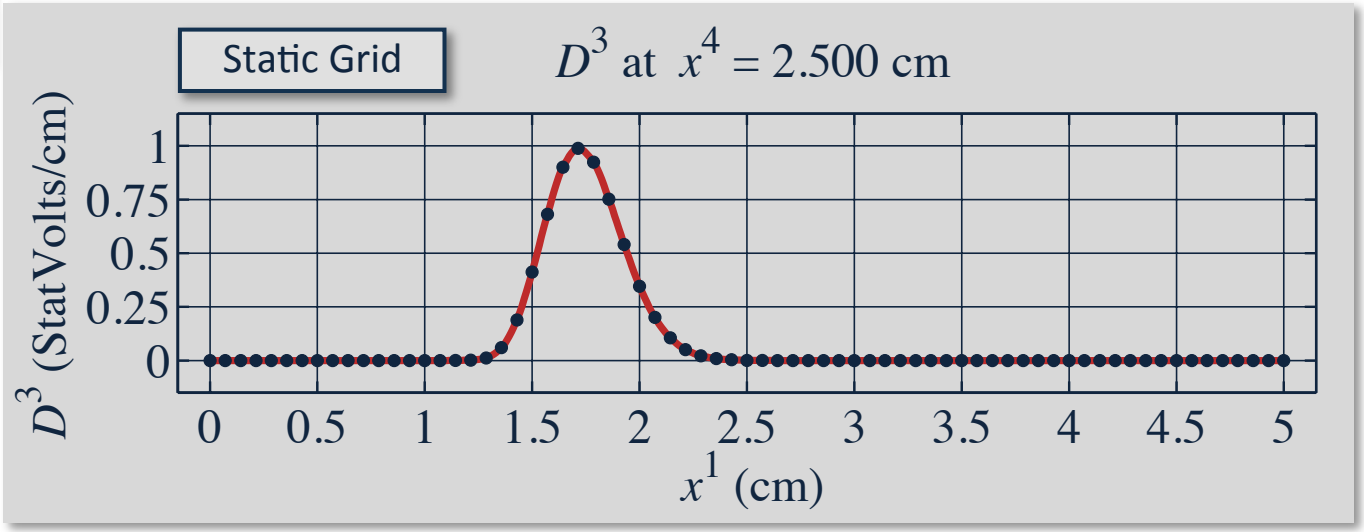

The dots show the location of the grid points.

Example: Pulse Tracking in 2D

The same number of grid points are used in both space and time.

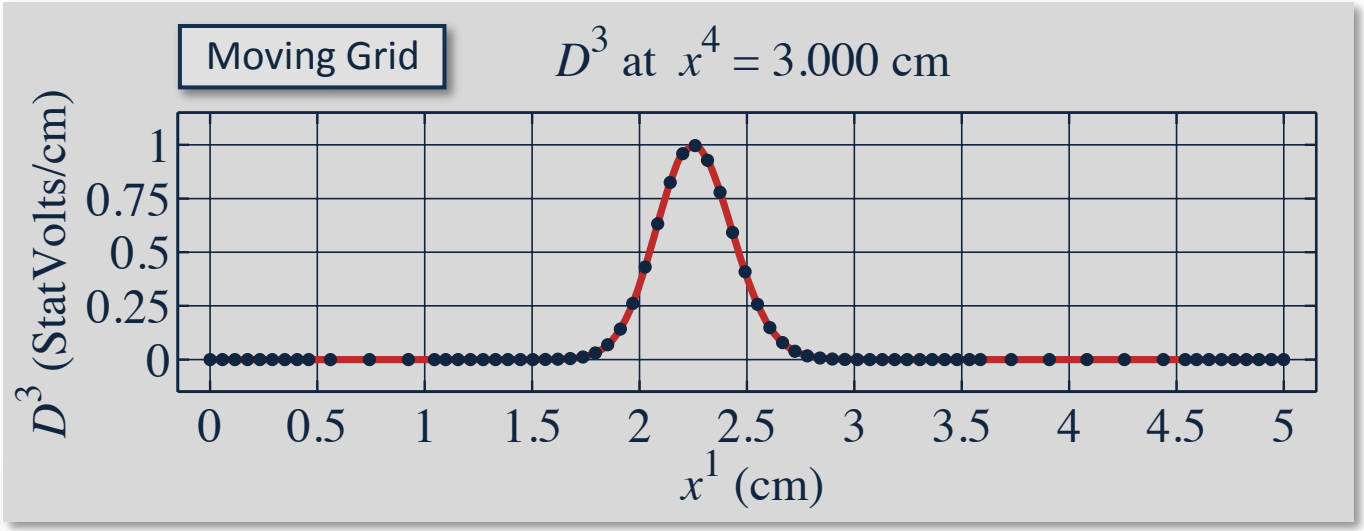

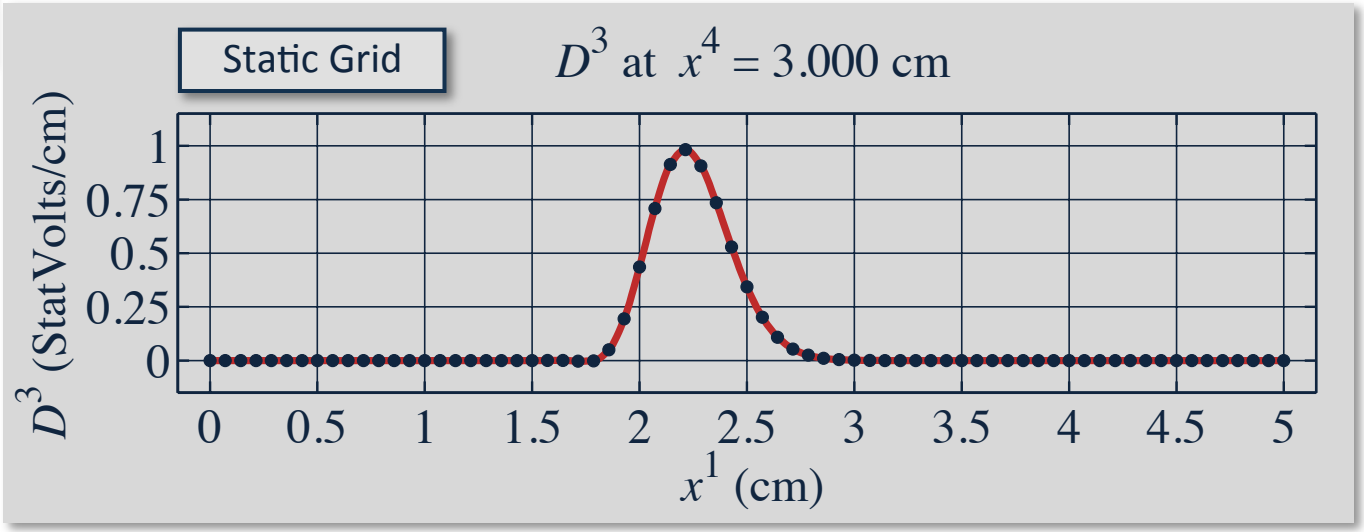

The dots show the location of the grid points.

Example: Pulse Tracking in 2D

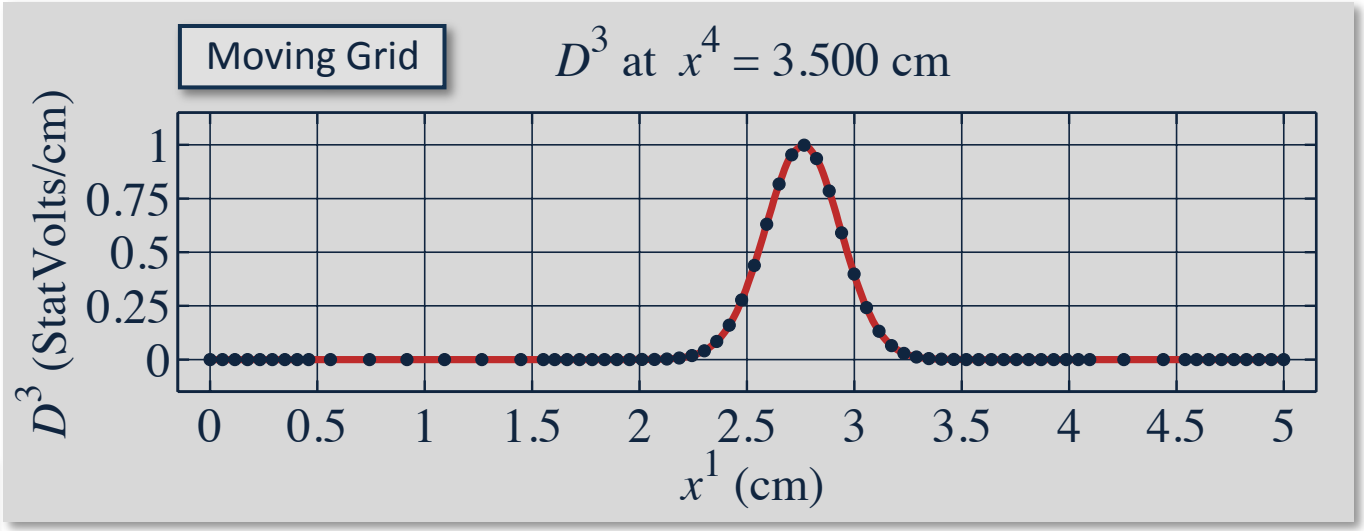

The same number of grid points are used in both space and time.

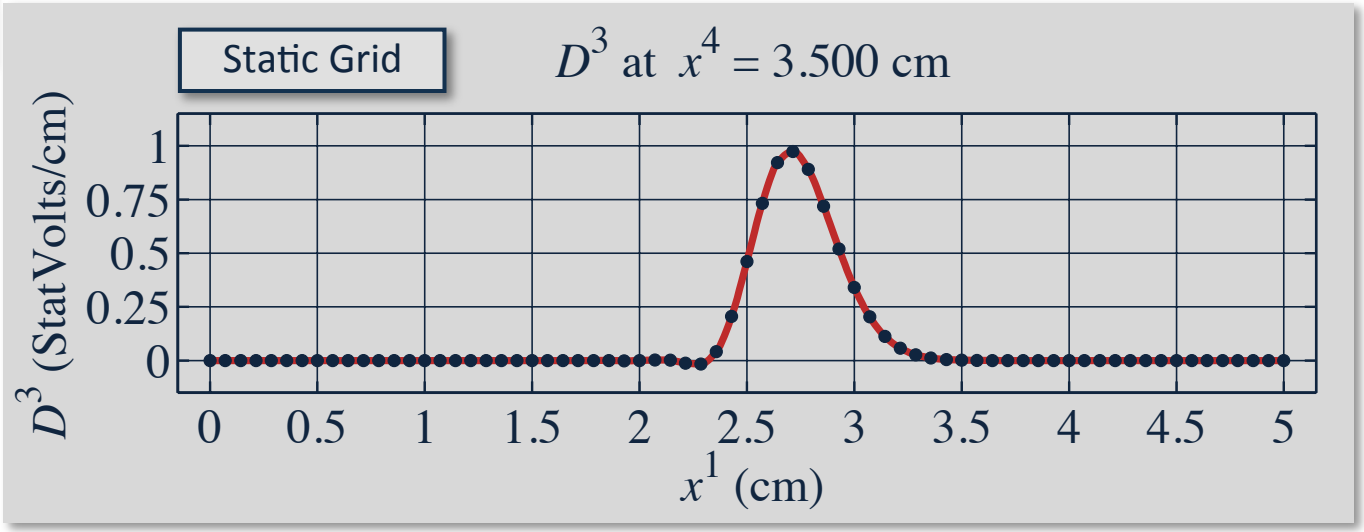

The dots show the location of the grid points.

Example: Pulse Tracking in 2D

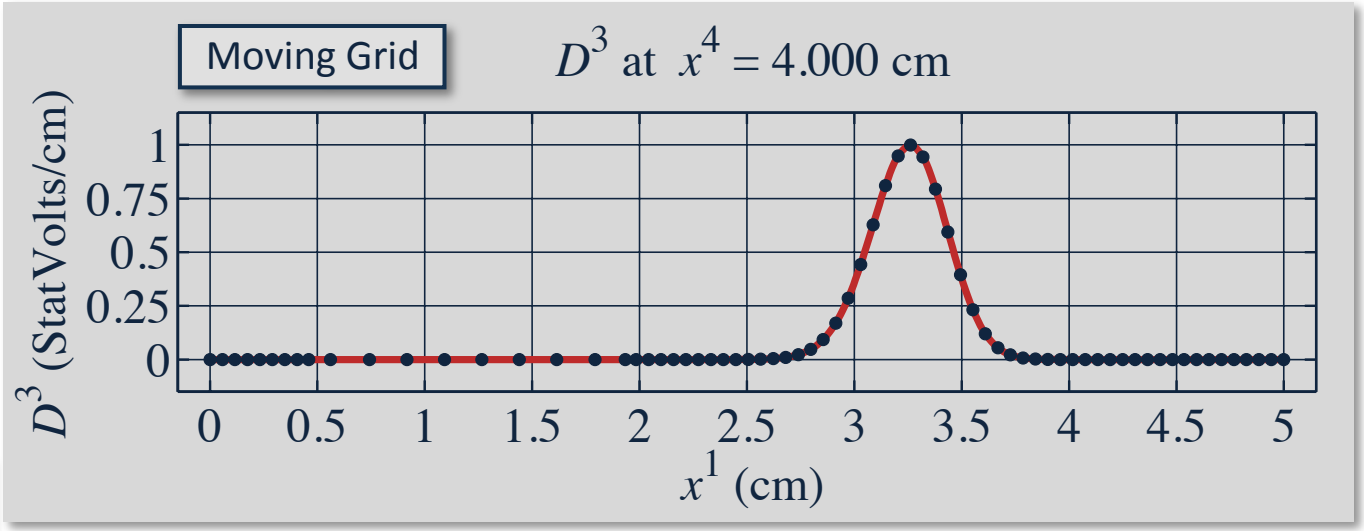

The same number of grid points are used in both space and time.

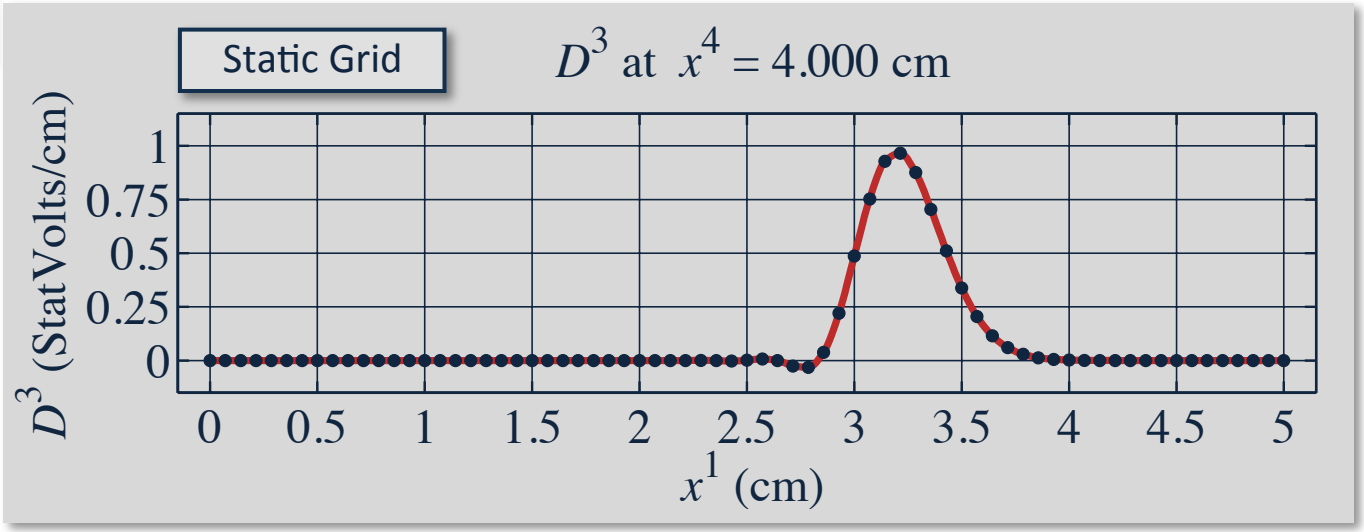

The dots show the location of the grid points.

Example: Pulse Tracking in 2D

The same number of grid points are used in both space and time.

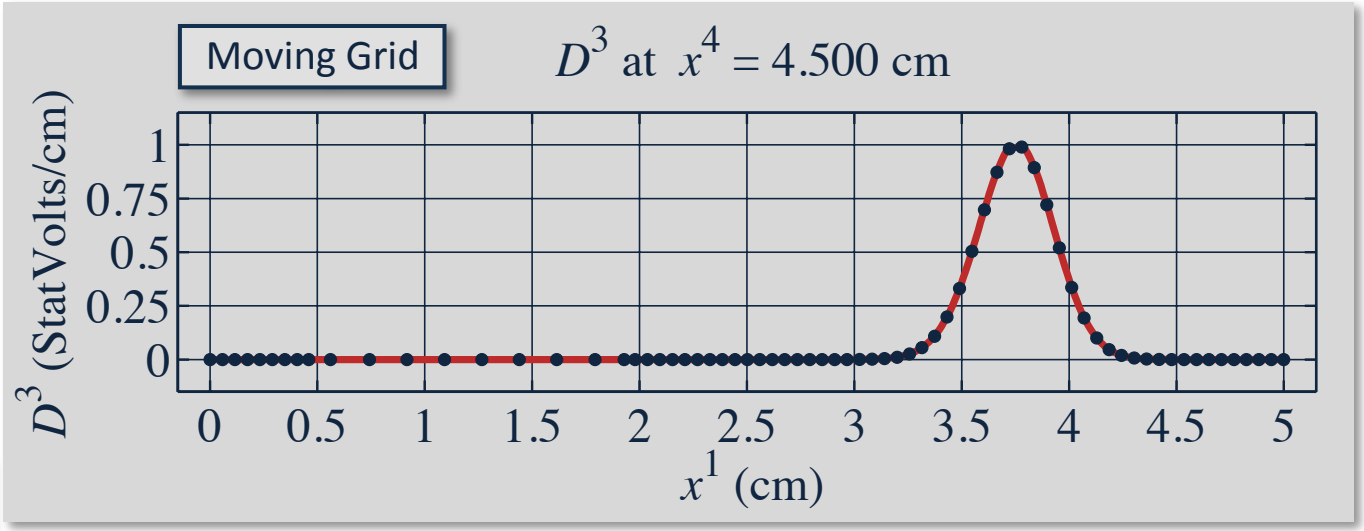

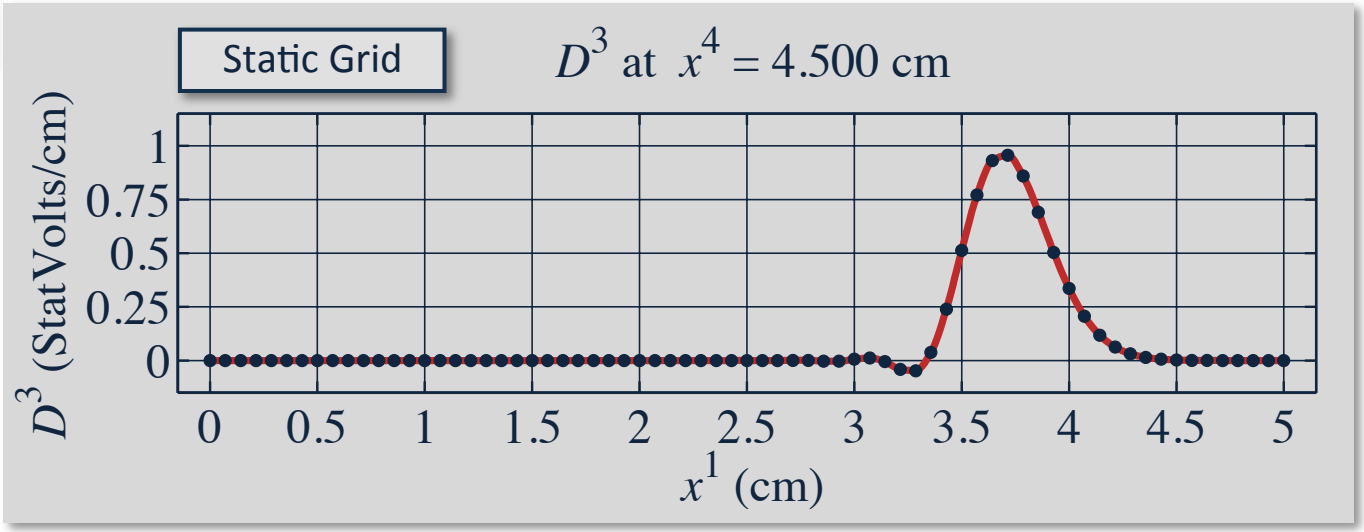

The dots show the location of the grid points.

Example: Pulse Tracking in 2D

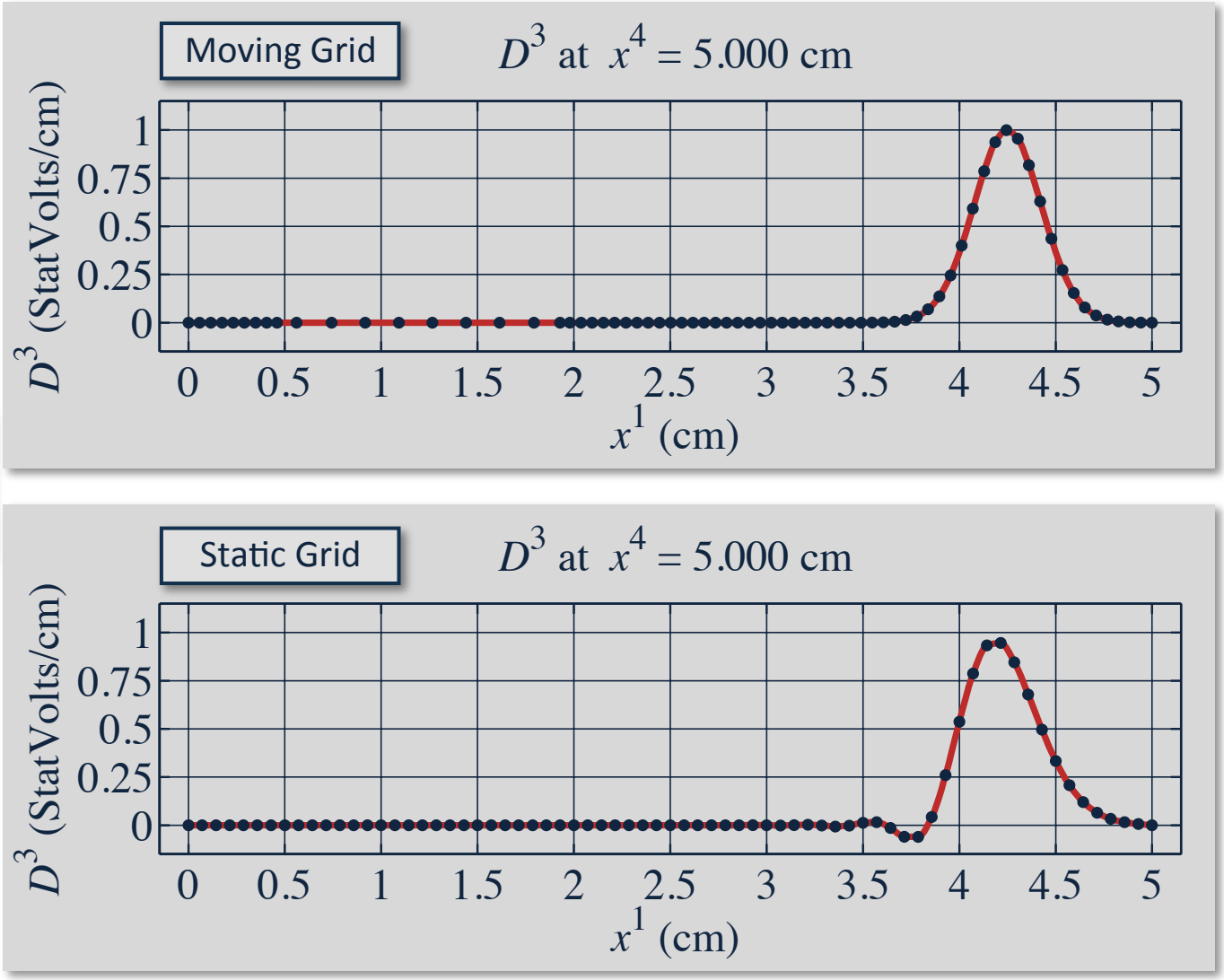

The same number of grid points are used in both space and time.

The dots show the location of the grid points.

Example: Pulse Tracking in 3D

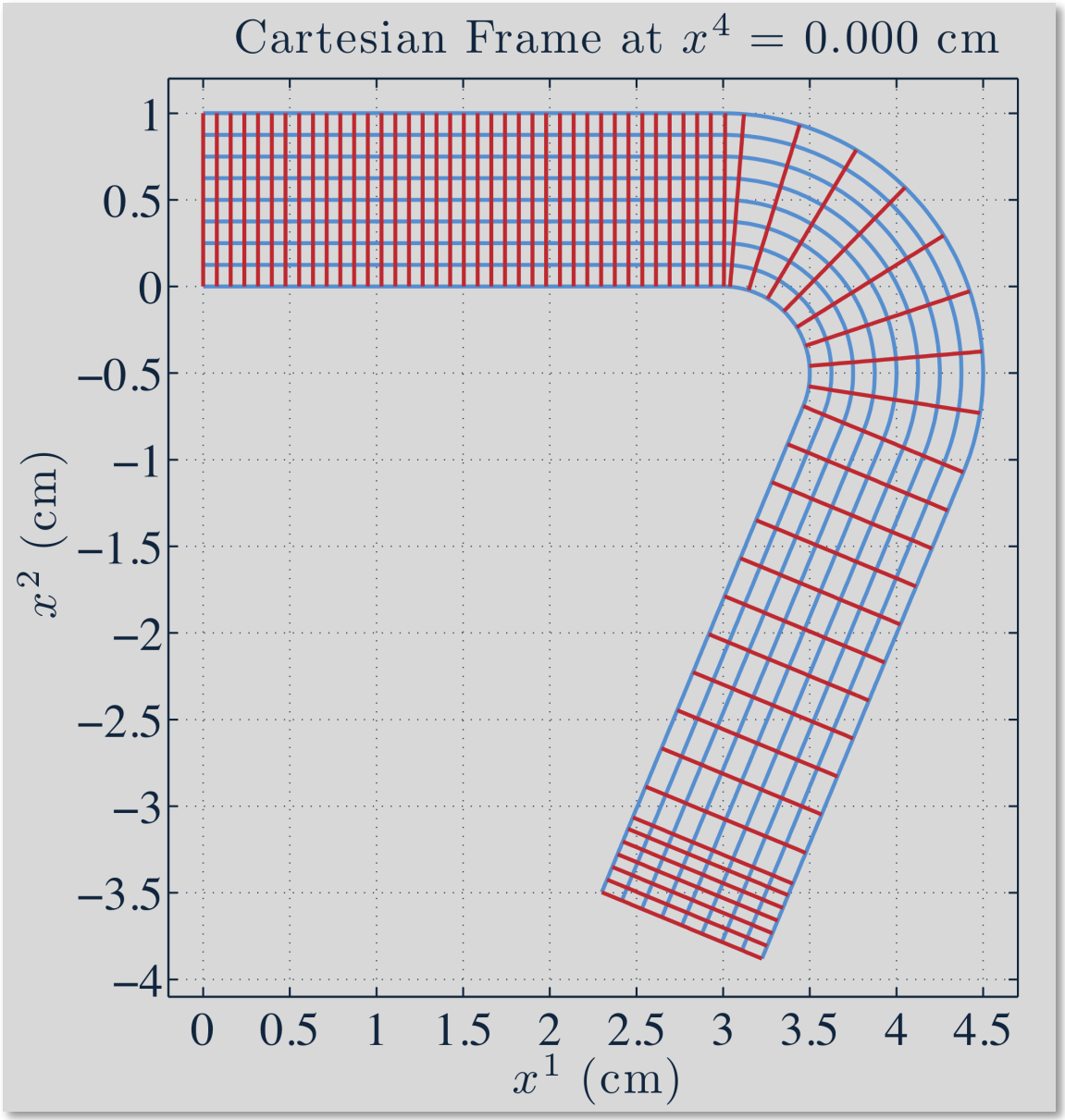

Going back to the example of a waveguide bend. A moving grid for this example was generated by putting together the two coordinate mappings presented thus far. v

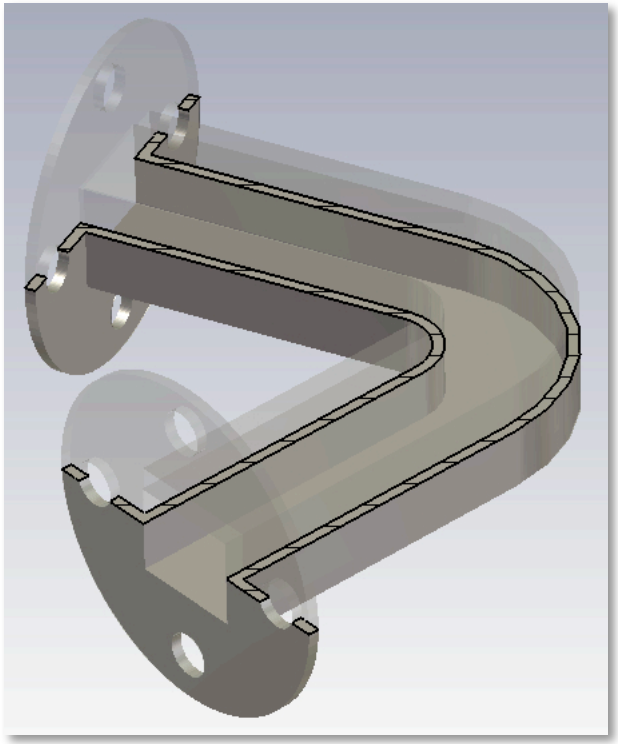

Example: Pulse Tracking in 3D

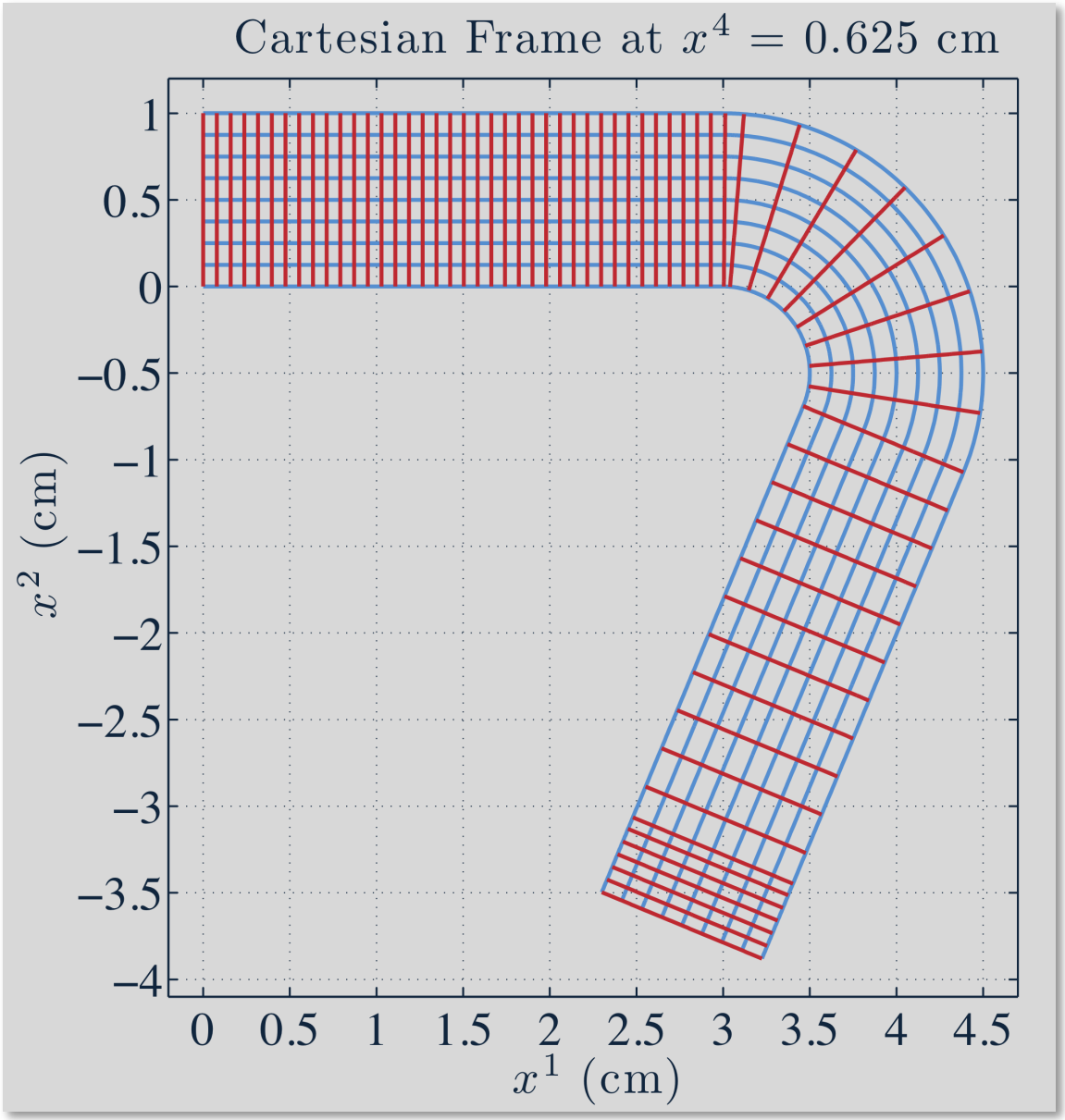

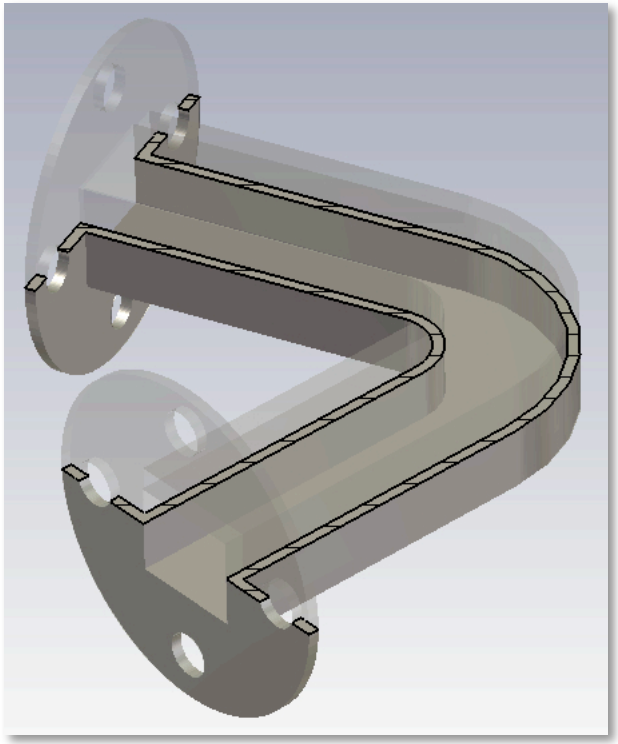

Example: Pulse Tracking in 3D

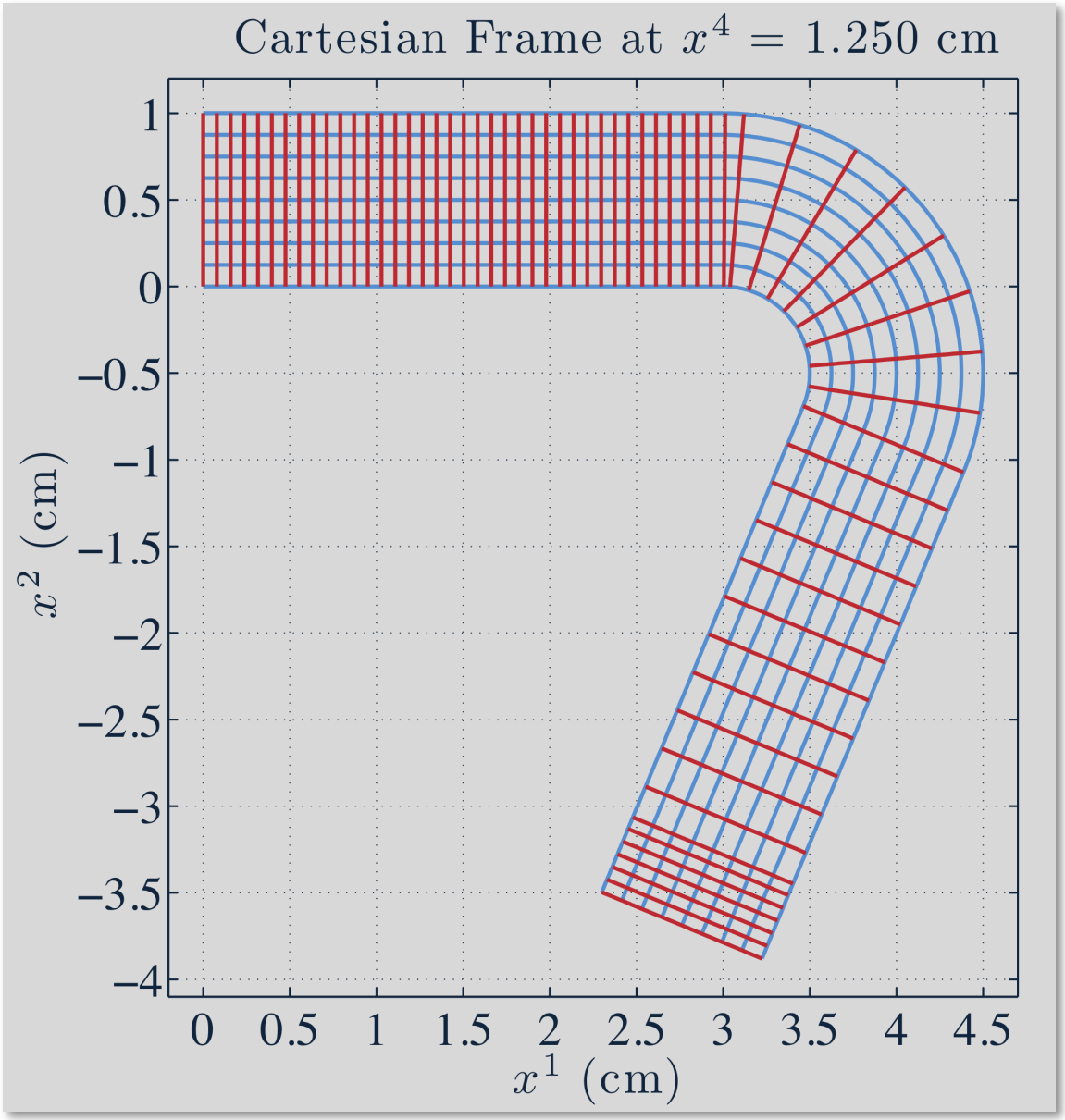

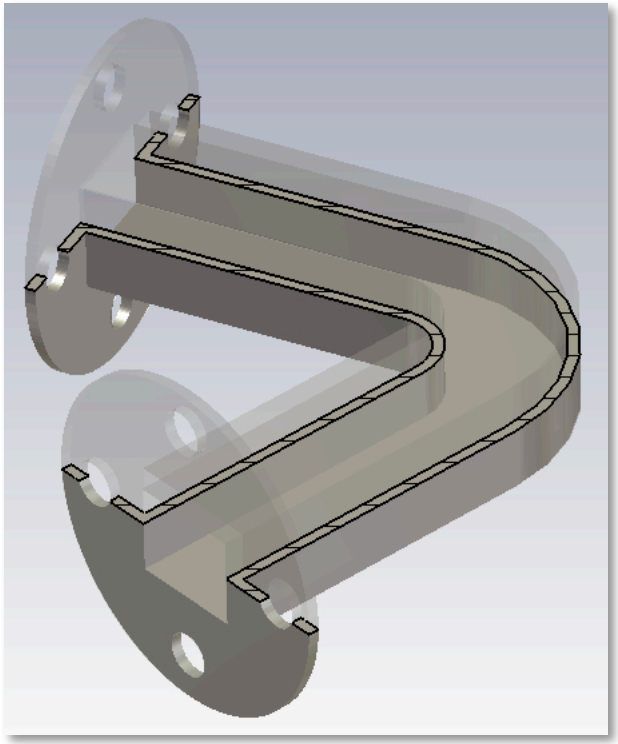

Example: Pulse Tracking in 3D

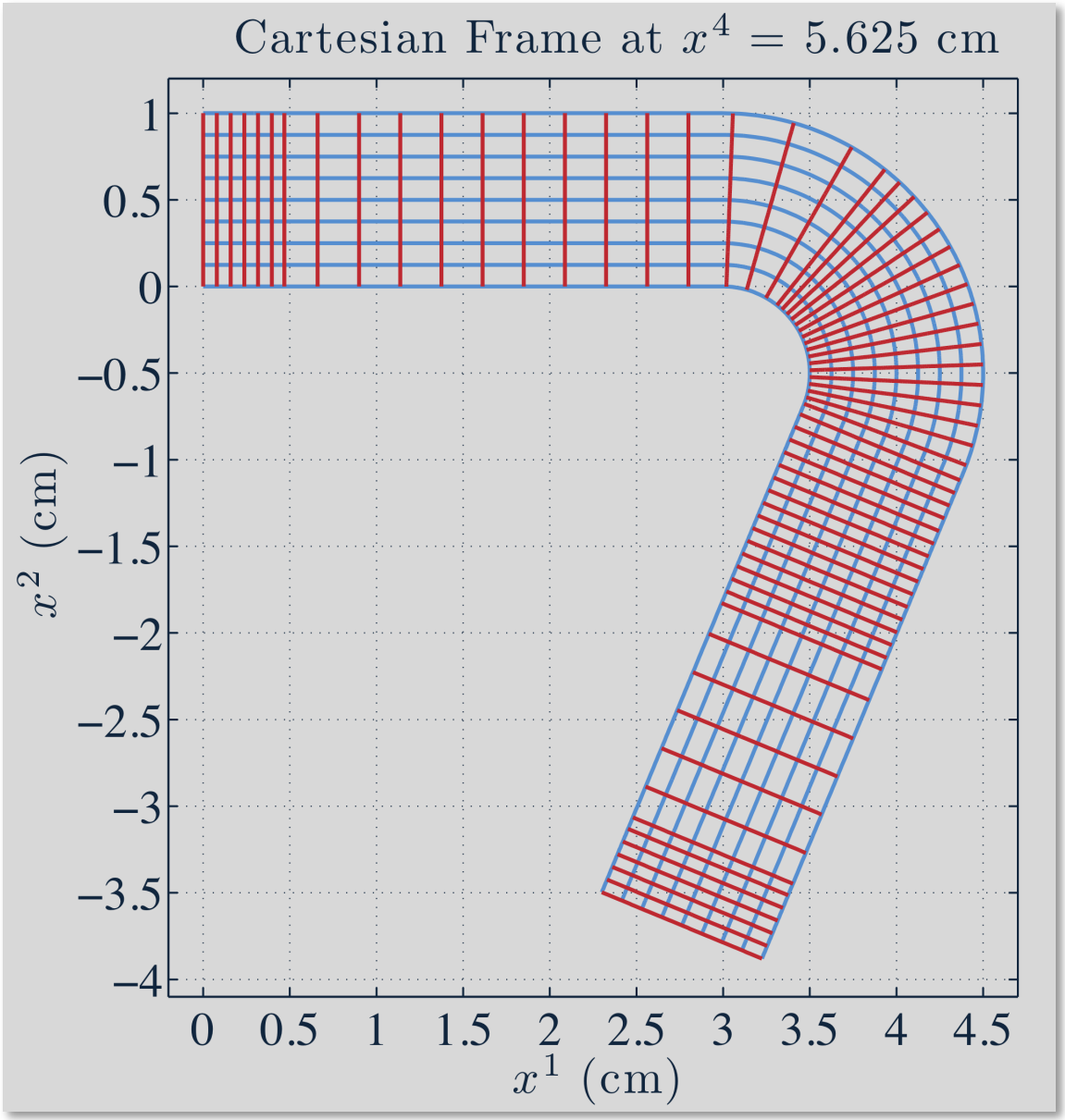

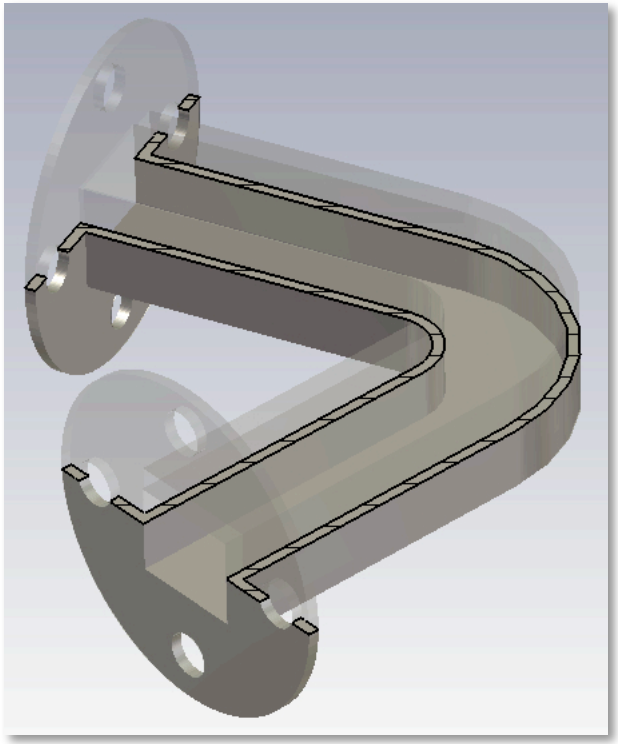

Example: Pulse Tracking in 3D

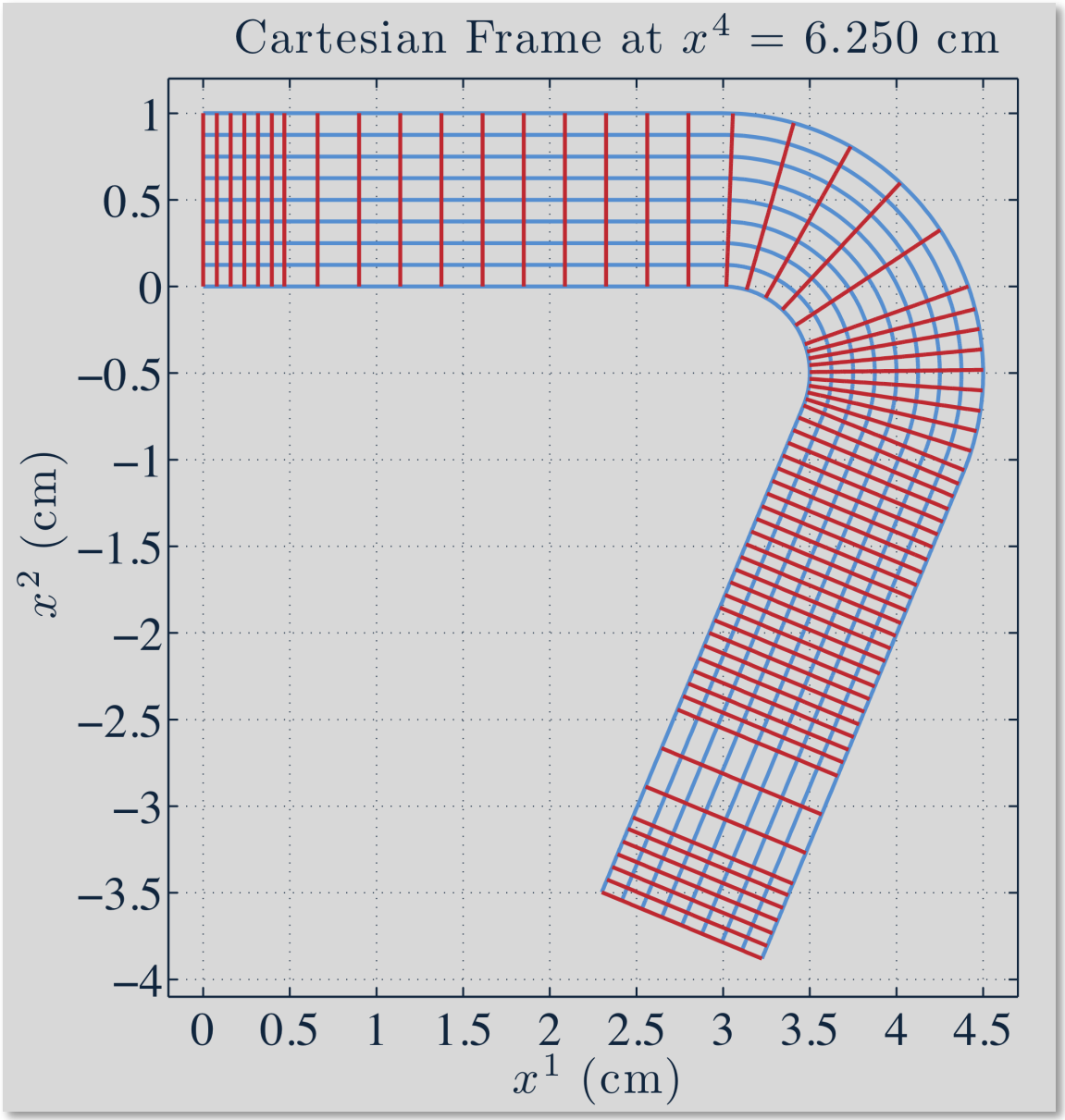

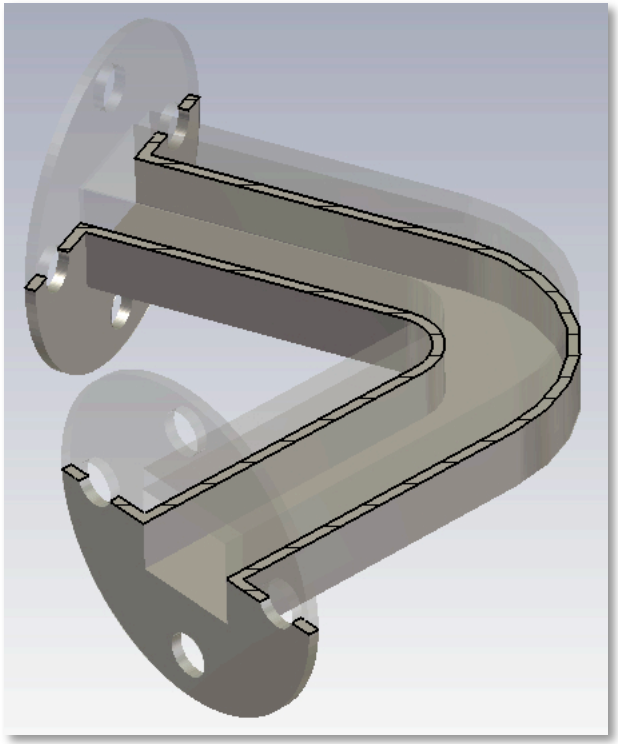

Example: Pulse Tracking in 3D

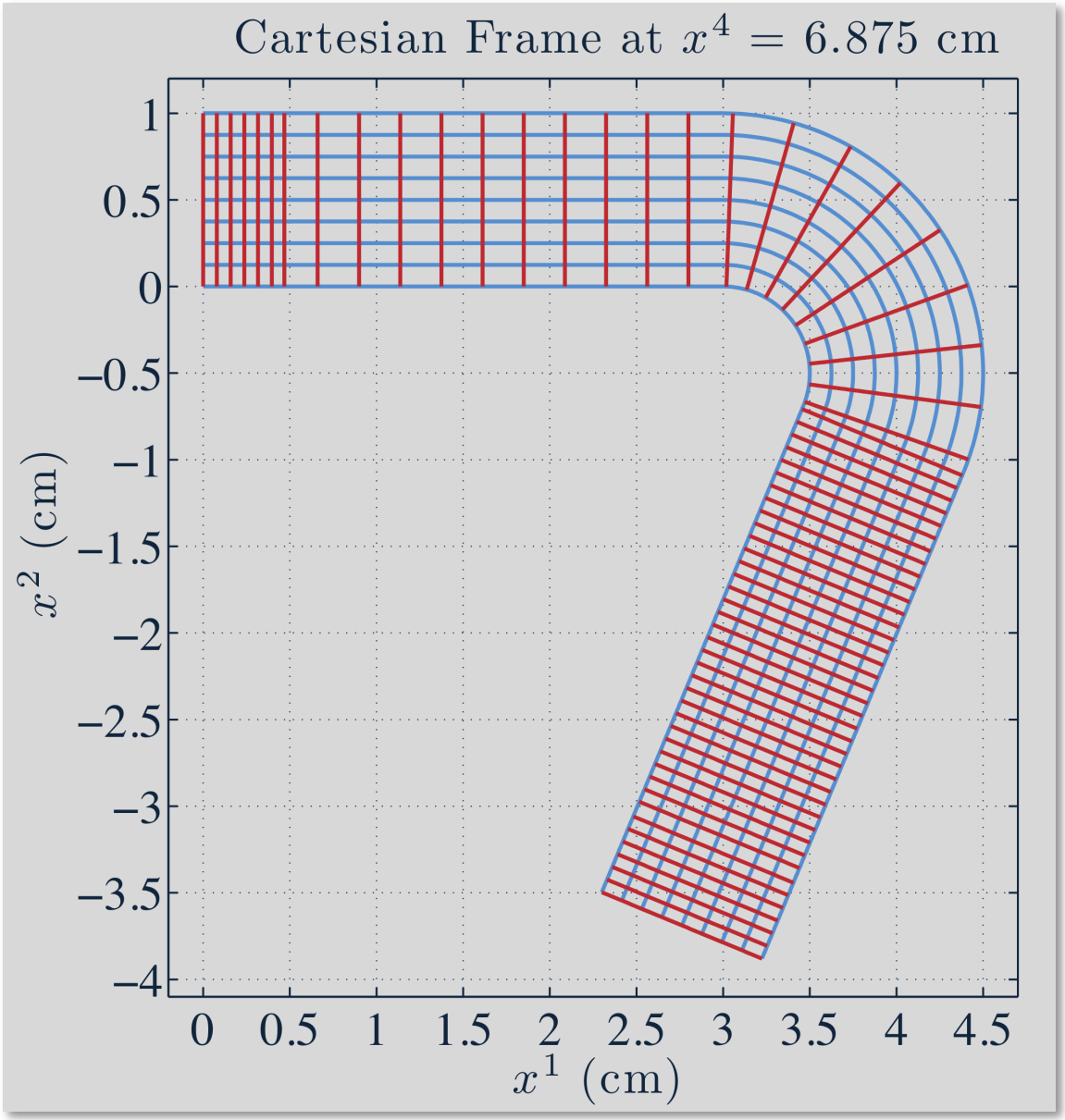

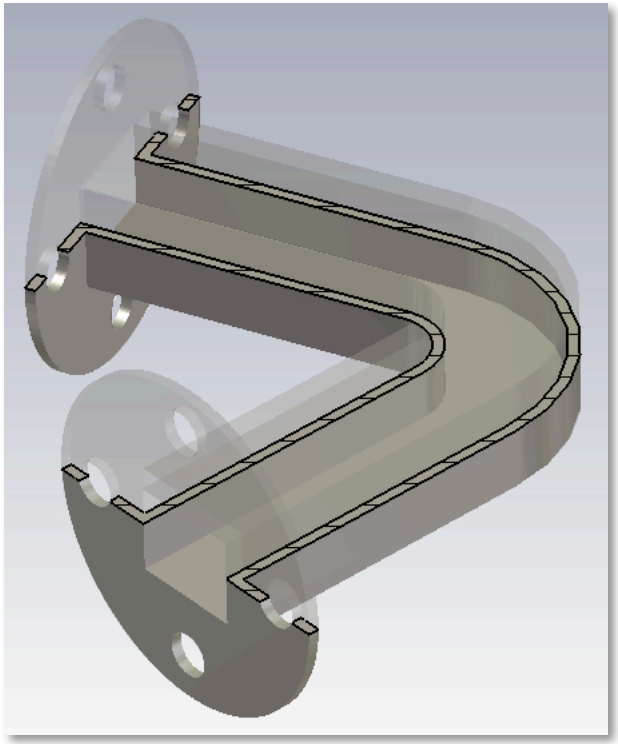

Example: Pulse Tracking in 3D

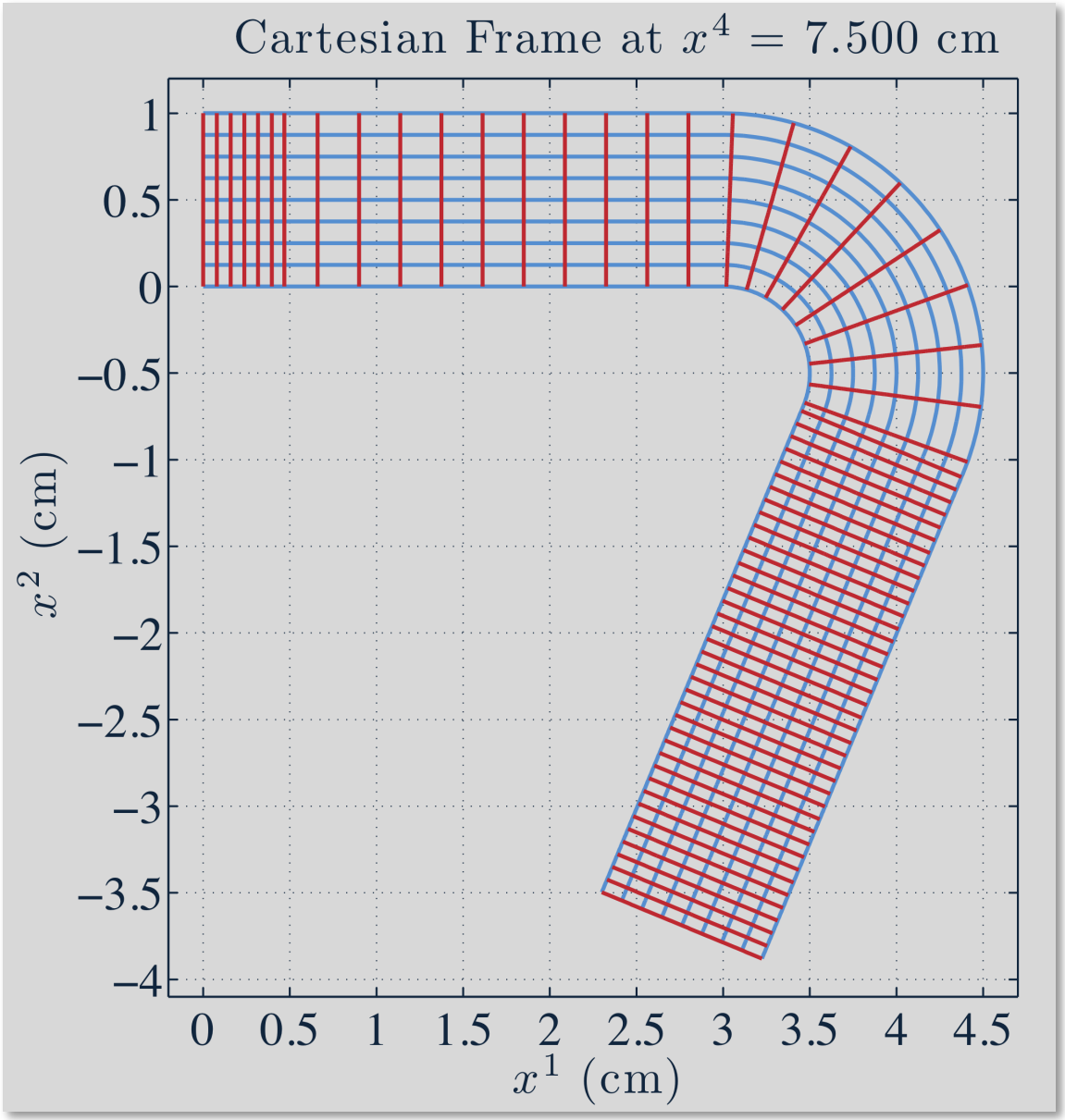

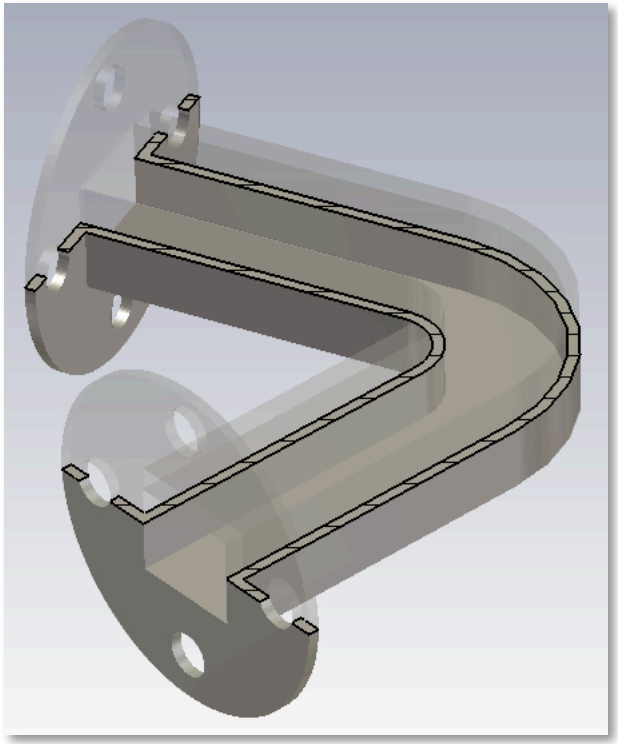

Example: Pulse Tracking in 3D

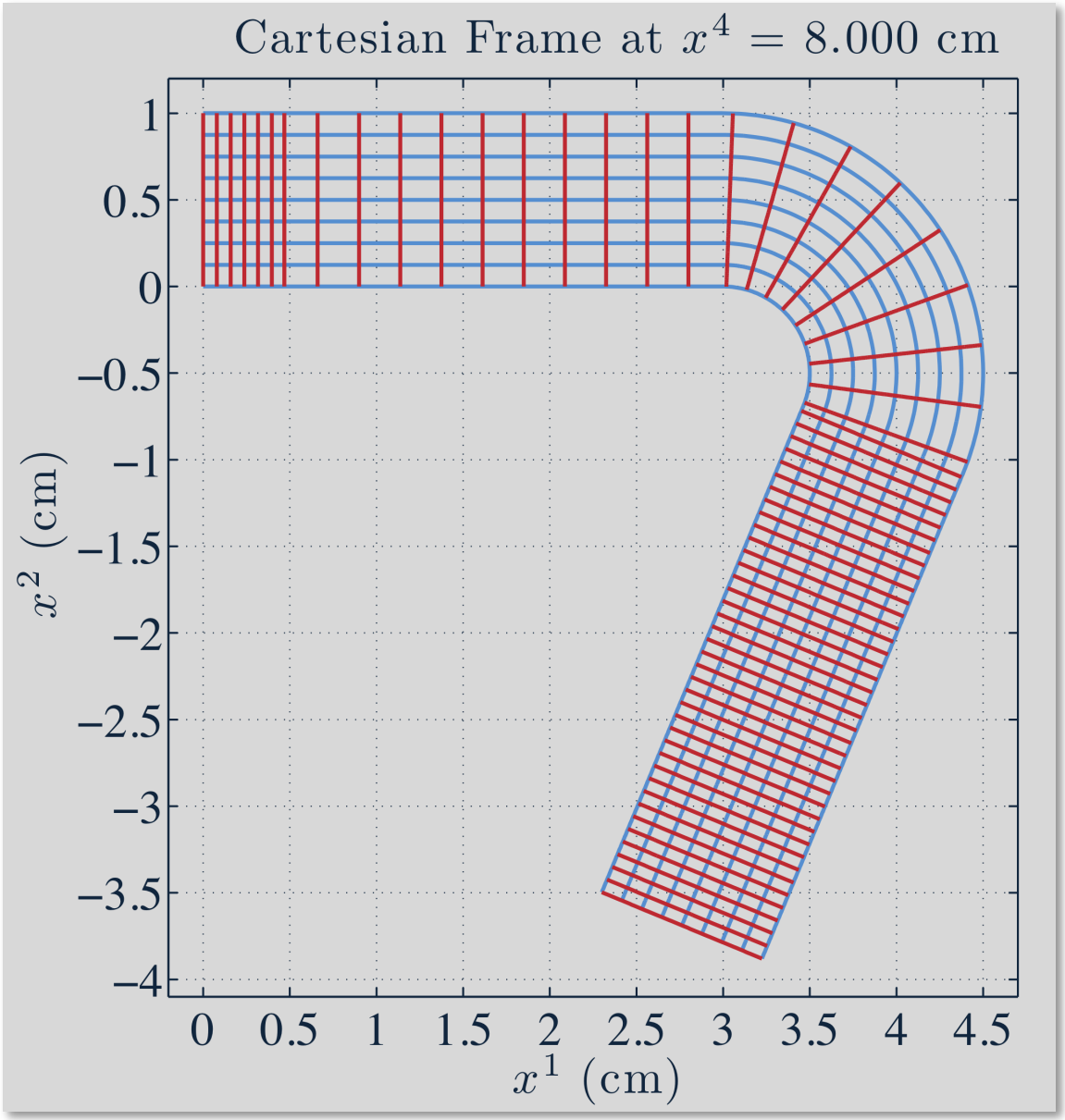

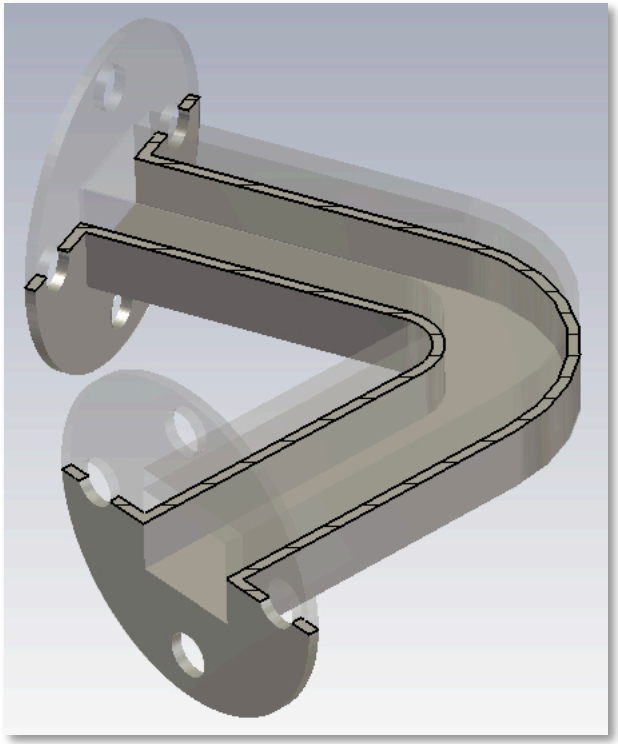

Example: Pulse Tracking in 3D

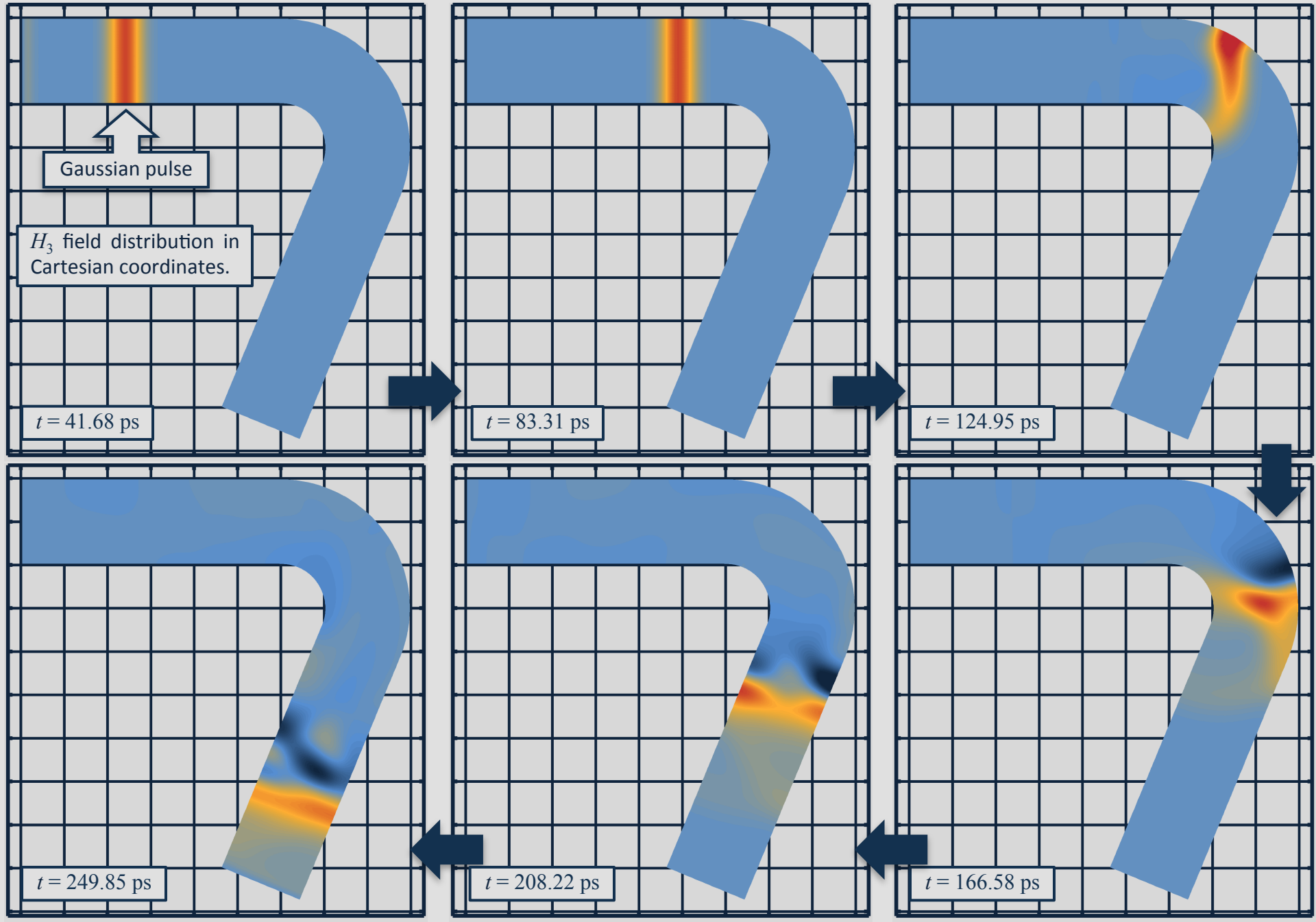

The relativistic formulation of Maxwell's equations can be used to introduce moving grids through time dependent coordinate transformations in a manner not permitted by the classical formulation.

Potential advantages of this approach:

① Stable: always leads to stable update equations.
② General: works regardless of what discretization
③ scheme is used.

Any type of material boundary shape can be accommodated.

Summary

FDTD Analysis of metamaterial structures

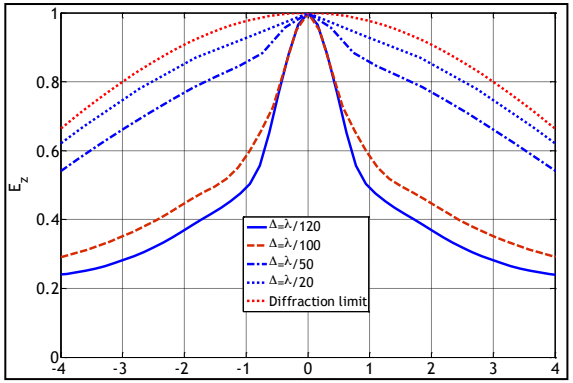

Dispersive models

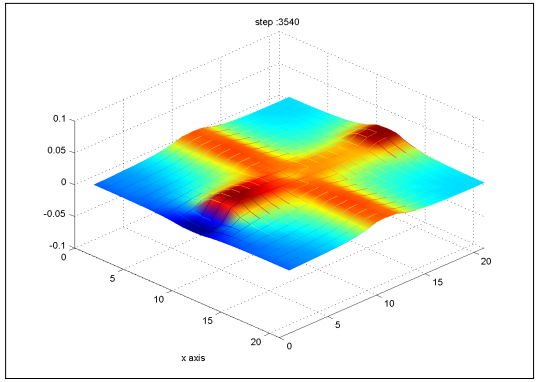

Periodic boundary conditions

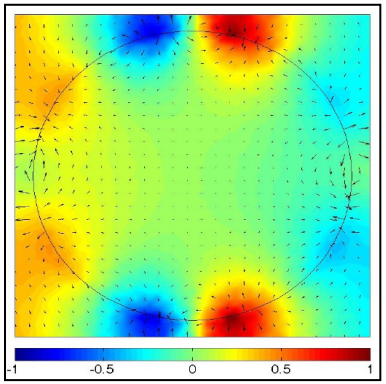

Plasmonic metamaterials

Methods inspired from transformation optics

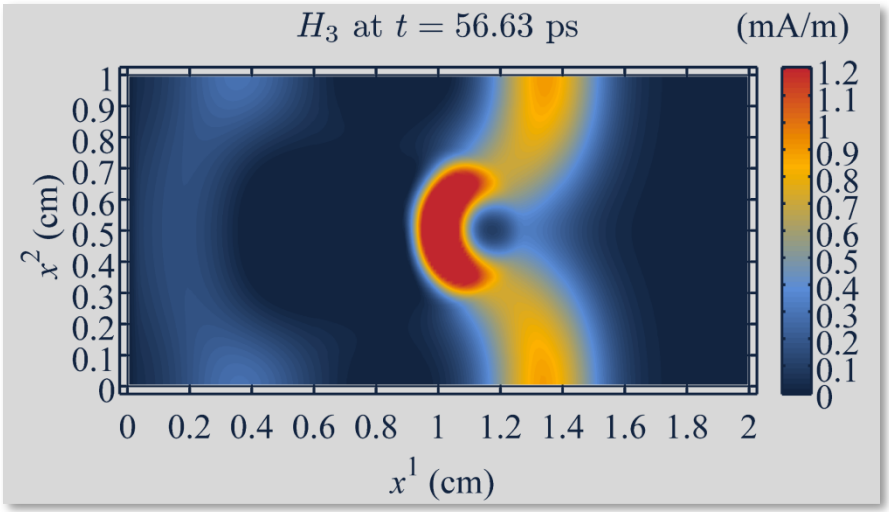

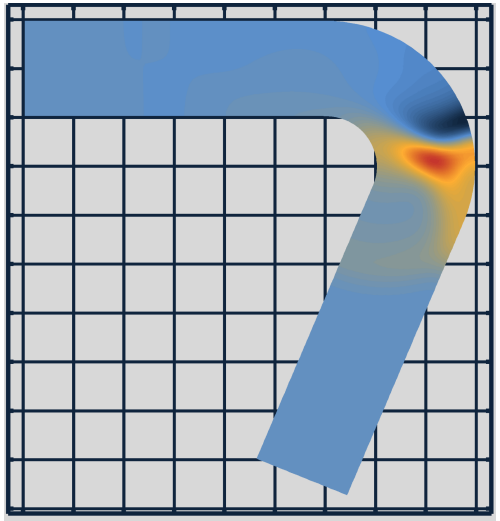

Space-time coordinate transformations

Questions ?

Thank you !

costas.sarris@utoronto.ca

The Edward S. Rogers Sr. Department
of Electrical & Computer Engineering
UNIVERSITY OF TORONTO

NSERC
CRSNG

Ontario Centres of
Excellence